https://ntrs.nasa.gov/search.jsp?R=19770007044 2020-03-22T12:19:45+00:00Z

TECH LIBRARY KAFB, NM
0061376
NASA CR-2
CAN COPY: RETURN TO
AFWL TECHNICAL LIBRARY
KIRTLAND AFB, N. M.

NASA CONTRACTOR REPORT

NASA CR-2767

# FURTHER STUDIES OF UNSTEADY BOUNDARY LAYERS WITH FLOW REVERSAL

*John F. Nash*

*Prepared by*
SYBUCON, INC.
Atlanta, Ga. 30339
*for Ames Research Center*

27 DEC 1976

NATIONAL AERONAUTICS AND SPACE ADMINISTRATION • WASHINGTON, D. C. • DECEMBER 1976

TECH LIBRARY KAFB, NM
0061376

| 1. Report No. | 2. Government Accession No. | 3. Recipient's Catalog No. |
|---|---|---|
| NASA CR-2767 | | |

| 4. Title and Subtitle | 5. Report Date |
|---|---|
| "Further Studies of Unsteady Boundary Layers with Flow Reversal" | December 1976 |
| | 6. Performing Organization Code |

| 7. Author(s) | 8. Performing Organization Report No. |
|---|---|
| John F. Nash | |
| | 10. Work Unit No. |

| 9. Performing Organization Name and Address | 11. Contract or Grant No. |
|---|---|
| Sybucon, Inc.<br>9 Perimeter Place, N.W. (Suite 960)<br>Atlanta, Georgia 30339 | NAS 2-8771 |
| | 13. Type of Report and Period Covered |
| 12. Sponsoring Agency Name and Address | Contractor Report |
| National Aeronautics & Space Administration<br>Washington, D. C. 20546 | 14. Sponsoring Agency Code |

15. Supplementary Notes

16. Abstract

Further computational experiments have been conducted to study the characteristics of flow reversal and separation in unsteady boundary layers. One set of calculations was performed using the first-order, time-dependent turbulent boundary-layer equations, and extended earlier work by Nash and Patel to a wider range of flows. Another set of calculations was performed for laminar flow using the time-dependent Navier-Stokes equations.

The results of the calculations confirm previous conclusions concerning the existence of a regime of unseparated flow, containing an embedded region of reversal, which is accessible to first-order boundary-layer theory. However, certain doubts are cast on the precise nature of the events which accompany the eventual breakdown of the theory due to singularity onset. The earlier view that the singularity appears as the final event in a sequence involving rapid thickening of the boundary layer and the formation of a localized region of steep gradients, is called into question by the present results. It appears, first, that singularity onset is not necessarily preceded by rapid boundary-layer thickening, or even necessarily produces immediate thickening. Furthermore, the formation of a region of steep gradients could not be reproduced in the solutions of the Navier-Stokes equations, and may, itself, prove to be a feature of first-order boundary-layer theory and not part of a more complete description of the flow.

| 17. Key Words (Suggested by Author(s)) | 18. Distribution Statement |
|---|---|
| Turbulent Flow Calculation<br>Navier-Stokes Equations<br>Unsteady Boundary Layers | UNCLASSIFIED - UNLIMITED<br><br>STAR Category 02 |

| 19. Security Classif. (of this report) | 20. Security Classif. (of this page) | 21. No. of Pages | 22. Price* |
|---|---|---|---|
| UNCLASSIFIED | UNCLASSIFIED | 97 | $4.00 |

*For sale by the National Technical Information Service, Springfield, Virginia 22161

CONTENTS


| | Page |
|---|---|
| FOREWORD | iii |
| SUMMARY | iv |
| SYMBOLS | v |
| LIST OF FIGURES | vii |
| INTRODUCTION | 1 |
| PART I. TURBULENT FLOW CALCULATIONS | 4 |
| I.1 NATURE OF THE FLOWS CONSIDERED | 4 |
| I.2 COMPUTATIONAL EXPERIMENTS | 7 |
| Frozen Flows | 7 |
| Oscillatory Flows | 12 |
| I.3 THE NATURE OF UNSTEADY SEPARATION | 19 |
| PART II. LAMINAR FLOW CALCULATIONS | 24 |
| II.1 NATURE OF THE FLOWS CONSIDERED | 24 |
| II.2 COMPUTATIONAL EXPERIMENTS | 29 |
| CONCLUDING REMARKS | 32 |
| APPENDIX A: CALCULATION METHOD FOR TIME-DEPENDENT TURBULENT BOUNDARY LAYERS | 35 |
| APPENDIX B: SOLUTION METHOD FOR TIME-DEPENDENT NAVIER-STOKES EQUATIONS | 40 |
| REFERENCES | 44 |
| FIGURES | 46 |

## FOREWORD

This report was prepared under Contract NAS2-8771 by

Sybucon, Inc.
Scientific and Business Consultants
9 Perimeter Place, N.W. (Suite 960)
Atlanta, Georgia 30339

for the

United States Army Air Mobility
Research and Development Laboratory
Ames Directorate
Moffett Field, California 94035.

The contract was administered by the National Aeronautics and Space Administration, Ames Research Center. The Technical Monitor was Dr. Lawrence W. Carr.

## SUMMARY

Further computational experiments have been conducted to study the characteristics of flow reversal and separation in unsteady boundary layers. One set of calculations was performed using the first-order, time-dependent turbulent boundary-layer equations, and extended earlier work by Nash and Patel to a wider range of flows. Another set of calculations was performed for laminar flow using the time-dependent Navier-Stokes equations.

The results of the calculations confirm previous conclusions concerning the existence of a regime of unseparated flow, containing an embedded region of reversal, which is accessible to first-order boundary-layer theory. However, certain doubts are cast on the precise nature of the events which accompany the eventual breakdown of the theory due to singularity onset. The earlier view that the singularity appears as the final event in a sequence involving rapid thickening of the boundary layer and the formation of a localized region of steep gradients, is called into question by the present results. It appears, first, that singularity onset is not necessarily preceded by rapid boundary-layer thickening, or even necessarily produces immediate thickening. Furthermore, the formation of a region of steep gradients could not be reproduced in the solutions of the Navier-Stokes equations, and may, itself, prove to be a feature of first-order boundary-layer theory and not part of a more complete description of the flow.

## LIST OF SYMBOLS

| | |
|---|---|
| $A$, $A_m$ | Imbalance between production and dissipation of turbulent kinetic energy (see Equation A8) |
| A,B,C,D,E | Coefficients appearing in Equation (B14) |
| $a_1$,$a_2$ | Empirical functions in the shear-stress model (Equation A3) |
| c | Chord length of the plate, and length of the integration domain |
| F | General function |
| f | Function defined by Equation (3) |
| j,n | Integers appearing in Equation (A11) |
| $\ell$ | Time-level integer |
| L | Dissipation length |
| m,n | Node-point indexing integers |
| p | Static pressure |
| q | Resultant fluctuating velocity ($q^2 = u^2 + v^2 + w^2$) |
| R,$R_1$,$R_2$ | Functions appearing in Equations (B14,B15,B16) |
| s | Height of the integration domain |
| t | Time |
| U,V,W | Ensemble average velocity components in the x-, y-, z-directions, respectively |
| u,v,w | Fluctuating velocity components corresponding to U,V,W, respectively |
| x,y,z | Cartesian coordinates fixed in the plate: x measured along the plate, y measured normal to it, and z measured laterally. |
| $x_o$,$x_1$ | Parameters appearing in Equations (2, 3) |
| $\alpha$ | Shear-stress gradient (see Equation A10) |
| $\Gamma$, $\Phi$ | Parameters appearing in Equations (A3,A5) |

| | |
|---|---|
| $\Delta$ | Step length in the numerical method |
| $\delta$ | Boundary-layer thickness |
| $\delta^*$ | Displacement thickness ($\delta^* = \int_0^\infty (1 - \frac{U}{U_e})\, dy$) |
| $\zeta$ | Vorticity component in the z-direction |
| $\kappa$ | Constant in the Law of the Wall |
| $\nu$ | Kinematic viscosity |
| $\rho$ | Density |
| $\tau$ | Shear stress |

Subscripts

| | |
|---|---|
| c | Convection values |
| e | Value at the edge of the boundary layer |
| m | Value at the matching station |
| o | Values at $x = 0$ (except $x_o$, which see) |
| p | Penetration value |
| s | Stagnation value |
| w | Value at the wall |

LIST OF FIGURES


| Figure | | Page |
|---|---|---|
| 1. | Definition of the External Velocity Distributions . . . . . | 46 |
| 2. | Wall Shear Stress Distributions for Increasing Time; Frozen Flow, $U_o t_f/c = 0.2$, $f_f = 0$ . . . . . | 47 |
| 3. | Displacement Thickness Distributions for Increasing Time; Frozen Flow, $U_o t_f/c = 0.2$, $f_f = 0$ . . . . . | 48 |
| 4. | Wall Shear Stress Distributions for Increasing Time; Frozen Flow, $U_o t_f/c = 2.0$, $f_f = 0$ . . . . . | 49 |
| 5. | Displacement Thickness Distributions for Increasing Time; Frozen Flow, $U_o t_f/c = 2.0$, $f_f = 0$ . . . . . | 50 |
| 6. | Wall Shear Stress Distributions for Increasing Time; Frozen Flow, $t_f = 2.0$, $f_f = 0.5$ . . . . . | 51 |
| 7. | Displacement Thickness Distributions for Increasing Time; Frozen Flow, $t_f = 2.0$, $f_f = 0.5$ . . . . . | 52 |
| 8. | Variation of Wall Shear Stress with Time; Frozen Flow . . . | 53 |
| 9. | Variation of Displacement Thickness with Time; Frozen Flow . . . . . | 54 |
| 10. | Movement of the Reversal Point with Time; Frozen Flow . . . | 55 |
| 11. | Prediction of Singularity Onset, Using the Criterion of Reference [7]; Frozen Flow . . . . . | 56 |
| 12. | The Function f(t) for Oscillatory Flows of Various Periods; A = 0.5 . . . . . | 57 |
| 13. | Variation of Pressure Gradient at $x = x_o$ with Time; Oscillatory Flow, A = 0.5 . . . . . | 58 |
| 14. | Wall Shear Stress Distributions for Increasing Time; $U_o t_p/c = 2.0$, A = 0.5. Oscillatory Flow . . . . . | 59 |
| 15. | Displacement Thickness Distributions for Increasing Time; $U_o t_p/c = 2.0$, A = 0.5. Oscillatory Flow . . . . . | 60 |
| 16. | Wall Shear Stress Distributions for Increasing Time; Oscillatory Flow, $U_o t_p/c = 4.0$, A = 0.5 . . . . . | 61 |
| 17. | Displacement Thickness Distributions for Increasing Time; Oscillatory Flow, $U_o t_p/c = 4.0$, A = 0.5 . . . . . | 62 |

Figure Page

18. Wall Shear Stress Distributions for Increasing Time; Oscillatory Flow, $U_o t_p/c = 8.0$, A = 0.5 . . . . . 63

19. Displacement Thickness Distributions for Increasing Time; Oscillatory Flow, $U_o t_p/c = 8.0$, A = 0.5 . . . . . 64

20. Movement of the Reversal Point with Time; Oscillatory Flow, $U_o t_p/c = 2.8$ . . . . . 65

21. Variation of Wall Shear Stress with Time . . . . . 66

22. Variation of Displacement Thickness with Time; Oscillatory Flow, $U_o t_p/c = 2.8$ . . . . . 67

23. The Function f(t) for Oscillatory Flows of Various Amplitudes; $U_o t_p/c = 2.0$ . . . . . 68

24. Variation of Pressure Gradient at $x = x_o$ with Time; Oscillatory Flow, $U_o t_p/c = 2.0$ . . . . . 69

25. Wall Shear Stress Distributions for Various Amplitudes; Oscillatory Flow, $U_o t_p/c = 2.0$, $U_o t/c = 4.0$ . . 70

26. Displacement Thickness Distributions for Various Amplitudes; Oscillatory Flow, $U_o t_p/c = 2.0$, $U_o t/c = 4.0$ . . 71

27. Wall Shear Stress Distributions for Various Amplitudes; Oscillatory Flow, $U_o t_p/c = 2.0$, $U_o t/c = 5.0$ . . 72

28. Displacement Thickness Distributions for Various Amplitudes; Oscillatory Flow, $U_o t_p/c = 2.0$, $U_o t/c = 5.0$ . . 73

29. Variation of Wall Shear Stress with Time; Oscillatory Flow, $U_o t_p/c = 2.0$, x = 0.65c . . . . . 74

30. Variation of Displacement Thickness with Time; Oscillatory Flow, $U_o t_p/c = 2.0$, x = 0.65c . . . . . 75

31. Movement of the Reversal Point with Time; Oscillatory Flow, $U_o t_p/c = 2.0$ . . . . . 76

32. The Function f(t) for Oscillatory Flows of Various Amplitudes; $U_o t_p/c = 4.0$ . . . . . 77

33. Variation of Pressure Gradient at $x = x_o$ with Time; Oscillatory Flow, $U_o t_p/c = 4.0$ . . . . . 78

34. Wall Shear Stress Distributions for Various Amplitudes; Oscillatory Flow, $U_o t_p/c = 4.0$, $U_o t/c = 4.0$ . . 79

| Figure | | Page |
|---|---|---|
| 35. | Displacement Thickness Distributions for Various Amplitudes; Oscillatory Flow, $U_o t_p/c = 4.0$, $U_o t/c = 4.0$ . . | 80 |
| 36. | Movement of the Reversal Point with Time: Oscillatory Flow, $U_o t_p/c = 4.0$ . . . . . | 81 |
| 37. | Velocity Profiles at $U_o t/c = 1.0$; Oscillatory Flow, $U_o t_p/c = 2.0$, $A = 0.5$ . . . . . | 82 |
| 38. | Velocity Profiles at $U_o t/c = 1.5$; Oscillatory Flow, $U_o t_p/c = 2.0$, $A = 0.5$ . . . . . | 83 |
| 39. | Velocity Profiles at $U_o t/c = 2.0$; Oscillatory Flow, $U_o t_p/c = 4.0$, $A = 0.5$ . . . . . | 84 |
| 40. | Velocity Profiles at $U_o t/c = 3.0$; Oscillatory Flow, $U_o t_p/c = 4.0$, $A = 0.5$ . . . . . | 85 |
| 41. | Velocities at $y = 0.1\delta$; Oscillatory Flow, $A = 0.5$ . . . . | 86 |
| 42. | Computed Velocity Profiles Over a Flat Plate; Laminar Flow, $U_o c/\nu = 10^4$ . . . . . | 87 |
| 43. | Velicity Profiles at $U_o t/c = 2.0$; Laminar Frozen Flow, $U_o t_f/c = 2.0$, $f_f = 0.5$ . . . . . | 88 |
| 44. | Velocity Profiles at $U_o t/c = 4.0$; Laminar Frozen Flow, $U_o t_f/c = 2.0$, $f_f = 0.5$ . . . . . | 89 |
| 45. | Velocity Profiles at $U_o t/c = 8.0$; Laminar Frozen Flow, $U_o t_f/c = 2.0$, $f_f = 0.5$ . . . . . | 90 |
| 46. | Wall Shear Stress Distributions for Increasing Time; Laminar Frozen Flow, $U_o t_f/c = 2.0$, $f_f = 0.5$ . . . . | 91 |
| 47. | Displacement Thickness Distributions for Increasing Time; Laminar Frozen Flow, $U_o t_f/c = 2.0$, $f_f = 0.5$ . . . . | 92 |
| 48. | Variation of Wall Shear Stress with Time; Frozen Flow; $U_o t_f/c = 2.0$, $f_f = 0.5$, $x = 0.65c$ . . . . . | 93 |
| 49. | Variation of Displacement Thickness with Time; Frozen Flow, $U_o t_f/c = 2.0$, $f_f = 0.5$, $x = 0.65c$ . . . . . | 94 |
| 50. | Vorticity Contours at $U_o t/c = 2.0$; Frozen Laminar Flow, $U_o t_f/c = 2.0$ . . . . . | 95 |
| 51. | Vorticity Contours at $U_o t/c = 4.0$; Frozen Laminar Flow, $U_o t_f/c = 2.0$ . . . . . | 96 |
| 52. | Vorticity Contours at $U_o t/c = 8.0$; Frozen Laminar Flow, $U_o t_f/c = 2.0$ . . . . . | 97 |

# INTRODUCTION

Extensive calculations have been performed, over the last several years, to study the characteristics of time-dependent turbulent boundary layers. These calculations have taken the form of numerical experiments, yielding data which -- although inferior in obvious respects to reliable wind-tunnel results -- have nevertheless served to fill the void which still exists because of the scarcity of comprehensive measurements. Indeed, much of what is known at this time about unsteady boundary layers has been derived from theory rather than from measurement, and, while the need for good wind-tunnel experiments to confirm the calculated results (or at least to validate the theoretical models) remains as acute as ever it was, the information content of calculations seems likely to "stay ahead" of that of measurements for some time to come.

The most recent work on unsteady turbulent boundary layers, done by the present author and his co-workers, has been concerned with the effects of time-dependence on reversal and separation onset. It was shown in References [1,2] that time-dependence results in a delay of reversal onset, and that this delay could not be related in any simple manner to an alleviation of the pressure gradients; indeed, some measure of delay was observed even when the pressure gradients were augmented by the effects of the unsteadiness. It was shown further, that the reversal point in an unsteady turbulent boundary layer is not a singular point -- an observation which confirmed earlier statements which had been made concerning laminar flow [3,4,5,6] -- and that the boundary layer remains thin even

though reversal had taken place [1]. Subsequent work was directed to studying a class of unsteady turbulent boundary layers in which a region of embedded reversal was allowed to develop but in which, under certain conditions, a singularity occurred sometime later [7,8]. This singularity is related to the final separation of the boundary layer, in the sense of detachment of the outer flow from the body surface, and represents the limit of validity of first-order boundary-layer theory. However, the regime between reversal and separation appears to be accessible to first-order theory [7], and the calculations which were performed in this regime are believed to be meaningful.

The present work, which forms a sequel to that of Reference [7], has two main objectives:

1. to extend the calculations of unsteady turbulent boundary layers to a wider range of flow configurations, and
2. to try to elucidate the mechanism of separation onset by performing higher-order calculations which would not break down as the result of the development of a singularity.

In pursuit of the first objective, calculations have been performed for two additional types of flow: flows in which an unsteady retardation is first imposed, but where the external velocity distribution is subsequently frozen allowing a relaxation towards steady-state conditions, and oscillatory flows in which reversal occurs during part of the cycle. The results of these calculations are presented in Part I of this report.

The second objective was pursued by programming a simple method for solving the unsteady Navier-Stokes equations, and performing some calculations

for laminar flow. It was recognized that the characteristics of turbulent flows would not be represented appropriately by this means, but it was hoped that the mechanism of separation would have sufficient generality to make these laminar calculations useful. The results of this study are presented in Part II of the report.

## PART I. TURBULENT FLOW CALCULATIONS

### I.1 NATURE OF THE FLOWS CONSIDERED

The turbulent boundary-layer studies reported here were carried out for incompressible, time-dependent flow over a two-dimensional surface of large or infinite radius. As in the earlier work [1,7], orthogonal coordinates are erected on the surface, with y measured normal to it and x measured along the surface from some origin where the boundary layer is already turbulent and of known properties: corresponding to steady, constant-pressure conditions. The main features of the calculation method are reviewed in Appendix A. The calculations relate to the boundary layer developing over a "plate" of chord c which extends downstream from the origin.

The external velocity: $U_e$, over the plate, is assumed to vary in a prescribed manner with x and time, t. Specifically, it is assumed that

$$U_e = U_o, \text{ for } t \leq 0 \text{ and all } x \tag{1}$$

$$\frac{U_e}{U_o} = 1 - \frac{x}{x_o}\{1 - f(t)\}, \text{ for } t \geq 0 \text{ and } 0 \leq x \leq x_o \tag{2}$$

$$\frac{U_e}{U_o} = 1 - \frac{x_1 - x}{x_o}\{1 - f(t)\}, \text{ for } t \geq 0 \text{ and } x_o < x \leq c \tag{3}$$

where $U_o$ is some reference velocity, and $x_o$ and $x_1$ are prescribed values of x: $x_o = 5c/7$ ( = 0.714c), $x_1 = 2x_o$. In Equations (2,3), f(t), which is the value of $U_e/U_o$ at $x = x_o$, is chosen to be a function of time, with

the restriction that $f = 1$ at $t = 0$ in order to satisfy Equation (1). The flows discussed in Reference [7] corresponded to

$$f = 1 - \omega x_o t/c, \tag{4}$$

where $\omega$ = constant, which imposed a distortion of the external flow which was monotonic in time.

Here, the emphasis is on patterns of distortion of the external velocity field which are of two other types:

(1) patterns in which an initial distortion, extending over a finite interval ($0 \leq t \leq t_f$), is followed by freezing of the external velocity field,

(2) oscillatory external velocity fields.

The "frozen" flows were generated by taking

$$f = 1 - (1 - f_f)t/t_f, \text{ for } 0 \leq t \leq t_f \tag{5}$$

$$f = f_f, \text{ for } t \geq t_f \tag{6}$$

Values of $f_f = 0$ and 0.5 were used, together with values of $t_f$ corresponding to $U_o t_f/c = 0.2$, 1.0, and 2.0.

The oscillatory flows were of a triangular waveform, and were generated by taking

$$f = 0.5 - A\ 4\{\frac{t - t_o}{t_p} - 1\} \tag{7}$$

over the first half of the cycle: $t_o \leq t \leq t_o + t_p/2$, and

$$f = 0.5 + A\{4 \frac{t - t_o}{t_p} - 3\} \qquad (8)$$

over the second half of the cycle: $t_o + t_p/2 \leq t \leq t_o$. Here, $t_p$ is the period of the oscillation, and $t_o$ refers to the beginning of the cycle. It will be noted that the mean value of f is 0.5, except* for the first half-cycle of the motion ($0 \leq t \leq t_p/2$) where an initial transient satisfies the requirement: $f = 1$ for $t = 0$; this transient is defined by

$$f = 1 - (1 + 2A) \frac{t}{t_p} . \qquad (9)$$

The period of the motion, which in dimensionless terms is $U_o t_p/c$, was varied between 2.0 and 8.0 in the calculations. The constant A, in Equations (7,8,9), controls the amplitude of the oscillatory external velocity distribution; values between 0 and 0.5 were chosen for the calculations. When $A = 0$, the flow degenerates from an oscillatory to a "frozen" flow (as defined above) with $f_f = 0.5$ and $t_f = t_p/2$.

When $A = 0.5$, in the oscillatory calculations, the external flow stagnates momentarily (i.e. $U_e = 0$), at the point on the surface: $x = x_o$, once during every cycle: namely, at $t = t_o + t_p/2$. With $f_f = 0$, in the "frozen flows," stagnation of the outer flow occurs at $x = x_o$ for all times subsequent to $t = t_f$. Stagnation does not occur at all if $A < 0.5$, in the oscillatory flows, and if $f_f > 0$ in the frozen flows.

Figure 1 illustrates the features of the two types of flow, and provides a graphical definition of the parameters $f_f$, $t_f$, $t_p$ and A.

---

*If $A = 0.5$ the mean value of f is 0.5 even during the first half-cycle.

## I.2 COMPUTATIONAL EXPERIMENTS

### Frozen Flows

A number of calculations were done for flows in which the external velocity distribution was frozen, at $t = t_f$, following an initial distortion starting at $t = 0$.

Figures 2 through 7 show the spacial distributions of wall shear stress and displacement thickness, respectively, at various time levels, for the following cases:

| $U_o t_f/c$ | $f_f$ |
|---|---|
| 0.2 | 0 |
| 2.0 | 0 |
| 2.0 | 0.5. |

In the first two cases, a region of reversed flow, of substantial extent, has already formed on the plate by the time ($t = t_f$) the external flow is frozen. In the third, reversal has not yet taken place at the time of freezing but occurs later. With $f_f = 0$, stagnation of the outer flow occurs at $x = x_o$, and $t \geq t_f$, and the displacement thickness takes on a locally infinite value. However, this infinity reflects the division by zero in the definition of displacement thickness and does not necessarily indicate the presence of a singularity in the solution of the boundary-layer equations.

Various criteria were described in Reference [7] for identifying the onset of a singularity: steepening of the gradients of wall shear stress and displacement thickness, versus x, the development of locally high displacement-thickness maxima, and breakdown of the boundary-layer approximationed. A surrogate criterion was also suggested: $\delta^* = 0.1c$, for flows

of the present type and at these Reynolds numbers, which appeared to correlate with the other criteria, and which helped to pinpoint the location of the locally high gradients between node points in the calculation. This surrogate criterion will be used here also, for the moment, although its usefulness is called into question later in the discussion. In any case, it is necessary to repeat the cautionary statements made in Reference [7] to the effect that the real measure of singularity onset is steepening of the velocity gradients rather than the attainment of some arbitrary value of $\delta^*$, and that the surrogate only has validity insofar as it helps to locate the formation of the steep gradients.

Figures 2 through 5, which relate to the two cases where $f_f = 0$, indicate that incipient singular conditions form at a time corresponding to $U_o t/c = 2.0$ for $U_o t_f/c = 0.2$, and at a time corresponding to $U_o t/c = 3.0$ for $U_o t_f/c = 2.0$. Thus the lower initial rate of distortion of the outer flow, in the latter case, results in a delay in the final onset of the singularity. Figures 8, 9, in which the wall shear stress and the displacement thickness are plotted versus time, emphasize this delay. The small dip in one of the curves of $\delta^*$ versus time (Figure 9) results from a forward movement of the $\delta^*$ maximum on the plate. It is interesting to note that, for these two cases with $f_f = 0$, there is a measure of similarity in the development of each solution towards singular conditions: the two sets of results (for $\tau_w$ or $\delta^*$) would roughly coincide if they were plotted against $t - t_s$, where $t_s$ refers to the onset of the singularity. This similarity does not extend to the case where $f_f = 0.5$ (Figures 6,7), where the approach to the singularity is somewhat slower (Figures 8,9). The slower approach to singular conditions presumably has to do with the smaller gradient of $U_e$ with respect to x, when $f_f = 0.5$, but direct comparison of the results for this case with those for $f_f = 0$ is difficult

because the singularity forms further aft when $f_f = 0.5$: at around $x = 0.6c$, rather than $x = 0.25c$ with $f_f = 0$.

In Reference [7] a semi-empirical model was proposed for predicting the onset of the singularity. The procedure was to compare the velocity of penetration of the reversal point, upstream into the oncoming boundary layer, with an average "convection" velocity in the reversed-flow region. For want of a better definition, this convection velocity was taken to be one-half of the maximum negative velocity in the region at the particular time level. The prediction criterion proved useful in correlating the results of Reference [7], and it was therefore of interest to see whether it would be valid here. To this end, estimates were made of the penetration velocity, for the three frozen flows considered here, by plotting the movement of the point of flow reversal (Figure 10), and differentiating the curves graphically. The values obtained in this manner are shown in Figure 11, and compared with data for the convection velocity, as defined above.

The points of intersection of the curves corresponding to the pairs of velocities yields the predicted times at which the singularity is supposed to form. These predictions are compared with the approximate observed values (indicated by $\delta^* = 0.1c$) in the following table:

| Case: | | Predicted onset | Observed onset |
|---|---|---|---|
| $U_o t_f/c$ | $f_f$ | $U_o t/c$ | $U_o t/c$ |
| 0.2 | 0 | 1.2 | 2.0 |
| 2.0 | 0 | 2.2 | 3.0 |
| 2.0 | 0.5 | 3.9 | 4.8. |

It will be seen that there is a constant discrepancy in $U_o t/c$, of about 0.8, between the predictions and the observations, and the criterion has no more than qualitative validity for these results. The reason why it does not apply here is not clear, although some suggestions can be made. It might be suggested that the assumed ratio of convection velocity to maximum negative velocity needs to be reduced. However the discrepancies are too large to be resolved in such a manner: the ratio would have to be reduced virtually to zero to make the predictions and observations agree. Indeed, for the present frozen flows, the singularity does not seem to form until the forward movement of the reversal point has ceased: i.e. until the penetration velocity has fallen to zero. In the flows discussed in Reference [7], the singularity was observed to develop while the reversal point was still moving forward. Another suggestion, anticipating some of the later discussion in this report, is that the real singularity, in the sense of steepening of the gradients, does form at the predicted times, and that the discrepancies simply measure the failure of the surrogate criterion to pinpoint its formation. Since the surrogate criterion was used in the derivation of the heuristic model, in Reference [7], the implication must be that the rates of increase of $\delta^*$ with time were so much greater than they are here that any differences in timing between true singularity onset and the condition: $\delta^* = 0.1c$, were masked. It is true that the rates of increase of $\delta^*$ were generally higher, in Reference [7], than they are in the present flows, and so the suggestion has some merit. On the other hand the discrepancies, between the predicted and the observed singularity onset are rather larger than can be explained entirely in this way, and for the moment the conclusion

must remain that the heuristic model, proposed in Reference [7], is not sufficiently general to make quantitative predictions outside the class of flows for which it was originally developed.

Oscillatory Flows

(a) Two sets of calculations were performed for oscillatory flows; the first set was concerned with the effects of variation of frequency, and included the following cases:

| $U_o t_p/c$ | A |
|---|---|
| 2.0 | 0.5 |
| 4.0 | 0.5 |
| 8.0 | 0.5. |

The function f(t), corresponding to each of these cases, is plotted in Figure 12. The pressure gradient over the plate: $\partial p/\partial x$, is given by

$$\frac{1}{\rho}\frac{\partial p}{\partial x} = -\frac{\partial U_e}{\partial t} - U_e\frac{\partial U_e}{\partial x} \qquad (10)$$

and varies with both x and t. The pressure gradient has a discontinuity at $x = x_o$; however, the value at $x = \bar{x}_o$ is representative of conditions over the forward portion of the plate: $0 \leq x \leq x_o$, and can be expressed as a function of f and its derivative f' (= df/dt) by:

$$\frac{c}{\rho U_o^2}\frac{\partial p}{\partial x} = \frac{c}{x_o} f(1 - f) - \frac{c}{U_o} f' \; . \qquad (11)$$

Now, since from Equations (7.8), $f' = -2/t_p$, over the first half of the cycle, and $-2/t_p$, over the second half, $\partial p/\partial x$ at $x = \bar{x}_o$ can be determined as a function of time, and is shown in Figure 13 for the three cases defined above.

The distributions of wall shear stress and displacement thickness, for the three cases, are presented in Figures 14 through 19. The emphasis, here, is on demonstrating the failure of the boundary layer to reach a stable oscillatory condition. By contrast, when reversal does not occur during part of the cycle, stable conditions are reached after a few cycles (see Reference [9]). For $U_o t_p/c = 2.0$ (Figures 14,15), the distributions at stages through the first cycle are compared with those at corresponding stages during the second cycle. It will be seen that the wall shear stress is typically lower, and the displacement thickness typically higher, during the second cycle than the first. The differences are most conspicuous over the range of x corresponding to the reversed-flow region. This trend continues through the third cycle, and is evidently associated with the gradual approach towards eventual separation and the formation of a singularity. Nevertheless, during the latter part of the first cycle and the early part of the second, the reversed-flow region shrinks and vanishes, and forward flow is temporarily reestablished over the whole of the plate. This intermittent behavior which will be discussed more fully later, is repeated for at least two more cycles.

For the intermediate frequency: $U_o t_p/c = 4.0$ (Figures 16,17), reversed flow persists throughout the first cycle and a singularity forms towards the end of the cycle. It will be recalled from Figure 13 that $\partial p/\partial x < 0$ during the second half of the cycle, and so we have the interesting situation here in which reversed flow exists on the plate in spite of a favorable pressure gradient. With $U_o t_p/c = 8.0$, a singularity forms during the first half-cycle and forward flow is never recovered once reversal is established.

The movement of the reversal point, with time, is plotted in Figure 20, for the three cases. In all three cases, reversal first occurs near $x = x_o$ and then moves rapidly upstream with increasing time. At the highest frequency considered ($U_o t_p/c = 2.0$), the reversal point reaches a furthest upstream position at the mid point of the cycle and then moves aft again, with reversed-flow vanishing at a point on the plate somewhat upstream of $x_o$. At the two lower frequencies ($U_o t_p/c = 4.0$ and $8.0$), the reversal point never moves appreciably aft from its furthest-upstream position. The approximate times at which $\delta^*$ first reaches the value $0.1c$ (other than when $U_e \to 0$) are shown on the curves in Figure 20.

In order to observe an intermediate behavior, between that for $U_o t_p/c = 2.0$ in which reversed flow temporarily vanishes during part of the cycle, and that for $U_o t_p/c = 4.0$ when it persists indefinitely, an additional calculation was made for $U_o t_p/c = 2.8$ and the results are shown by the dashed curve in Figure 20. Here, forward flow is reestablished for a short time, at the end of the first cycle, but reversed flow persists during the second cycle with $\delta^*$ reaching the value $0.1c$ about half-way through the second cycle.

Figures 21, 22 show the variation, with time, of the wall shear stress and displacement thickness at two neighboring positions on the plate, for this last case. The displacement thickness reaches $0.1c$ at about $U_o t/c = 4.0$, although steep gradients of wall shear stress occur somewhat earlier. It is of interest to note the pronounced phase shift between the displacement thickness and the external velocity gradients (which are symmetrical about the mid point of the cycle) even during

the first cycle when the flow is still far from developing a singularity. The magnitude of this phase lag is considerably greater than the lags found in Reference [9] for flows which did not suffer reversal during part of the cycle.

The limited data presented here suggest that there is some connection between the persistence of reversal during the cycle, even when the pressure gradient becomes negative, and the appearance of the singularity. This may simply mean that a singularity can only develop when reversed flow is present; but, if so these results are at variance with suggestions which have been made that a singularity can occur upstream of reversal. Alternatively, the incipient formation of a singularity may somehow inhibit the shrinkage and disappearance of the reversed-flow region which would otherwise take place.

(b) The second set of calculations for oscillatory flow was concerned primarily with the effects of variation of amplitude, and included the following cases:

| $U_o t_p/c$ | A |
|---|---|
| 2.0 | 0 |
| 2.0 | 0.1 |
| 2.0 | 0.3 |
| 2.0 | 0.5 |
| 4.0 | 0 |
| 4.0 | 0.1 |
| 4.0 | 0.3 |
| 4.0 | 0.5. |

The two cases with A = 0.5 are the same as two of the oscillatory flows mentioned above, and the case: A = 0, $U_o t_p/c = 4.0$ is the same as the frozen flow, where $U_o t_f/c = 2.0$ and $f_f = 0.5$, which was discussed

earlier. The function f(t) is plotted in Figure 23, for the cases where $U_o t_p/c = 2.0$, and in Figure 32 for the cases where $U_o t_p/c = 4.0$. The corresponding plots of the pressure gradient, at $x = \bar{x}_o$, are shown in Figures 24 and 33, respectively.

The distributions of wall shear stress and displacement thickness, over the plate, for the cases where $U_o t_p/c = 2.0$, are shown in Figures 25, 26 for a time corresponding to $U_o t/c = 4.0$: i.e., at the end of two complete cycles, and in Figures 27, 28 for $U_o t/c = 5.0$, which corresponds to the mid point of the third cycle. In Figures 29, 30 the wall shear stress and displacement thickness at one point on the plate, are plotted versus time, and Figure 31 shows the movement of the reversal point with time.

It will be noted from Figure 29 that, for A = 0 and 0.1, reversal does not occur until some time during the second cycle. However, once it does take place, it persists until a singularity develops in the third cycle (Figure 28). In contrast, for A = 0.3 and 0.5, reversal appears during the first cycle but subsequently vanishes again, later in the cycle, leaving forward flow reestablished over the whole plate. This intermittent formation and subsequent disappearance of reversed flow is repeated for at least two more cycles (Figure 29). The displacement thickness reaches a value of 0.1c at around the mid point of the third cycle, when A = 0.3, but there is no evidence of singular behavior anywhere in the first three cycles when A = 0.5 (the calculation was not continued beyond $U_o t/c = 6$: the end of the third cycle); the large values of $\delta^*$ at $U_o t/c = 5$ (Figure 28) result from the stagnation of the outer

flow and do not indicate the onset of a singularity in the solution. The difference in behavior between the two low-amplitude cases, in which reversal persists throughout the second and subsequent cycles, and the two high-amplitude cases, where reversal is intermittent, correlates with the sign of $\partial p/\partial x$ during the second half of the cycle (Figure 24): positive for A = 0, 0.1 and negative for A = 0.3, 0.5. On the other hand it has already been observed that reversal can persist even when the pressure gradient is favorable, and, clearly, the mechanism which controls the appearance and disappearance of the reversed-flow region is not simply a function of the pressure gradient. Indeed, as already mentioned, it was shown in Reference [1] that time-dependence caused a delay in the first appearance of reversal even when $\partial U/\partial t$ made a positive contribution to the pressure gradient.

Figures 34 through 36 present data for the lower frequency calculations ($U_o t_p/c = 4.0$). Here, it will be seen that forward flow is not recovered for any of the amplitudes considered; once formed, reversal persists until $\delta^*$ reaches 0.1c near the end of the first cycle. Specifically, singularity onset (according to this criterion) occurs earliest for the high-amplitude case: at $U_o t/c = 3.7$, and latest for A = 0: at about $U_o t/c = 4.7$. This order of onset, in terms of the values of A, is opposite to the order observed at the higher frequency. The difference is probably associated with the failure of the reversal point to move aft, during the second half of the cycle, when $U_o t_p/c = 4.0$ (Figure 36). At the lower frequency, the reversal point moves forward, during the first half-cycle, and subsequently remains near its furthest-forward position, leaving an extensive region of reversed flow, for the duration of the motion. It is interesting to note the wide variation in the terminal positions of the reversal point, over the range of amplitudes considered:

from about x = 0.6c, when A = 0, to about 0.34c when A = 0.5 (Figure 36).

It is clear that, at this relatively low frequency, the behavior of the boundary layer is strongly influenced by the adverse pressure gradients present during the first half cycle. The alleviation of these gradients, during the second half cycle, has less effect than it does at higher frequencies, although the effects are still noticeable. This can be seen by comparing the movement of the reversal point for the case: $U_o t_p/c = 4.0$, A = 0.5, in Figure 36, with the dashed curve which corresponds to the frozen flow: $U_o t_f/c = 2.0$, $f_f = 0$; the two flows suffer the same retardation during the interval $0 \leq U_o t/c \leq 2.0$, but different retardations thereafter.

## I.3 THE NATURE OF UNSTEADY SEPARATION

Some important conclusions concerning the nature of unsteady separation of the turbulent boundary layer are suggested by the results of the computational experiments presented above.

First: the relaxation of a turbulent boundary layer, which has been subjected to an initial retardation strong enough to cause reversal, towards a steady state separation, is achieved in a finite time. It was suggested, in Reference [1], that the relaxation time is of the same order as the time taken for the fluid to be convected off the part of the surface ahead of the ultimate point of separation. The present results support this hypothesis: the calculations for the frozen flow in which $U_o t_f/c = 0.2$, $f_f = 0$, indicate incipient separation at $x = 0.27c$ in a time $U_o t/c = 2.0$, implying that all of the fluid with an average velocity exceeding $0.15U_o$ had been replaced by new fluid entering the boundary layer after time $t_f$. In the case, just mentioned, the initial retardation was abrupt; in cases where the retardation is more gradual the time necessary to reach incipient separation is longer. However, the final divergence towards singular conditions, as separation is approaches, is rapid, with the displacement thickness increasing roughly exponentially with time.

Second: the approach to the separation singularity, in oscillatory flows, appears to be a function of both the long-time-average, and the instantaneous, pressure gradients. At low frequencies, the effects of the adverse instantaneous pressure gradients seem to dominate, and separation

can occur during the first half-cycle if the gradients are sufficiently severe. At higher frequencies, the approach to separation appears to depend more on the time-average pressure gradients, while the nature of the instantaneous gradients may be such as to have a delaying effect on separation onset. In one of the cases examined ($U_o t_p/c = 2.0$, $A = 0.5$), three complete cycles were completed without evidence of imminent separation even though the average gradients were large enough to provoke separation after two cycles (as can be seen from the results for $U_o t_p/c = 2.0$, $A = 0$).

The delay of separation onset, observed in the oscillatory cases, where the amplitude in large, is evidently associated with the alleviation of the pressure gradients during the parts of the cycle when the external velocities are increasing with time: instantaneously favorable gradients can exist, at sufficiently high amplitudes and frequencies, which offset the time-average adverse gradients. On the other hand, the existence of favorable instantaneous pressure gradients is not enough to guarantee the avoidance of separation -- or even to guarantee the reestablishment of forward flow in place of a reversed-flow region.

In some cases the reversed-flow region did vanish during the phases of the motion when the pressure gradients were favorable. In others, not only did the reversed-flow region persist during such phases, but the extent of the region actually increased. This type of behavior seemed to occur when the flow in the boundary layer was already retarded to a degree where separation could be expected to occur shortly: the change to favorable pressure gradients was then "too late" to save the boundary

layer from separating. Figures 37 through 40 contrast, in more detail, the cases where recovery was achieved, with those where it was not achieved. Figures 37,38 show a typical recovery from reversed flow to forward flow, as the pressure gradient changes sign from positive to negative. These results, which are for the oscillatory flow: $U_o t_p/c$ = 2.0, A = 0.5, show the velocity profiles before and after the recovery. The boundary-layer thickness increases as a result of the recovery, although the displacement thickness decreases (Figure 15). Figures 39, 40 show a case which fails to recover ($U_o t_p/c$ = 4.0, A = 0.5) despite a similar change in the pressure gradient; instead, the reversal point moves further upstream, accompanied by an abrupt increase in the boundary-layer thickness over the reversed-flow region. This latter effect is reminiscent of the flow patterns, reported in Reference [7], depicting the approach to singular conditions, although the onset of a singularity (according to the surrogate criterion: $\delta^*$ = 0.1c) has not yet been reached in the solution plotted in Figure 40. A more detailed examination of the results indicates, however, that the solution in Figure 40 already contains a singularity. Figure 41 shows a plot of the velocity at y = 0.1, versus x, for the two sets of results, before and after the change in pressure gradient. In the case where recovery is achieved, the progression from reversed to forward flow is accompanied by a smooth, continuous variation of velocity with x. In contrast, in the case where recovery did not take place, a discontinuity in velocity occurs, and the part of the solution where U > 0 loses contact with the part where U < 0. The large values of $\partial U/\partial x$, across the discontinuity, give rise to large values of $\partial V/\partial y$, and correspondingly large values of V, which are

reflected in the growth of the boundary-layer thickness seen in Figure 40, but they have not yet been translated into values of $\delta^*$ exceeding 0.1c. Nor does the solution imply an excessively large normal pressure gradient, at this stage. Two conclusions therefore seem to emerge: (1) that the failure of a boundary layer to recover forward flow upon a change in the pressure gradient is indicative of an incipient singularity, and (2) that the onset of a singularity may not always result in an immediate gross thickening of the boundary layer. This second conclusion needs to be examined more carefully in future work because singularity onset has normally been identified with imminent separation. The present computational framework would not be particularly appropriate for such an examination because of the coarseness of the mesh in the x - y plane, and because there may be some suppression of large temporal gradients (even though short time steps were used). Some analytical studies would appear to offer more prospect of success.

Meanwhile, the possibility exists that a sequence of events takes place, prior to the final separation of the flow, in which the extent of flow reversal increases, and thickening of the boundary layer occurs, regardless of any alleviation of the separation-provoking pressure gradients. In none of the cases discussed here was a retreat from imminent separation observed, although it may be demonstrated by further work that the imposition of sufficiently strong favorable gradients would bring this about. It is interesting to draw a parallel, here, with the hysteresis effect observed in dynamic stall: the recovery of the flow on the airfoil is not achieved until the incidence is reduced substantially below the level reached before stall occurred [10]. The flow around a pitching airfoil

is clearly more complicated than the flows discussed in this report; in particular, the vortex shed from the leading edge of the airfoil plays an important role in the hysteresis process. Nevertheless, a general rule may be emerging that, once the separation mechanism is initiated, it is necessary to take drastic steps, in terms of a change of external-velocity conditions, to restore the boundary layer to an attached condition. Some further calculations, on the present lines could usefully be done to pursue this particular objective.

## PART II. LAMINAR FLOW CALCULATIONS

### II.1 NATURE OF THE FLOWS CONSIDERED

The laminar-flow studies were carried out for incompressible, two-dimensional, time-dependent flow over a flat surface. The viscous portion of the flow was taken to be boundary-layer-like, insofar as the longitudinal extent of the flow was assumed to be large compared with its transverse extent, and the potential-flow velocity was prescribed along the upper edge of the integration domain, which ran parallel to the wall. On the other hand, no assumption was made about the smallness of second derivatives in the longitudinal direction (except at the downstream end of the domain), and no restriction was placed upon the variation of static pressure normal to the wall: the solution in the interior of the domain corresponds to the full unsteady Navier-Stokes equations. Details of the equations, and the numerical scheme used to solve them, are given in Appendix B.

It was assumed that the upstream edge of the plate, upon which the flow was developing, was a sharp leading edge. At the downstream end of the plate, it was assumed that (regardless of its earlier condition, further upstream) the flow had recovered to a form which was consistent with the first-order boundary-layer approximations; this assumption was made in order to avoid the need for specifying the downstream velocity and vorticity profiles. The region of interest was the portion of the flow over the central part of the plate, where reversal was induced by suitable choice of the external velocity distributions. These distributions were similar to those defined by Equations (1,2,3), above, and the same values of $x_o/c$ and $x_1/c$

were used. The Reynolds number: $U_o c/\nu$, was taken to be $10^4$.

Results are presented here for a single case, viz. a "frozen flow," of the type considered in Part I, above with $U_o t_f/c = 2.0$, and $f_f = 0.5$. These results are of interest both in themselves and insofar as they may be compared and contrasted with the results of the corresponding turbulent calculation which has already been described.

The initial conditions, at t = 0, correspond to steady, constant-pressure flow, and were generated by means of a time-relaxation calculation; an approximate solution was assumed, and then the calculation was advanced in time until the steady-state solution was obtained; At the high Reynolds number, for which the calculation was performed, it would be expected that the exact solution of the Navier-Stokes equations would be close to the Blasius solution of the laminar boundary-layer equations, the only significant difference in boundary conditions lying in the confined domain in which the present flow was assumed to be developing; the height of the domain was taken to be 0.1c at t = 0. The velocity profiles produced by the time relaxation process are compared with the Blasius profiles in Figure 42. Calculations were done for three different mesh densities:

(a) $\Delta x = 0.1c$, $\Delta y = 0.01c$ (11 x 11 node points)

(b) $\Delta x = 0.05c$, $\Delta y = 0.005c$ (21 x 21 node points)

(c) $\Delta x = 0.025c$, $\Delta y = 0.0025c$ (41 x 41 node points)

It will be seen from Figure 42 that the agreement with the Blasius solution is good for the finest mesh, tolerable for the medium-density mesh, and poor for the coarse mesh, particularly over the upstream half of the plate. There are two main reasons for the poor agreement, in this last

case: first, the number of node points through the boundary layer is too small to give proper resolution of the higher derivatives in the y-direction, and second, the wide mesh spacing in the x-direction leads to inadequate resolution of the longitudinal derivatives associated with the flow near the leading-edge.

Some comments need to be made here concerning the artificial viscosity, introduced by the finite mesh size, and its effect on the quality of the solution. The appropriate measures of artificial viscosity are the two cell Reynolds numbers: $U\Delta x/\nu$ and $V\Delta y/\nu$, which multiply second derivatives in the x- and y-directions, respectively. If these cell Reynolds numbers are everywhere small compared to 2, the solution can be regarded as valid; otherwise the effective Reynolds number of the solution is reduced, at least in the regions of the flow where those conditions are not satisfied. Now, in the present flow, at $t = 0$, the transverse cell Reynolds number: $V\Delta y/\nu$ is at most about unity, even for the coarse mesh, and so its effects on the derivatives: $\partial^2/\partial y^2$, cannot be considered serious. The longitudinal cell Reynolds number: $U\Delta x/\nu$, is much higher than 2, even for the finest mesh, and can scarcely be reduced to 2 without placing an enormous number of node points in the x-direction. However, it affects only the second derivatives in x which, fortuitously are small for the constant-pressure flow; these derivatives are neglected altogether in the Blasius solution. Consequently, the solution for $t = 0$ appears to be relatively free of the effects of artificial-viscosity. The same cannot be said of the subsequent solutions for $t > 0$, however. There, $V\Delta y/\nu$ would begin to exceed 2, even for the finest mesh, and, also, second derivatives in x start to become significant. Thus artificial-viscosity becomes a more serious problem as time increases, and this fact

needs to be borne in mind during the discussion of the results throughout this section.

On the basis of the comparisons shown in Figure 42, and for reasons of computational economy, it was decided to use the medium-density mesh for the time-dependent calculations for $t > 0$. In order to allow for the growth of the viscous region, the height of the domain was allowed to increase with time: from 0.1c, at $t = 0$, to 0.2c, at $t = 5c/U_o$, after which the height was held constant. This scheme proved to be satisfactory, in the light of the solutions obtained, but it must be remembered that the solutions are not independent of the extent of the domain because the Navier-Stokes equations permit pressure gradients to develop normal to the wall. The specified rate of increase of height must, therefore, be included among the significant boundary conditions imposed on the flow.

The prescribed variation of U, along the upper edge of the domain -- according to the definition of the frozen flow considered -- represents a second boundary condition, and the variation of V represents a third. It emerged that the proper variation of V, along the upper edge, had to be chosen with some care. If V is taken to be zero, there, continuity demands that the retardation of U, at the boundary, has to be offset by an acceleration within the domain. Consequently, the flow near the wall feels less retardation than the flow at the upper boundary, and the alleviation of the longitudinal pressure gradients, due to the effects of the normal ones, increases with the height of the domain. A retardation imposed at a large distance from the wall has little or no effect on the

viscous flow, and may not be large enough to produce reversal. In an attempt to reduce the extent of the accelerations within the domain, V was given a positive value, on the upper boundary, for $0 \leq x < x_o$, and a negative value for $x_o < x < c$. Specifically, V was put equal to $s\partial U/\partial x$, where s is the height of the domain, which extracted enough mass to offset the decrease in U at the boundary. It was not large enough to prevent accelerations entirely, within the domain, but experimentation showed that such large values of V were needed to achieve this that the cell Reynolds-number problem was seriously aggravated. It suffices to say that the performance of the present laminar calculations was not as straightforward as it might seem, at first sight. Three seemingly separate problems: the choice of the height of the domain, the choice of the V-distribution along the upper boundary, and the artificial-viscosity problem, are actually closely related (computer time is a fourth related problem), and a suitable compromise had to be found that attempted to satisfy all of them.

## 11.2 COMPUTATIONAL EXPERIMENTS

The calculations for the frozen flow (in which $U_o t_f/c = 2.0$) were continued up to a time level: $U_o t/c = 8.0$. Typical velocity profiles through the viscous-flow region are shown in Figures 43 through 45, and the longitudinal distributions of wall shear stress and displacement thickness are plotted in Figures 46,47. Several of the velocity profiles exhibit an overshoot which reflects the acceleration within the domain, mentioned above, which tends to alleviate the applied retardation. Nevertheless, in spite of this degree of alleviation, reversal occurs at the wall, and the region of reversal extends over most of the plate at the highest time level reached.

Figures 46,47 may be compared with Figures 6,7 which relate to the corresponding turbulent boundary layer. A number of significant differences may be noted between the two sets of results. First, reversal takes place before $t = t_f$, in the laminar flow, whereas it did not occur until some time later in the turbulent flow. Second, the extent of reversed flow is substantially larger in the laminar case. Third, the variation of wall shear stress is characteristically different in the two cases: it is not only more gradual, in the laminar flow, but it exhibits a double minimum at the higher time levels: a double minimum did not occur in the present turbulent flows, and indeed has never been observed in any of the turbulent calculations performed by us so far. Finally, and perhaps most important. The abrupt changes of displacement thickness, associated with singularity onset in the turbulent boundary layer, are completely absent in the laminar flow. Figure 47 indicates that the displacement

thickness is tending towards a stable, steady-state solution; it must be remembered that the Navier-Stokes equations admit solutions corresponding to steady-state separation, whereas the first-order boundary-layer equations do not. The trend towards an asymptotic solution is emphasized in Figures 48,49 which show the variation of the wall shear stress and displacement thickness with time, for one point on the plate. It is interesting to note, from Figure 48, that the wall shear stress in the laminar flow is of substantially larger magnitude than that in the turbulent case. This difference is partly due to the difference in the Reynolds number: laminar, flat-plate skin friction at $R_e = 10^4$ is roughly twice the turbulent, flat-plate skin friction at $R_e = 10^7$. The difference is accentuated, here, because of the larger extent of the reversed-flow region, in the laminar case, and because of the nature of the velocity gradients within the region. The displacement thickness in a laminar flow at $R_e = 10^4$ is about the same as that in a turbulent boundary layer at $R_e = 10^7$, and Figure 49 shows that $\delta^*$ is of comparable magnitude, in the two cases considered here, over the initial time steps. The major difference in behavior for larger times, lies in the abrupt increase of $\delta^*$ with time, in the turbulent flow, compared with the progressive increase towards an asymptote in the laminar flow.

It might have been expected that the laminar calculations would exhibit some development which, although not of the proportions of a singularity, would in some way resemble the steepening gradients characteristic of the singularity observed in the turbulent boundary-layer calculations. However, the velocity profiles in Figures 43 through 45 show no such development: the abrupt changes in the x-direction -- typified by Figure 40,

for example -- seem to be completely absent in the present laminar results. Inclusion of the second derivatives in x appear to have had the effect of inhibiting the formation of any region of unusually large gradients. The only fear is that artificial-viscosity effects may have had too large an inhibiting effect on those derivatives, and that a more accurate solution of the Navier-Stokes equations, for a Reynolds number of order $10^4$, might indeed exhibit features somewhat intermediate between those of the laminar and turbulent results obtained here. Further studies, perhaps in which a large number of node points could be concentrated within a limited region of the flow field, might serve to resolve these fears.

Be that as it may, another area of interest, in the laminar calculations, involves the distribution of vorticity throughout the flow, and its variation with time. Figures 50 through 52 show contours of constant vorticity at three time levels. In the initial phases of the motion, the vorticity contours lie essentially parallel to the wall. Subsequently, with increase of time, the contours become distorted, and a tongue of high-vorticity fluid moves out into the body of the flow, leaving a region of low or negative vorticity between it and the wall. Figure 52 may demonstrate, on a small scale, how vorticity is shed from a boundary layer, near separation, and moves away from the body surface. There is, of course, no separation "point" as such; separation is a progressive phenomenon, associated with steadily thickening regions of viscous flow, and corresponding modification of the outer inviscid flow.

## CONCLUDING REMARKS

The calculations reported herein: on the one hand, using the turbulent boundary-layer equations, and, on the other, using the laminar Navier-Stokes equations, were intended to shed some light on the phenomenon of unsteady boundary-layer separation.

Earlier work had shown that flow reversal, in time-dependent boundary layers, is not a singular event, and is not associated with the breakdown of the boundary-layer approximations. However, it was also demonstrated that a singularity could develop some time later: associated with steepening streamwise gradients, gross thickening of the boundary layer, and the breakdown of those approximations, and that the onset of the singularity could be identified with the physical separation of the flow. The present calculations of unsteady turbulent boundary layers, which included flows relaxing in time and oscillatory flows, confirm the existence of a flow regime in which reversal, but not singular conditions, prevails. However, they also suggest that singularity onset may not always correlate with the immediate gross thickening of the boundary layer characteristic of separation. In some of the cases examined, it appeared that singularity onset was followed by a phase of only progressive boundary-layer thickening; indeed the only unusual gross feature of the solution was a lack of responsiveness to changes of the pressure gradient. In this situation, alleviation of the adverse pressure gradients did not bring about a contraction of the reversed-flow region and the reestablishment of forward flow over the surface; in some cases the extent of the reversed-flow region actually increased. The phenomenon

described was most noticeable in oscillatory flows, when reversal was found to persist throughout the cycle, despite the presence of instantaneously favorable pressure gradients.

It is, of course, of dubious validity to draw conclusions from the behavior of a solution after a singularity has developed, and there is no direct evidence that the relatively slow increase of boundary-layer thickness, accompanied by the insensitivity to changes of the pressure gradient, has any analog in a real flow. On the other hand, there is an interesting parallel that can be drawn with the histeresis effect observed on airfoils undergoing dynamic stall.

The laminar-flow calculations, based on the Navier-Stokes equations, were performed so as to study separation solutions which would not be contaminated by singularity onset and the breakdown of the boundary-layer equations. The solutions obtained certainly had this property, but, surprisingly, they did not exhibit any of the features associated with the early stages of singularity onset: steepening gradients or rapid thickening of the viscous region. The calculations were performed for a flow relaxing towards a steady-state separation, and the development of the solution was almost disappointingly uneventful. The reversed-flow region was found to increase steadily in extent, the displacement thickness increased progressively, approaching an asymptote, and vortical fluid moved away from the wall into the interior of the flow.

The major enigma posed by these results concerns the physical significance of the events leading up to singularity onset in the unsteady boundary-

layer equations. It was to be expected that the singularity itself was simply a feature of the boundary-layer approximations. It was somewhat less expected that the formation of a region of locally steep gradients, and rapid thickening of the layer, might also prove to be no more than a figment of the boundary-layer imagination.

The matter is not yet resolved, however, and further work needs to address a number of specific questions. First, what is the significance of a singularity whose only observable effect is to dissociate the subsequent boundary-layer development from the imposed pressure gradients? Second, to what extent was the uneventful development of the laminar solutions, obtained here, a result of excessive artificial viscosity, and would it genuinely be that uneventful in a high Reynolds-number viscous flow? Perhaps it would be less uneventful in a flow of larger extent than the one considered here. Third, at what point, in the introduction of higher-order terms into the boundary-layer equations, does the transition from a singularity-dominated separation to a nonsingular one occur, and is that transition the same for a laminar flow as it is for a turbulent flow?

## APPENDIX A

## CALCULATION METHOD FOR TIME-DEPENDENT TURBULENT BOUNDARY LAYERS

### 1. Governing Equations

The velocity components in the x -, y -, z - directions are expressed in the form U + u, V + v, W + w, respectively, where U,V,W are defined as ensemble average velocities, with $W \equiv 0$ for a two-dimensional flow, and u,v,w are the residual fluctuating components about those ensemble averages. The governing equations are similar to those used in earlier studies [1,7,9,11], namely, the momentum equation:

$$\frac{DU}{Dt} + \frac{1}{\rho}\frac{\partial p}{\partial x} + \frac{\partial}{\partial y}(\overline{uv}) = 0 \qquad (A1)$$

the continuity equation:

$$\frac{\partial U}{\partial x} + \frac{\partial V}{\partial y} = 0 \ , \qquad (A2)$$

and the empirically-modified turbulent kinetic-energy equation:

$$\frac{D\overline{uv}}{Dt} + 2a_1\left[|uv|\frac{\partial U}{\partial y} + \Phi + \frac{\partial}{\partial y}(a_2\,\overline{uv}) + \frac{\overline{uv}}{L}|uv|^{1/2}\right] = 0 \qquad (A3)$$

In Equations (A1,A3) the convective derivative is defined by

$$\frac{D}{Dt} = \frac{\partial}{\partial t} + U\frac{\partial}{\partial x} + V\frac{\partial}{\partial y} \ . \qquad (A4)$$

In Equation (A3) the empirical convective constant, $a_1$, and the empirical functions of position through the boundary layer, $a_2$ and L, are taken to

be the same as those used in Reference [1]; accordingly, the same cautionary statements apply to their continued use. Experimental substantiation of the appropriateness of Equation (A3) and of the empirical parameters in it - or guidance as to how they should be modified or improved - are still urgently needed and awaited. The quantity $\Phi$ in Equation (A3) is the two-dimensional equivalent of the functions $\Phi_x$, $\Phi_z$ in Reference [12], and is defined by

$$\Phi = \Gamma\{|\overline{uv}|\ \frac{\partial U}{\partial y} + \overline{uv}\ |\frac{\partial U}{\partial y}|\}\ , \qquad (A5)$$

where $\Gamma$ is some large number. The inclusion of this term has no effect on the resultant shear stress, but serves to maintain directionality of the shear-stress vector according to

$$\overline{uv} = a_1\ \overline{q^2}\ \text{sgn}\ (\frac{\partial U}{\partial y})\ , \qquad (A6)$$

where $\overline{q^2}$ is the resultant mean-square velocity fluctuation. Equation (A6) expresses an assumption which is implied in all the two-dimensional applications of Townsend's structural similarity hypothesis (see Ref. [12]), on which the present model is based.

## 2. Solution of the Equations

The solution of the governing equations follows the approach of References [1,7,9]. The flow is divided into an inner and an outer layer, with the matching station between them lying at about $y = 0.05$ . In the outer layer the equations are integrated by an explicit, staggered-mesh finite-difference scheme, advancing in the positive x-direction. The only aspect of the finite-difference scheme, worth mentioning here concerns the method of obtaining x-derivatives. In order to avoid

violation of the relevant zones of dependence, derivatives with respect to x are formed using two-point backward differences in region of positive U, and two-point forward differences in region of reversed flow ($U < 0$). At stations where the local flow direction is ambiguous: i.e. where the sign of U at some node point $(x,y,t)$ is different from that at the adjacent points: $(x - \Delta x,y,t)$ and $(x + \Delta x,y,t)$, the x-derivatives are set equal to zero. This refinement leads to improved smoothness of the solution at points of incipient flow reversal. Little loss of accuracy results because U, which is multiplied by the x-derivative in the momentum equation, is inevitably close to zero at such points. It should be stressed that $\partial U/\partial x$ is not set equal to zero throughout the reversed-flow region, as has been done in certain other analyses of flows with reversal; such a procedure clearly leads to an invalid solution because typical values of $U\partial U/\partial x$ are by no means numerically small compared to the other terms in the momentum equation.

Further details of the numerical scheme, in the outer layer, can be found in References [1,9,12,13,14], and the reader is referred thereto.

In the inner layer, near the surface of the plate, the numerical solution is again matched to an approximate solution based on the Law of the Wall. The details of this inner solution have been modified, as compared with the earlier work, in order to handle the transition from positive to negative values of the wall shear stress. In the present work, the turbulent kinetic-energy equation, for the inner layer, is written

$$\frac{\partial U}{\partial y} = \{\frac{|\overline{uv}|^{1/2}}{\kappa y} + A(x,y,t)\} \text{ sgn } (\overline{uv}) , \qquad (A7)$$

where the dissipation length, L, has been equated, in the usual way, to $\kappa y$. The function A, where

$$A = \frac{1}{2a_1\overline{uv}} \frac{D\overline{uv}}{Dt} + \frac{1}{\overline{uv}} \frac{\partial}{\partial y} (a_2\overline{uv}) \quad , \tag{A8}$$

represents the residual imbalance between production and dissipation of turbulent kinetic energy which, near the wall, corresponds chiefly to convective transport. In the inner layer $A << |\partial U/\partial y|$, and is replaced by its value, $A_m$ at the matching point with the outer-solution domain. With $A_m$ now independent of y, we have, upon formal integration of Equation (A7):

$$U = - \int_o^y \{ \frac{|\overline{uv}|^{1/2}}{\kappa y} + A_m \} \text{ sgn } (\overline{uv}) dy \quad . \tag{A9}$$

The integral is evaluated, following Townsend [15], by prescribing a linear stress relationship

$$- \overline{uv} = \tau_w/\rho + \alpha y \quad , \tag{A10}$$

where $\alpha$ is independent of y, and typically of the same order as $\partial p/\partial x$. It is not difficult to perform the integration analytically; however the resulting forms: one, if $\overline{uv}$ is of the same sign throughout the inner layer, and two, if it changes sign, do not lend themselves readily to programming for the computer. To avoid these problems, Equation (A9) is integrated by a simple iterative numerical scheme. With U and $\overline{uv}$ known at the matching point, an approximate value of $\tau_w$ is estimated from which $\alpha$ is determined; $\overline{uv}$ and U can then be found, as functions of y, for $0 < y < y_m$. The value of $\tau_w$ is adjusted, by means of a simple predictor-corrector method, until the associated values of U merge smoothly into those for the outer domain.

## 3. Integration Domain

The integration domain extended from $x = 0$ to $x = c$, and from $y = 0$ to $y = s(x)$ where $s = 1.25\delta$, approximately. The collocation points in the y-direction, 20 in number, were distributed, as in Reference [13], to give increased density near the wall. The collocation points in the x-direction were also distributed nonuniformly, so as to give increased density in the center portion of the plate. Specifically, the 24 points were distributed according to

$$x_j = 1.5 \frac{j}{n} \{1 - \frac{j}{n} + \frac{2}{3} (\frac{j}{n})^2\}, \qquad (A11)$$

with $n = 24$ and $0 \leq j \leq n$.

## 4. Boundary Conditions

For times $t \leq 0$, the flow corresponds to steady, constant-pressure flow in the x-direction. The boundary layer is in constant-pressure equilibrium, with a thickness, $\delta$, at $x = 0$, of 0.00444 c. The Reynolds number: $U_o c/\nu$, is taken to be $10^7$.

At $x = 0$, the velocity and shear-stress profiles are maintained, for all time, in the same form as at $t = 0$; i.e., in steady constant-pressure equilibrium with an external velocity of $U_o$ and the Reynolds-number conditions specified above.

## APPENDIX B

## SOLUTION METHOD FOR THE TIME-DEPENDENT NAVIER-STOKES EQUATIONS

### 1. Governing Equations

The Navier Stokes equations, for incompressible, time-dependent flow, can be written in vorticity-transport form as

$$\frac{D\zeta}{Dt} = \frac{\partial \zeta}{\partial t} + U \frac{\partial \zeta}{\partial x} + V \frac{\partial \zeta}{\partial y} = \nu \nabla^2 \zeta \ , \tag{B1}$$

in which the single non-zero component of vorticity is $\zeta$, where

$$\zeta = \frac{\partial V}{\partial x} - \frac{\partial U}{\partial y} \ , \tag{B2}$$

and

$$\nabla^2 = \frac{\partial^2}{\partial x^2} + \frac{\partial^2}{\partial y^2} \ . \tag{B3}$$

From Equation (B2), together with the continuity equation:

$$\frac{\partial U}{\partial x} + \frac{\partial V}{\partial y} = 0 \ , \tag{B4}$$

a Poisson equation can be derived for the velocity components, in terms of derivatives of the vorticity:

$$\nabla^2 U = - \frac{\partial \zeta}{\partial y} \tag{B5}$$

$$\nabla^2 V = \frac{\partial \zeta}{\partial x} \ . \tag{B6}$$

Equations (B1,B5,B6) form a parabolic set, and represent the governing equations, in three unknowns: $\zeta$,U,V, which are integrated in a three-

dimensional domain consisting of two space dimensions and time. The method of solution is closely related to that of References [16,17] for solving the parabolicized Navier-Stokes equations in three-dimensional steady flow.

## 2. Solution of the Equations

The governing equations are integrated by means of an implicit, alternating-direction (ADI) scheme, advancing in the positive time direction. A rectangular mesh: $x = m\Delta x$, $y = n\Delta y$, is erected on the plate, permitting discretization of the derivatives at each time level, $\ell$:

$$\frac{\partial F}{\partial x} = \frac{F^{(\ell)}_{m-1,n} - F^{(\ell)}_{m,n}}{\Delta x}, \quad \text{if } U < 0, \tag{B7}$$

$$= \frac{F^{(\ell)}_{m,n} - F^{(\ell)}_{m-1,n}}{\Delta x}, \quad \text{if } U \geq 0; \tag{B8}$$

$$\frac{\partial F}{\partial y} = \frac{F^{(\ell)}_{m,n+1} - F^{(\ell)}_{m,n}}{\Delta y}, \quad \text{if } V < 0, \tag{B9}$$

$$= \frac{F^{(\ell)}_{m,n} - F^{(\ell)}_{m,n-1}}{\Delta y}, \quad \text{if } V \geq 0; \tag{B10}$$

$$\frac{\partial^2 F}{\partial x^2} = \frac{F^{(\ell)}_{m+1,n} - 2F^{(\ell)}_{m,n} + F^{(\ell)}_{m-1,n}}{(\Delta x)^2}, \tag{B11}$$

$$\frac{\partial^2 F}{\partial y^2} = \frac{F^{(\ell)}_{m,n+1} - 2F^{(\ell)}_{m,n} + F^{(\ell)}_{m,n-1}}{(\Delta y)^2}; \tag{B12}$$

$$\frac{\partial F}{\partial t} = \frac{F^{(\ell)}_{m,n} - F^{(\ell-1)}_{m,n}}{\Delta t}, \tag{B13}$$

where F is any variable. Any one of the governing equations can then be

written in difference form as

$$AF^{(\ell)}_{m+1,n} + BF^{(\ell)}_{m,n+1} + CF^{(\ell)}_{m,n} + DF^{(\ell)}_{m-1,n} + EF^{(\ell)}_{m,n-1} = R \qquad (B14)$$

where A through E are coefficients which, in general, depend on the solution, but which are regarded as known at each iteration level reflecting the customary linearization procedure. R, in Equation (B14) involves the solution at time level $\ell$-1, which has already been calculated. The field, m,n, is scanned alternately in the m-, and n-directions, converting Equation (B14) into the successive forms:

$$AF^{(\ell)}_{m+1,n} + CF^{(\ell)}_{m,n} + DF^{(\ell)}_{m-1,n} = R_1 \qquad (B15)$$

$$BF^{(\ell)}_{m,n+1} + CF^{(\ell)}_{m,n} + EF^{(\ell)}_{m,n-1} = R_2 \qquad (B16)$$

where $R_1$ and $R_2$ have absorbed the passive terms on the left-hand side of Equation (B14). Equations (B15,B16) are solved by the extended Choleski method [18], for which efficient solution algorithms are available.

The procedure during any iteration cycle is to solve the vorticity equation to provide updated values of $\zeta$, and then, in a second step, to solve the two Poisson equations to provide updated values of the velocities U,V. The Poisson equations were solved simultaneously, by regarding F and R, in equation (B14) as two-dimensional vectors, and A through E as square matrices.

3. Boundary Conditions

It is assumed that the upper surface of the integration domain (y = s) is outside the viscous region, so that $\zeta$ = 0. The velocity components

are assumed to be prescribed. At the upstream boundary ($x = 0$), the vorticity is assumed to be zero except at the wall where a delta function is imposed, corresponding to the no-slip condition. At the downstream boundary ($x = c$), the vorticity is assumed to be zero outside the boundary layer, while conditions inside the boundary layer are assumed to conform to the first-order boundary-layer approximations: $\partial^2/\partial x^2 = 0$. At the wall: $y = 0$, the boundary conditions are $U = V = 0$; the vorticity at the wall is determined as part of the solution, and is proportional to the wall shear stress.

## REFERENCES


1. J. F. Nash, L. W. Carr and R. E. Singleton, "Unsteady Turbulent Boundary Layers in Two-Dimensional Incompressible Flow," AIAA J. 13, No. 2, February 1975.

2. R. M. Scruggs, J. F. Nash and R. E. Singleton, "Analysis of Flow-Reversal Delay for a Pitching Foil," A.I.A.A. 12th Aerospace Sciences Meeting, Paper No. 74-183, Feb. 1974.

3. Sears, W. R. and Telionis, D. P., "Unsteady Boundary-Layer Separation," Recent Research Boundary Layers (Proc. I.U.T.A.M. Symposium, Quebec 1971), E. A. Eichelbrenner, ed., Presses de L'Université Laval, Quebec 1972.

4. D. P. Telionis and M. J. Werle, "Boundary-Layer Separation from Downstream Moving Boundaries," J. Appl. Mech., p. 369, June 1973.

5. D. P. Telionis and D. Th. Tsahalis, "The Response of Unsteady Boundary-Layer Separation to Impulsive Changes of Outer Flow," AIAA 6th Fluid and Plasma Dynamic Conf., Paper No. 73-684, July 1973.

6. D. P. Telionis, "Calculations of Time-Dependent Boundary Layers," Unsteady Aerodynamics, Vol. 1, Univ. of Arizona (R. B. Kinney, Ed.), 1975.

7. J. F. Nash and V. C. Patel, "Calculations of Unsteady Turbulent Boundary Layers with Flow Reversal," NASA CR-2546, May 1975.

8. V. C. Patel and J. F. Nash, "Unsteady Turbulent Boundary Layers with Flow Reversal," Unsteady Aerodynamics, Vol. 1, Univ. of Arizona (R. B. Kinney, Ed.), 1975.

9. R. E. Singleton and J. F. Nash, "A Method for Calculating Unsteady Turbulent Boundary Layers in Two- and Three-Dimensional Flows," AIAA J. 12, No. 5, May 1974.

10. W. J. McCroskey: "Recent Developments in Dynamic Stall," Unsteady Aerodynamics, Vol. 1, Univ. of Arizona (R. B. Kinney, Ed.), 1975.

11. V. C. Patel and J. F. Nash, "Some Solutions of the Unsteady Turbulent Boundary Layer Equations," Recent Research on Unsteady Boundary Layers (Proc. I.U.T.A.M. Symposium, Quebec 1971), A. E. Eichelbrenner, ed., Presses de l'Université Laval, Quebec 1972.

12. J. F. Nash and V. C. Patel, "Three-Dimensional Turbulent Boundary Layer," SBC Technical Books, 1972.

13. J. F. Nash, "An Explicit Scheme for the Calculation of Three-Dimensional Turbulent Boundary Layers," J. Basic. Eng., 94D, p. 131, March 1972.

14. J. F. Nash and V. C. Patel, "A Generalized Method for the Calculation of Three-Dimensional Turbulent Boundary Layers," Proc. Project SQUID Workshop, Ga. Inst. Tech., (Ed. J. F. Marshall), June 1971.

15. A. A. Townsend, "Equilibrium Layers and Wall Turbulence," J. Fluid Mech., p. 97, 1961

16. R. M. Scruggs and C. J. Dixon, "Vortex/Jet/Wing Viscous Interaction Theory and Analysis," Final Report, O.N.R. Contract N00014-74-C-0151, Feb. 1976.

17. R. M. Scruggs, C. J. Dixon and J. F. Nash, "Vortex/Jet/Wing Interaction Loads by Viscous Numerical Analysis," Proc. A.G.A.R.D. Symposium: Prediction of Aerodynamic Loading, Sept. 1976.

18. R. D. Richtmyer and K. W. Morton, Difference Methods for Initial-Value Problems, Wiley, 1967.

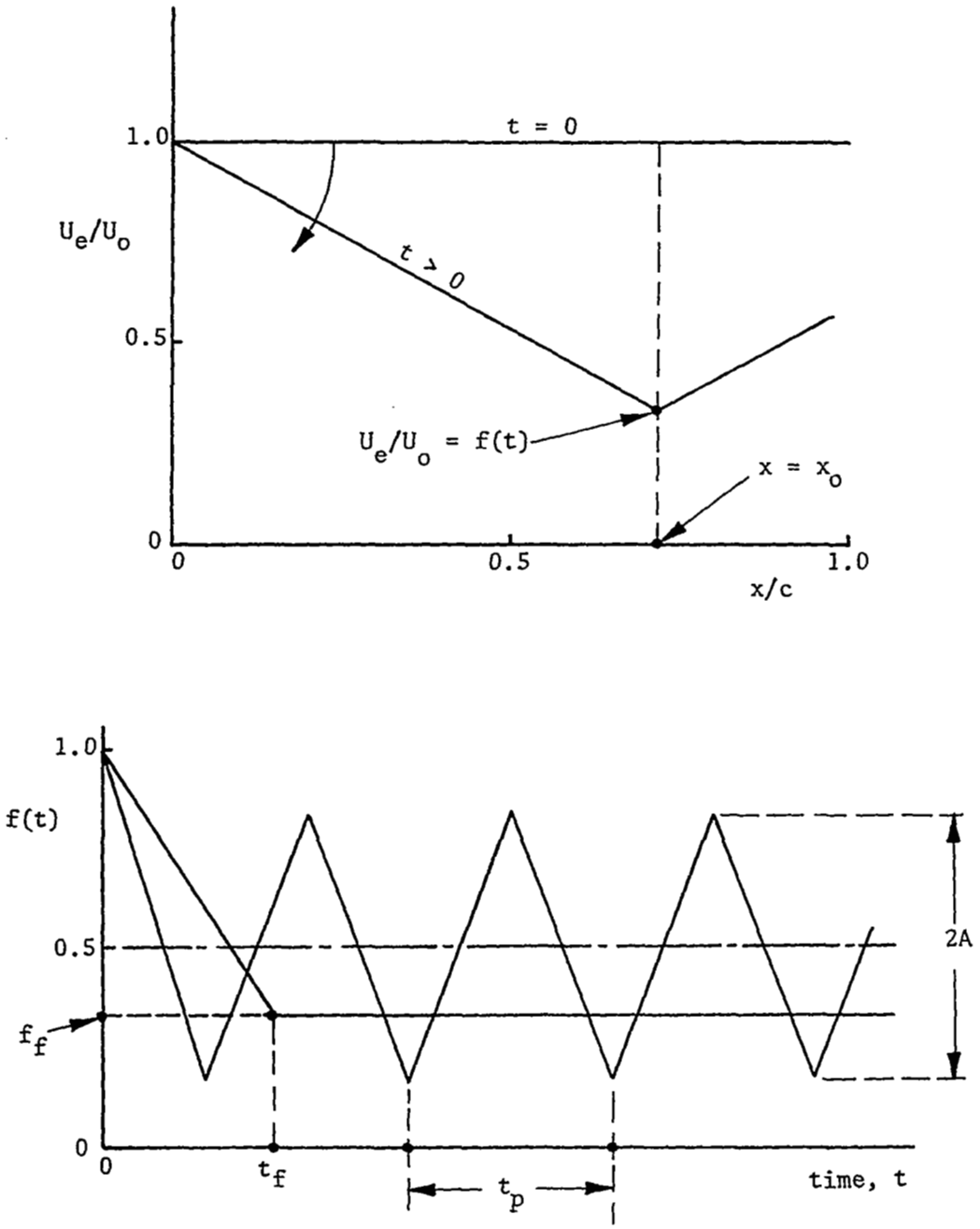


Figure 1 Definition of the External Velocity Distributions.

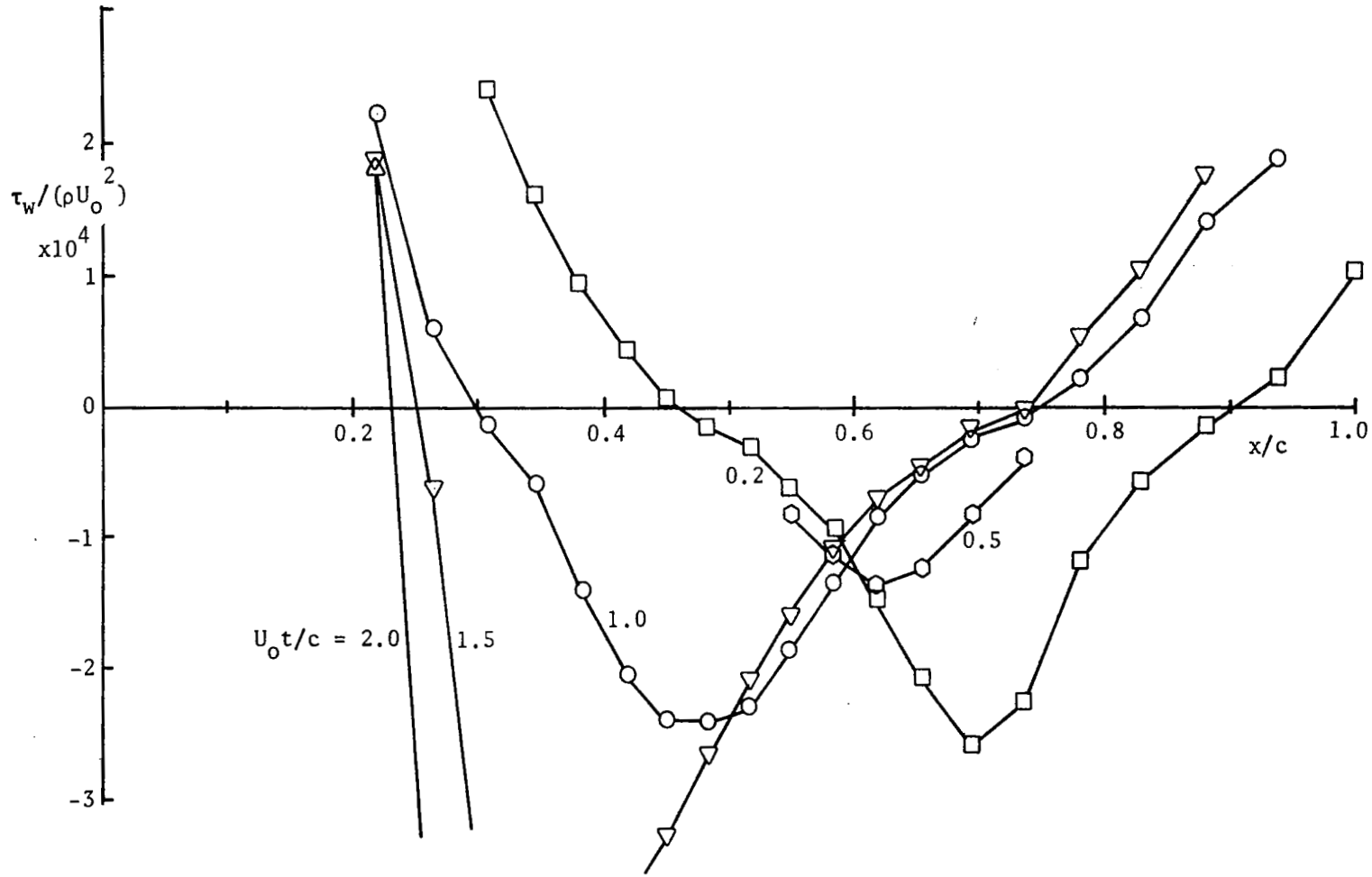


Figure 2 Wall Shear Stress Distributions for Increasing Time; Frozen Flow, $U_o t_f/c = 0.2$, $f_f = 0$.

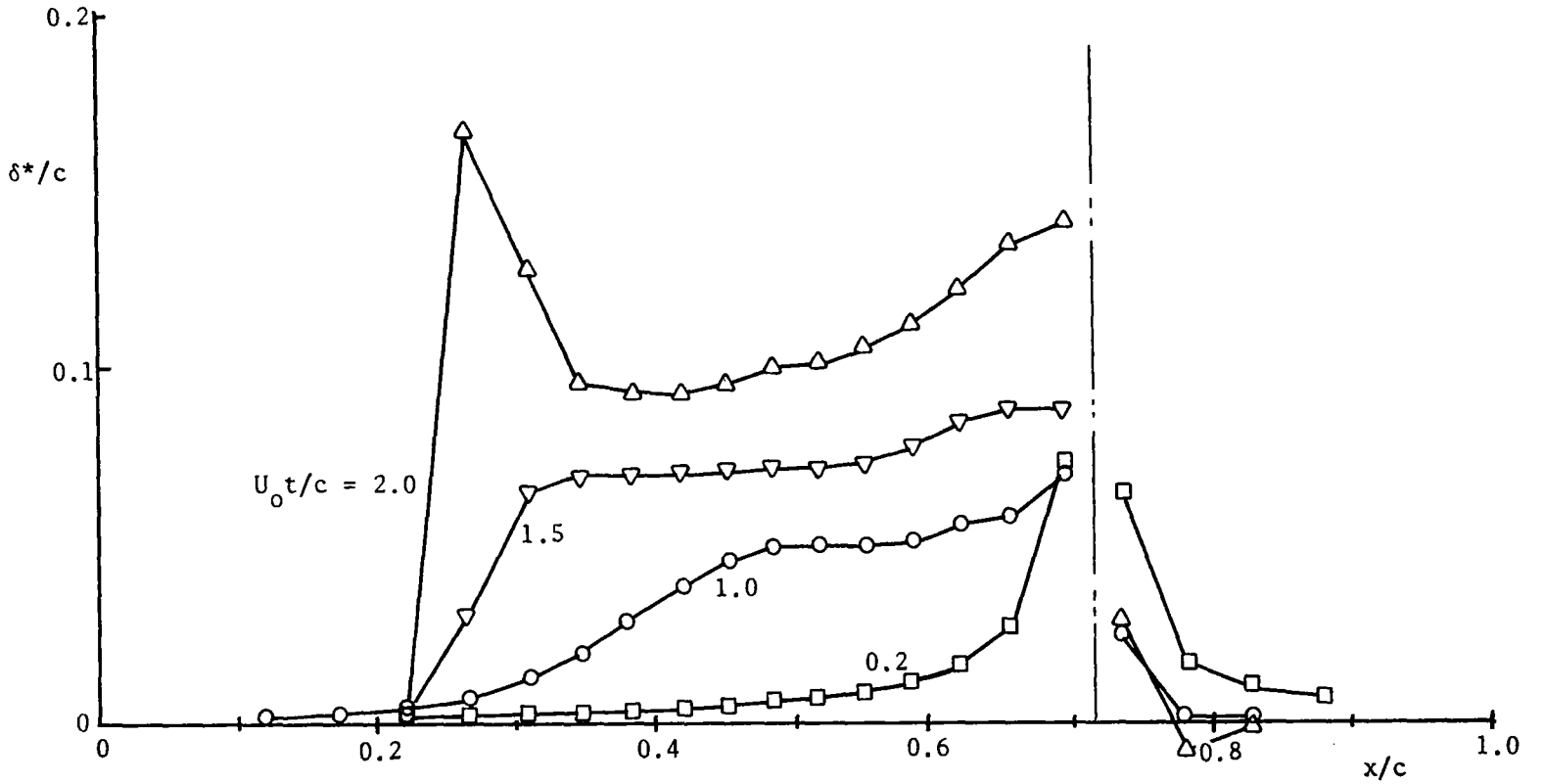


Figure 3 Displacement Thickness Distributions for Increasing Time; Frozen Flow, $U_o t_f/c = 0.2$, $f_f = 0$.

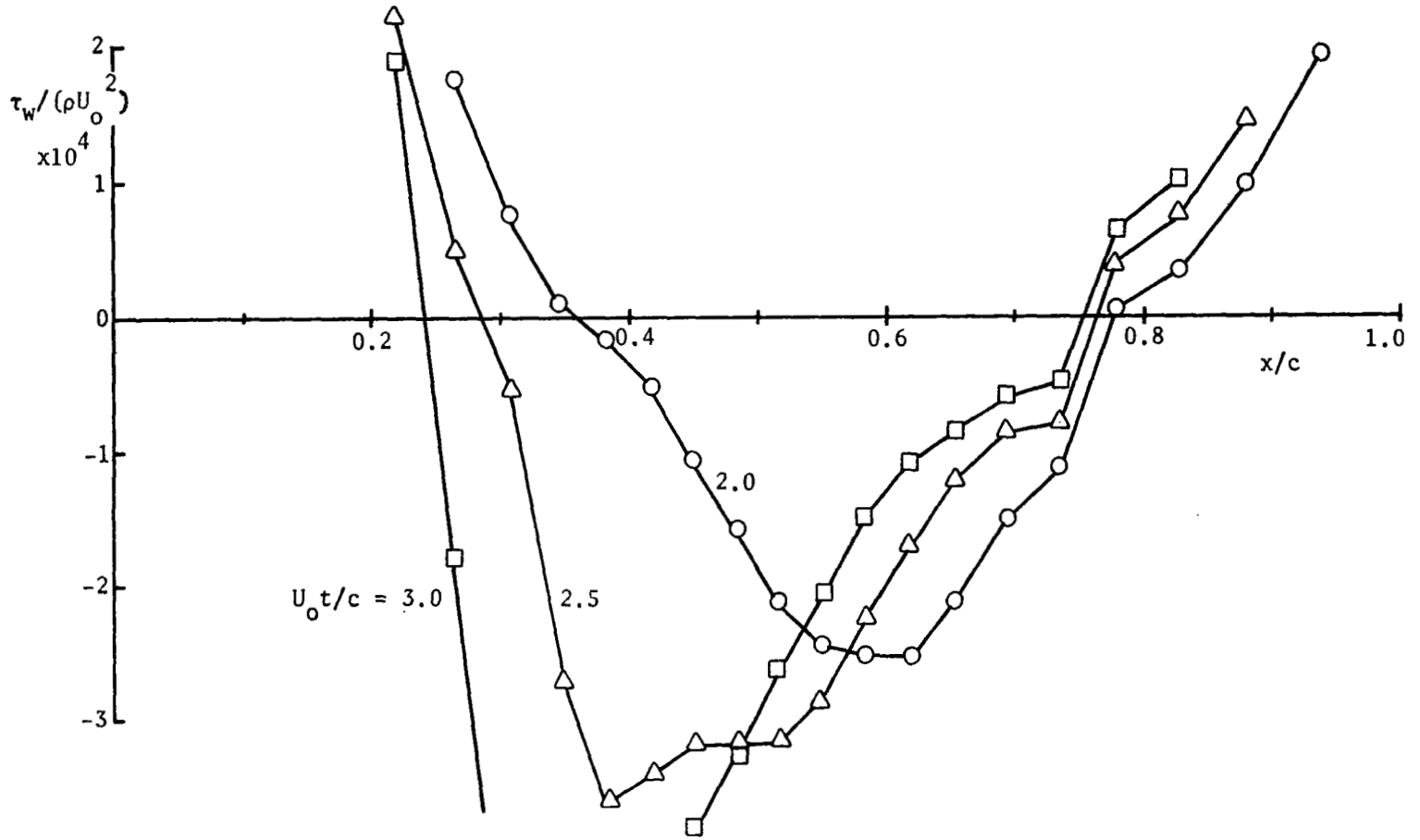


Figure 4 Wall Shear Stress Distributions for Increasing Time; Frozen Flow, $U_o t_f/c = 2.0$, $f_f = 0$.

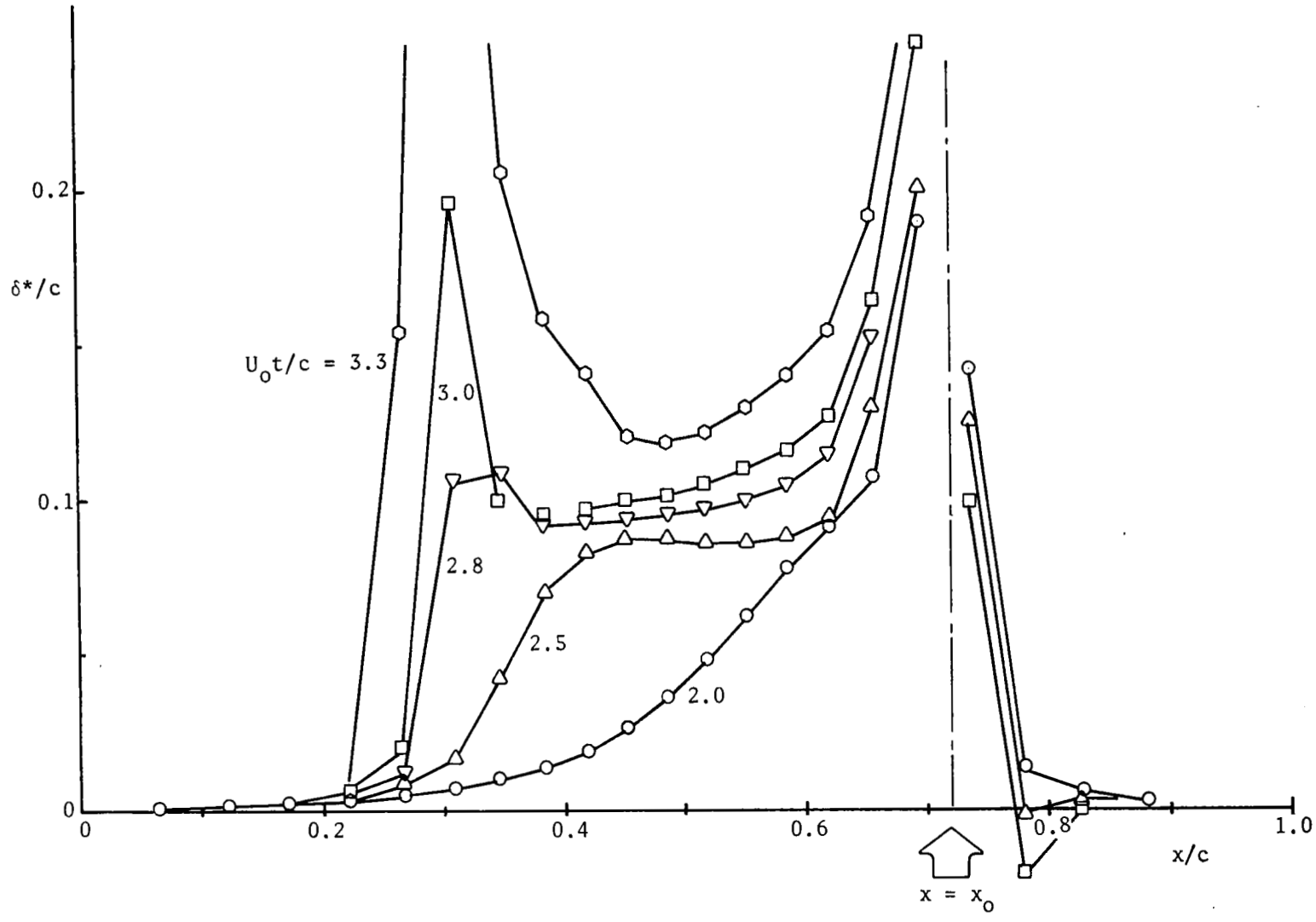


Figure 5 Displacement Thickness Distributions for Increasing Time, Frozen Flow, $U_o t_f/c = 2.0$, $f_f = 0.$

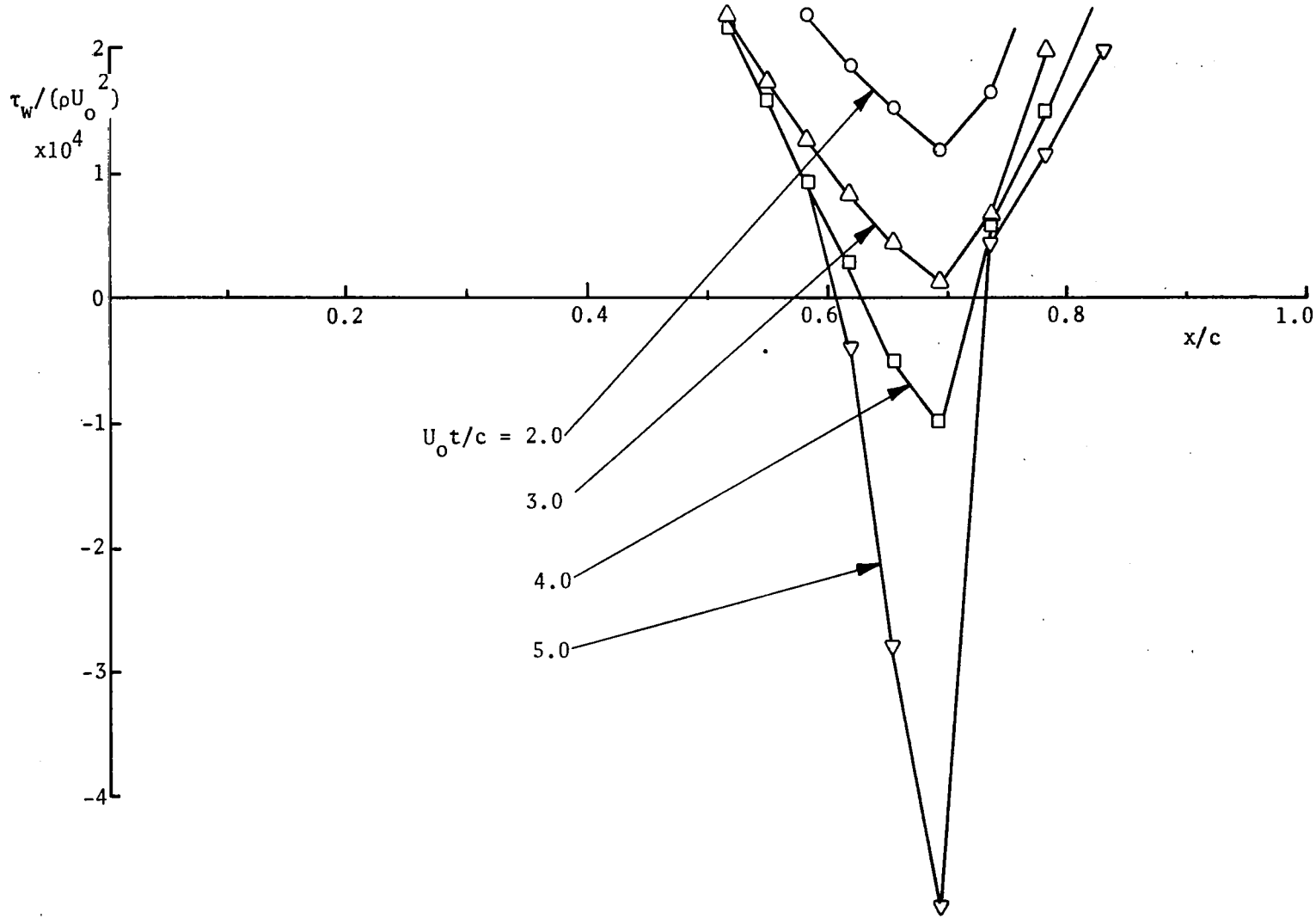


Figure 6 Wall Shear Stress Distributions for Increasing Time; Frozen Flow, $t_f$ = 2.0, $f_f$ = 0.5.

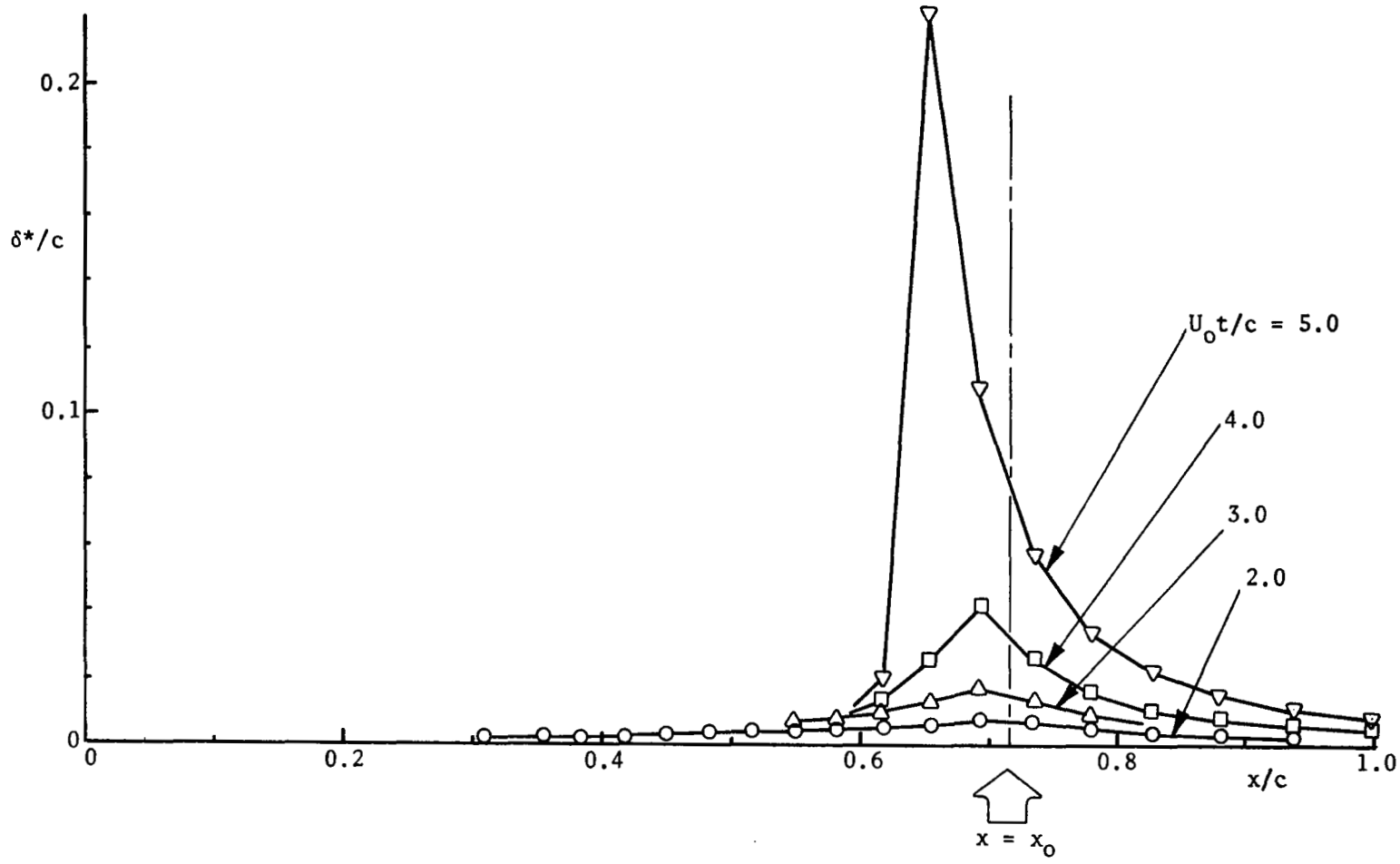


Figure 7 Displacement Thickness Distributions for Increasing Time; Frozen Flow, $t_f = 2.0$, $f_f = 0.5$.

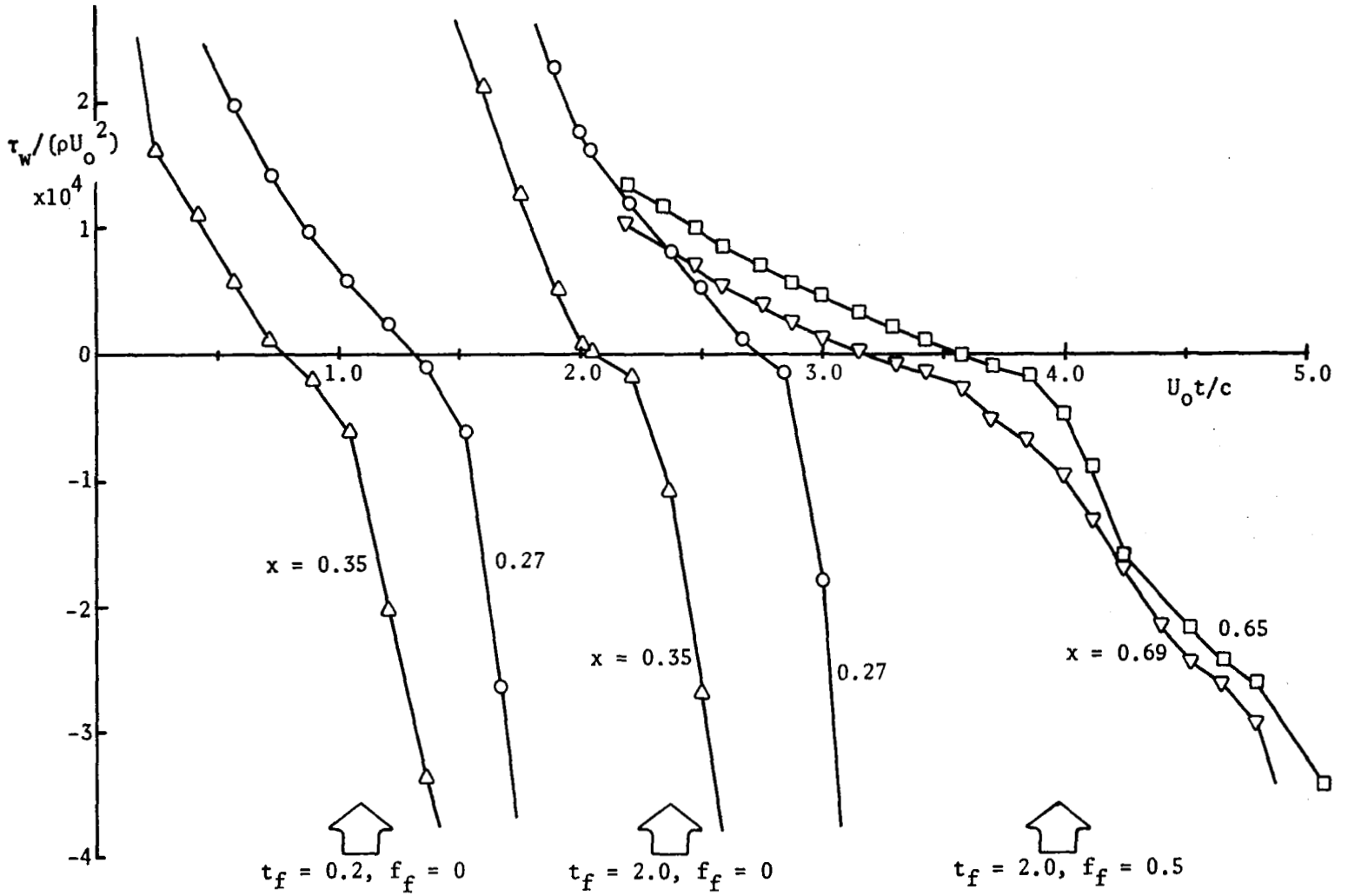


Figure 8 Variation of Wall Shear Stress with Time; Frozen Flow.

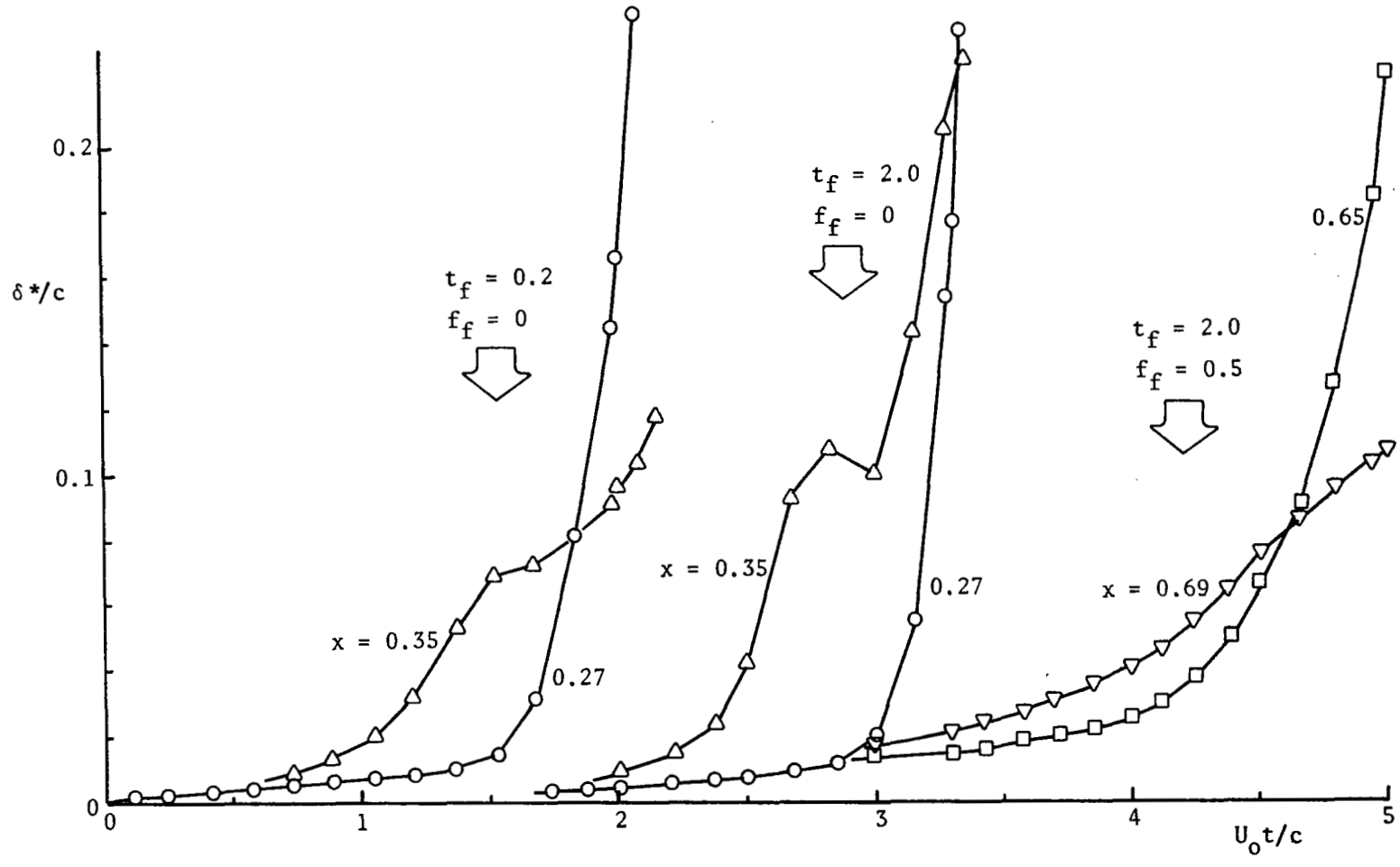


Figure 9 Variation of Displacement Thickness with Time; Frozen Flow.

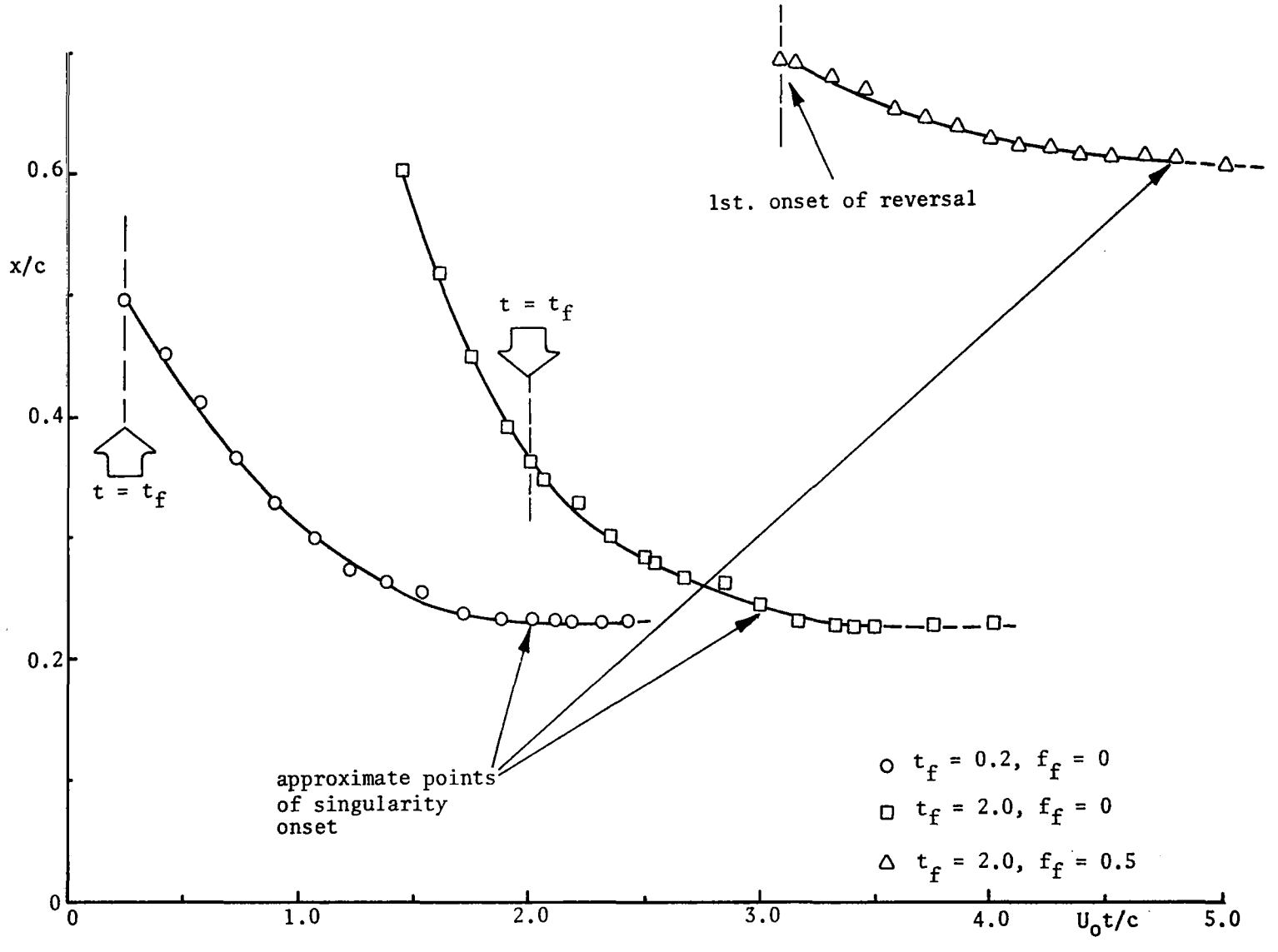


Figure 10 Movement of the Reversal Point with Time; Frozen Flow.

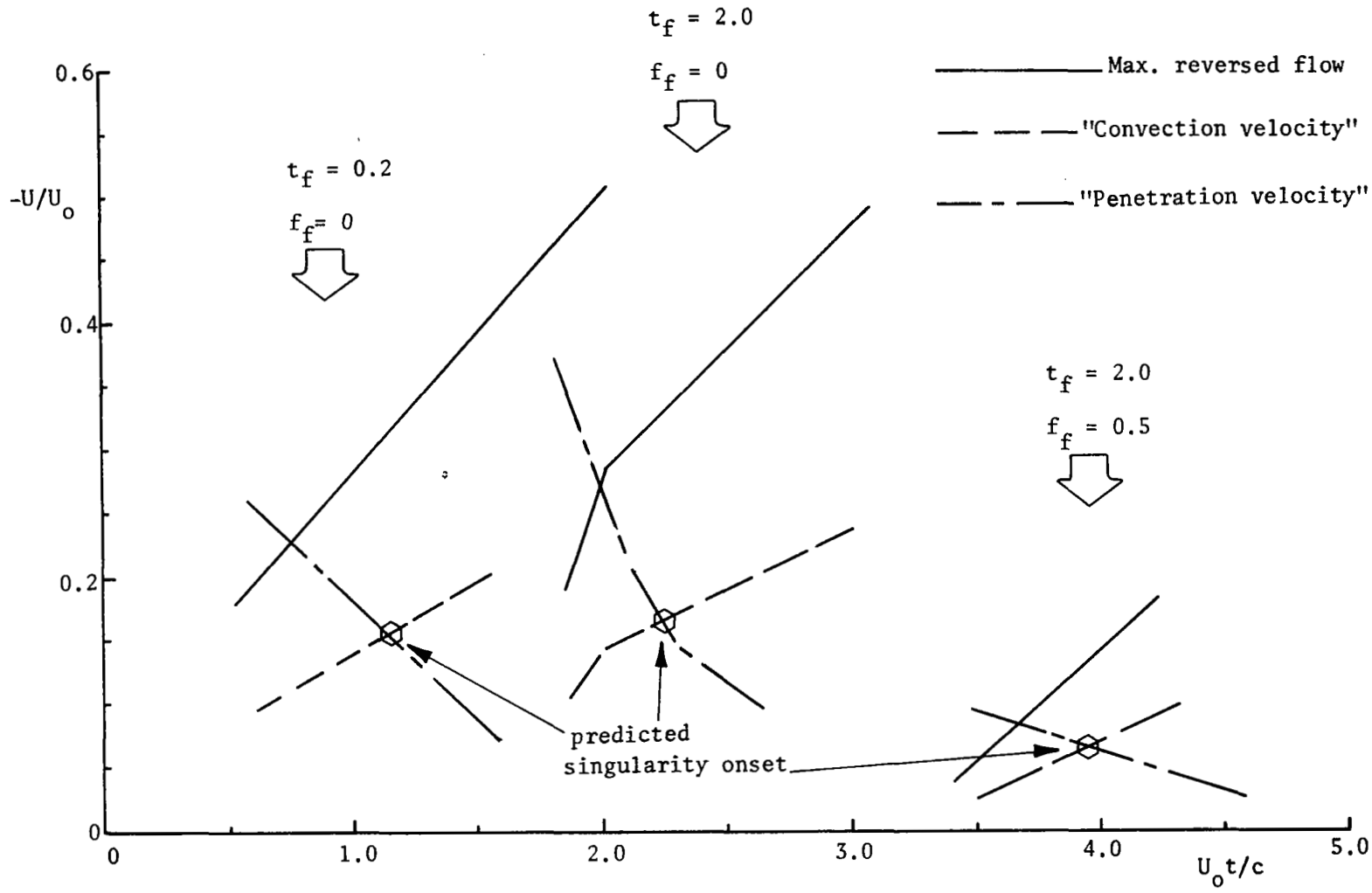


Figure 11 Prediction of Singularity Onset, Using the Criterion of Reference 7/; Frozen Flow.

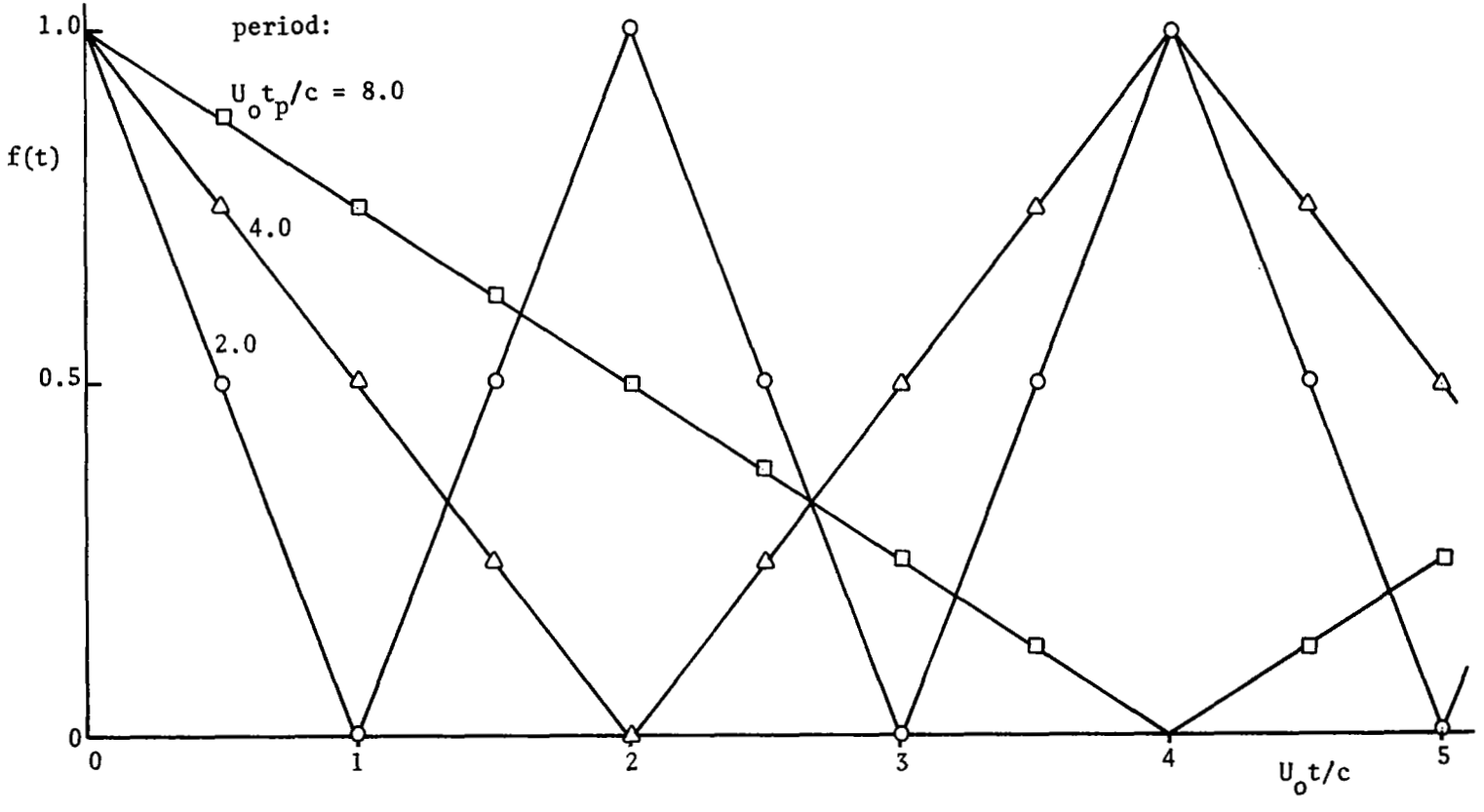


Figure 12 The Function f(t) for Oscillatory Flows of Various Periods; A = 0.5.

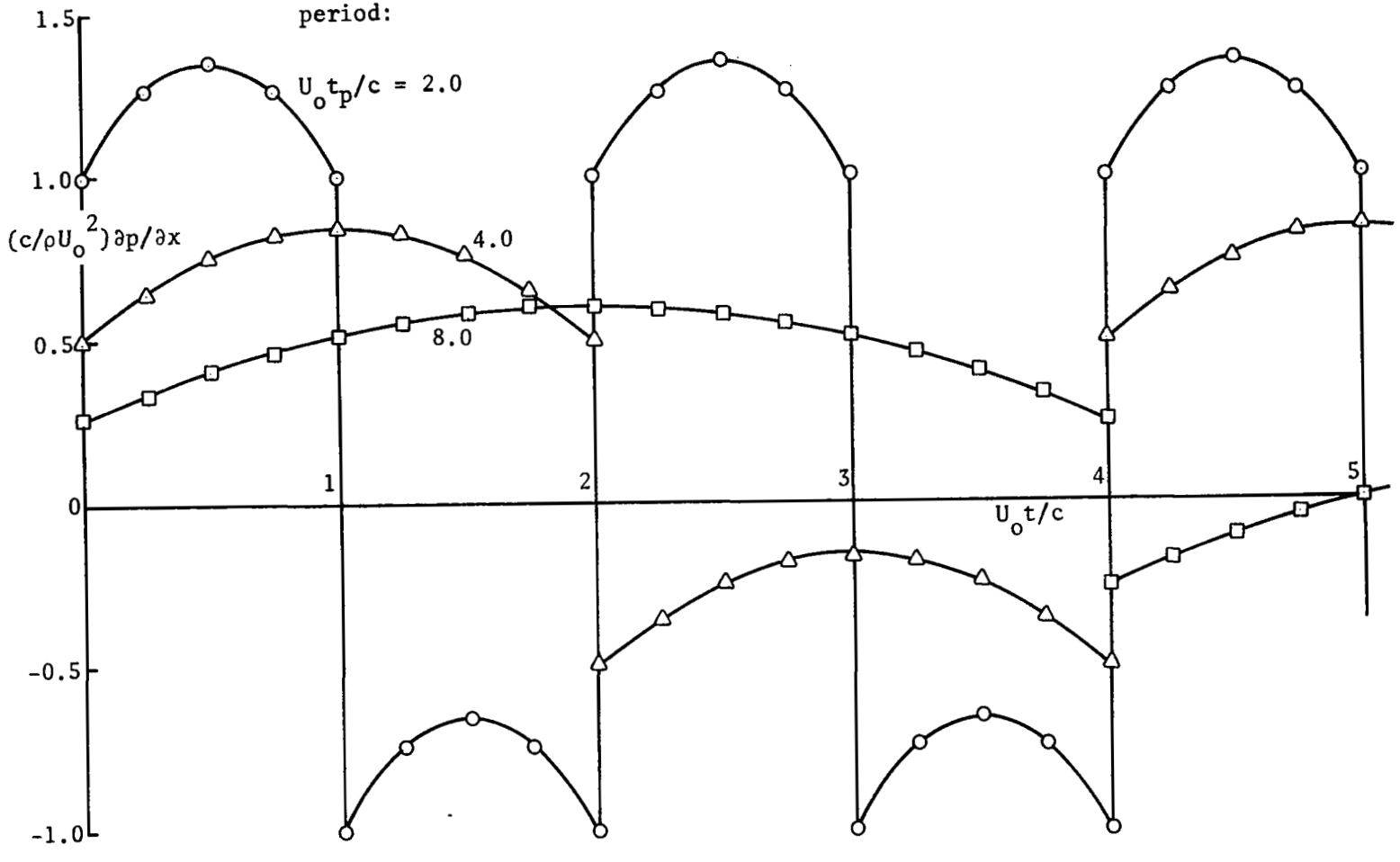


Figure 13 Variation of Pressure Gradient at $x = x_o$ with Time; Oscillatory Flow, A = 0.5.

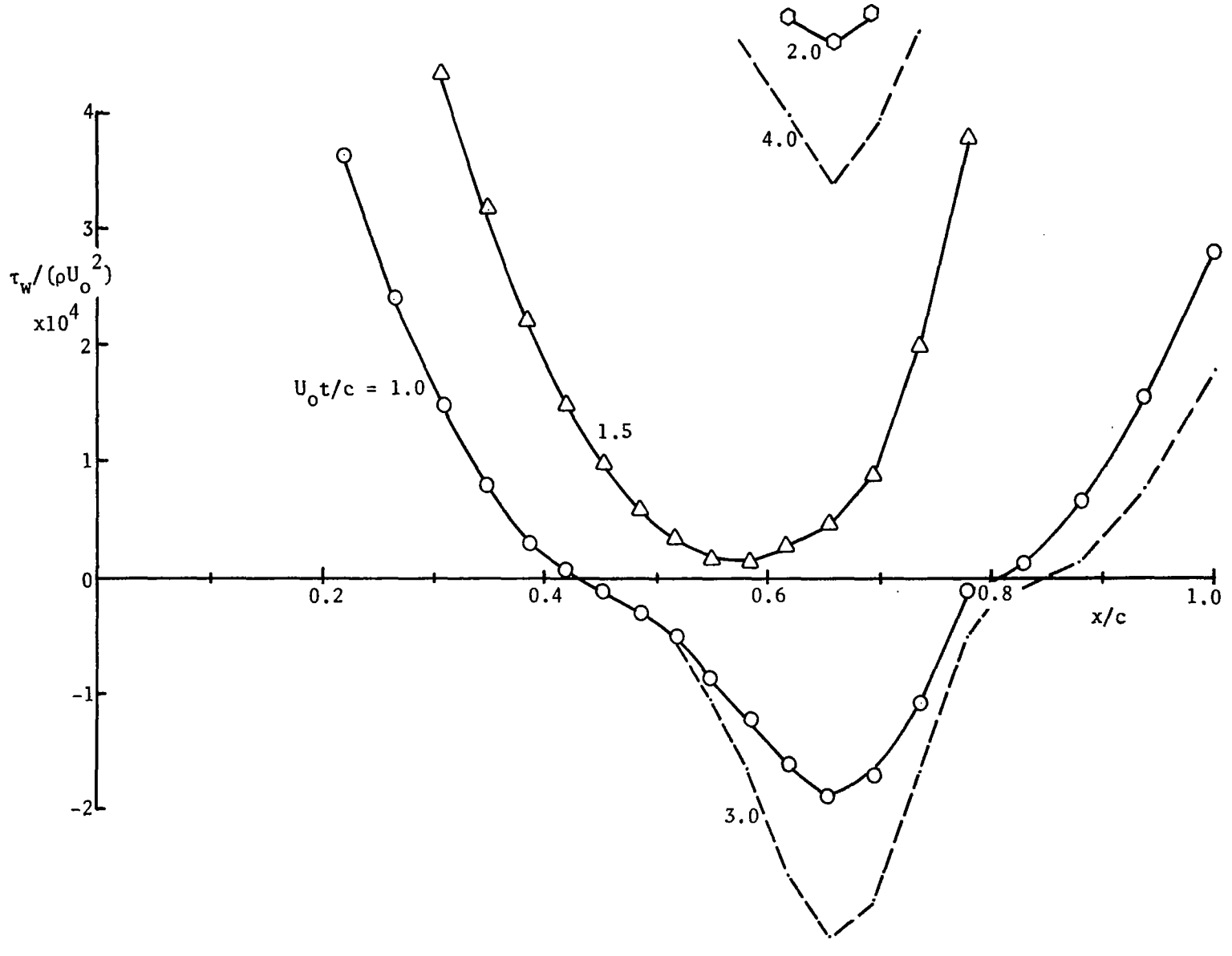


Figure 14 Wall Shear Stress Distributions for Increasing Time; $U_o t_p/c$ = 2.0, A = 0.5. Oscillatory Flow

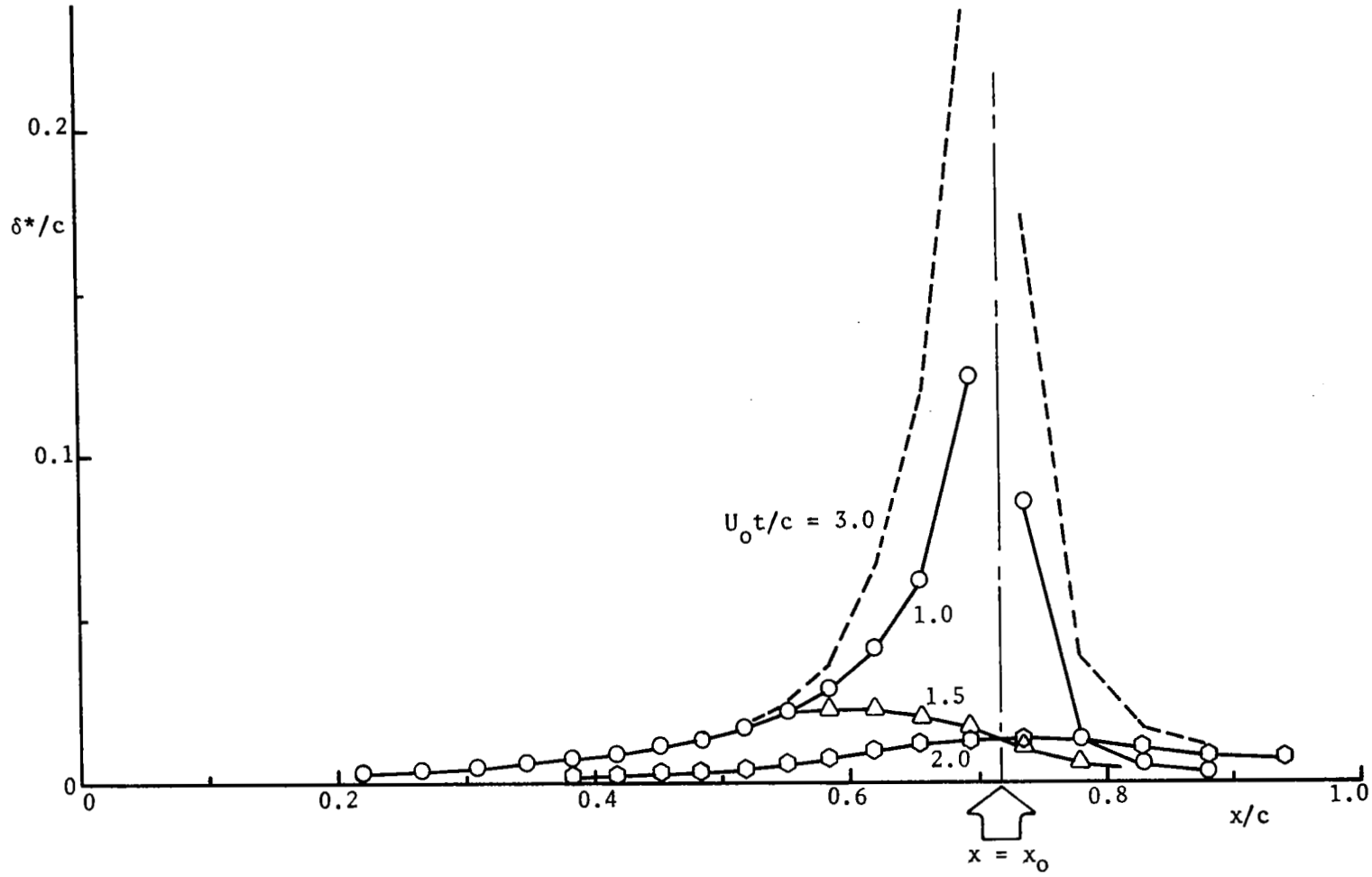


Figure 15 Displacement Thickness Distributions for Increasing Time; $U_o t_p/c = 2.0$, A = 0.5. Oscillatory Flow

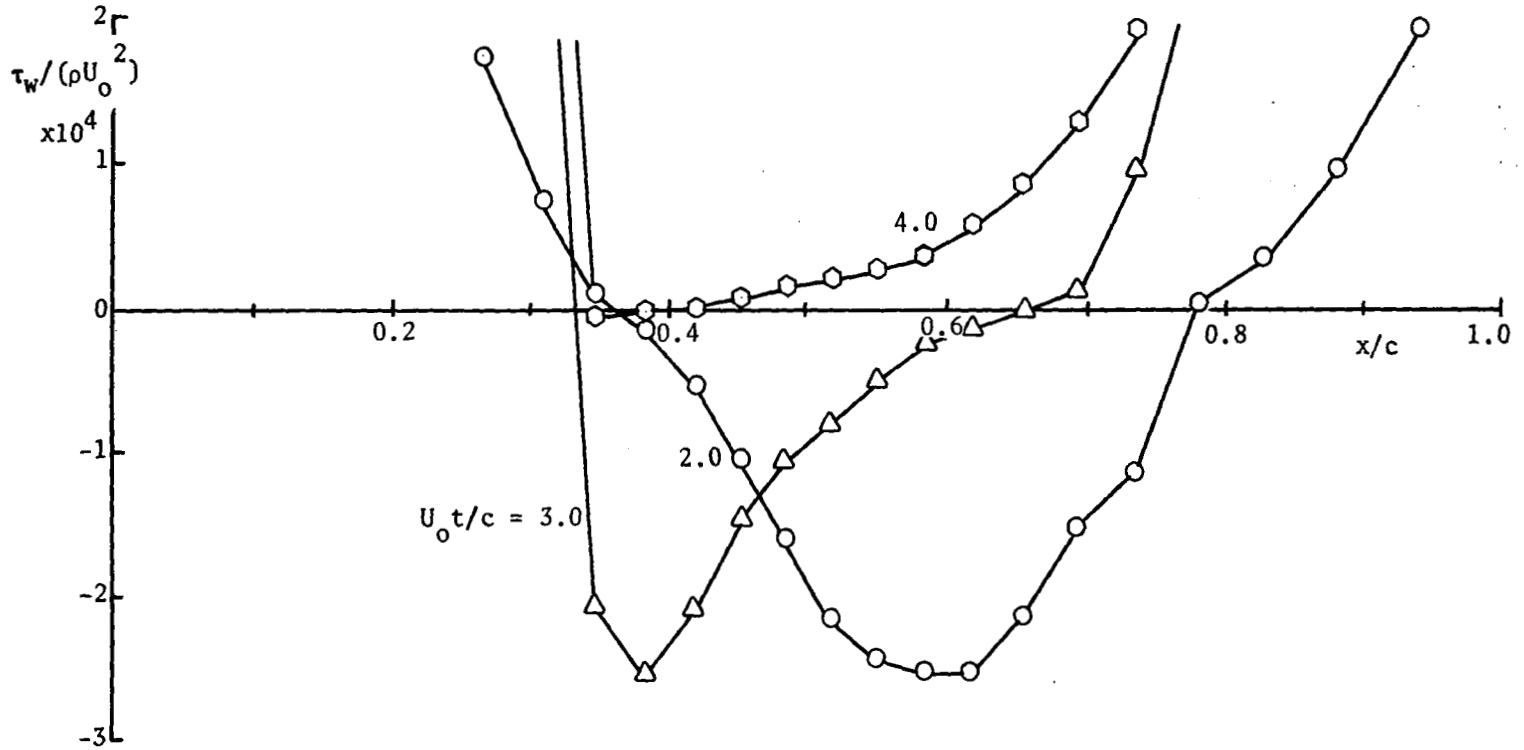


Figure 16 Wall Shear Stress Distributions for Increasing Time;

Oscillatory Flow, $U_o t_p/c$ = 4.0, A = 0.5.

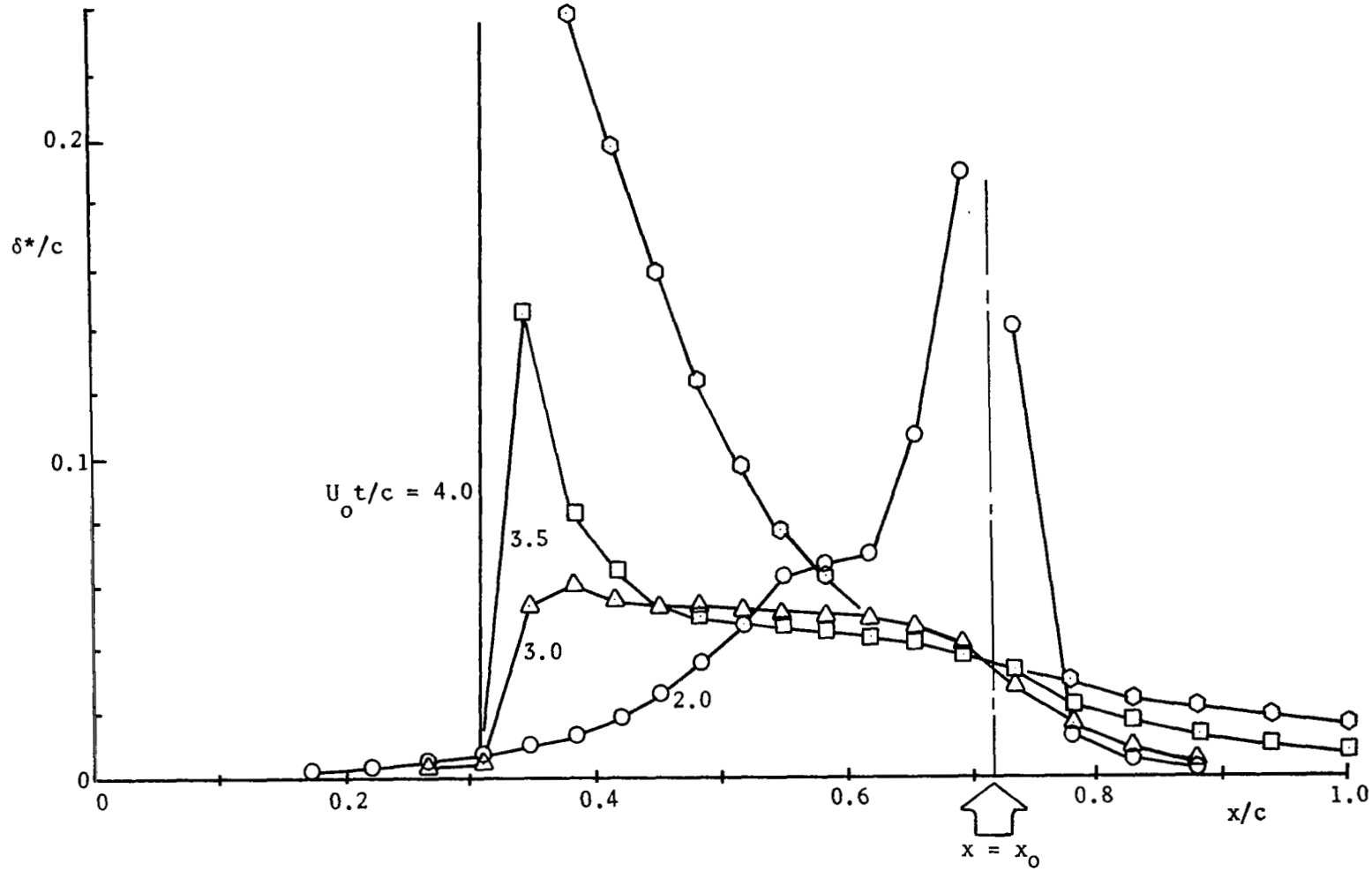


Figure 17 Displacement Thickness Distributions for Increasing Time; Oscillatory Flow, $U_o t_p/c = 4.0$, A = 0.5.

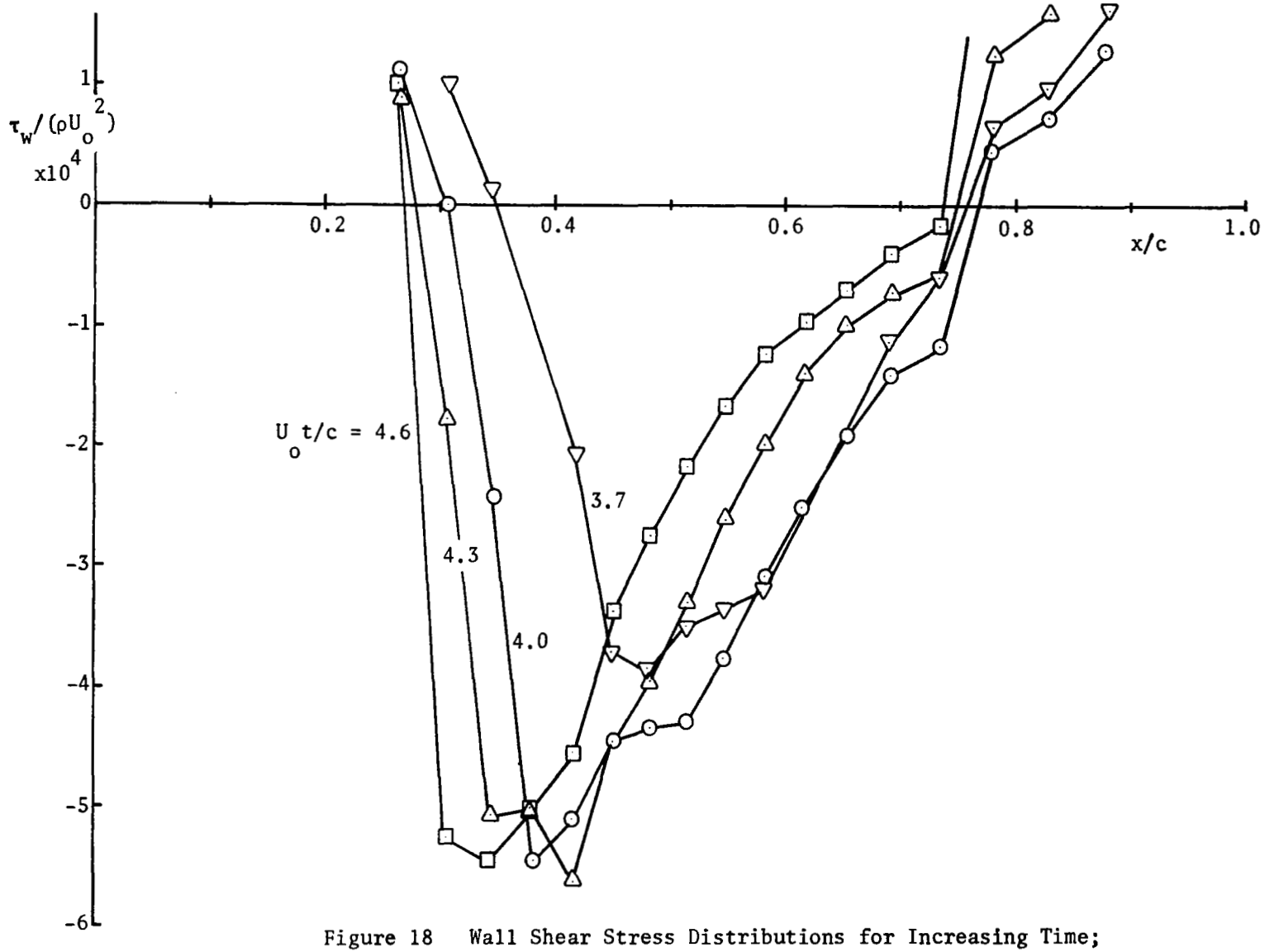


Figure 18 Wall Shear Stress Distributions for Increasing Time; Oscillatory Flow, $U_o t_p/c$ = 8.0, A = 0.5.

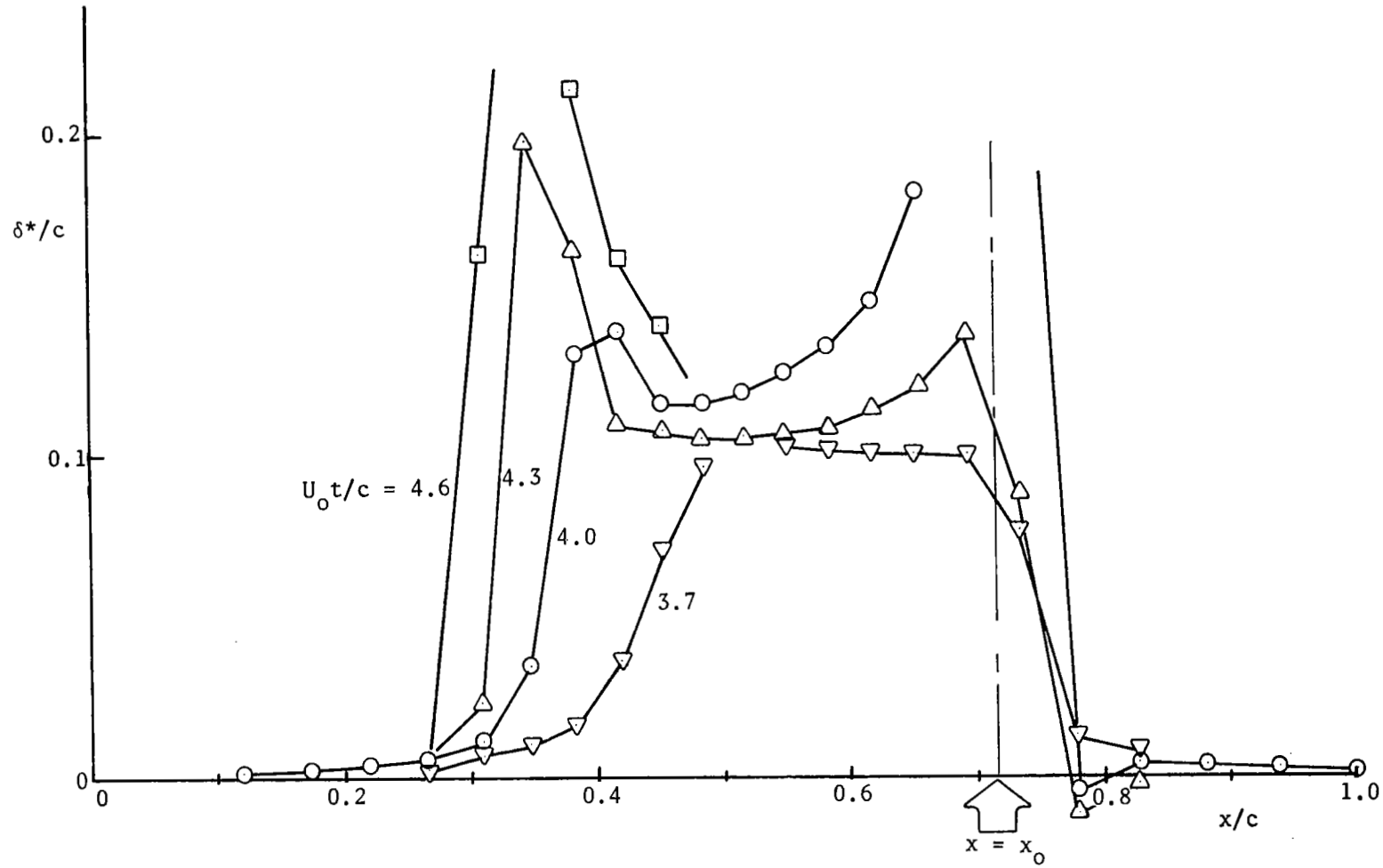


Figure 19 Displacement Thickness Distributions for Increasing Time; Oscillatory Flow, $U_o t_p/c = 8.0$, A = 0.5.

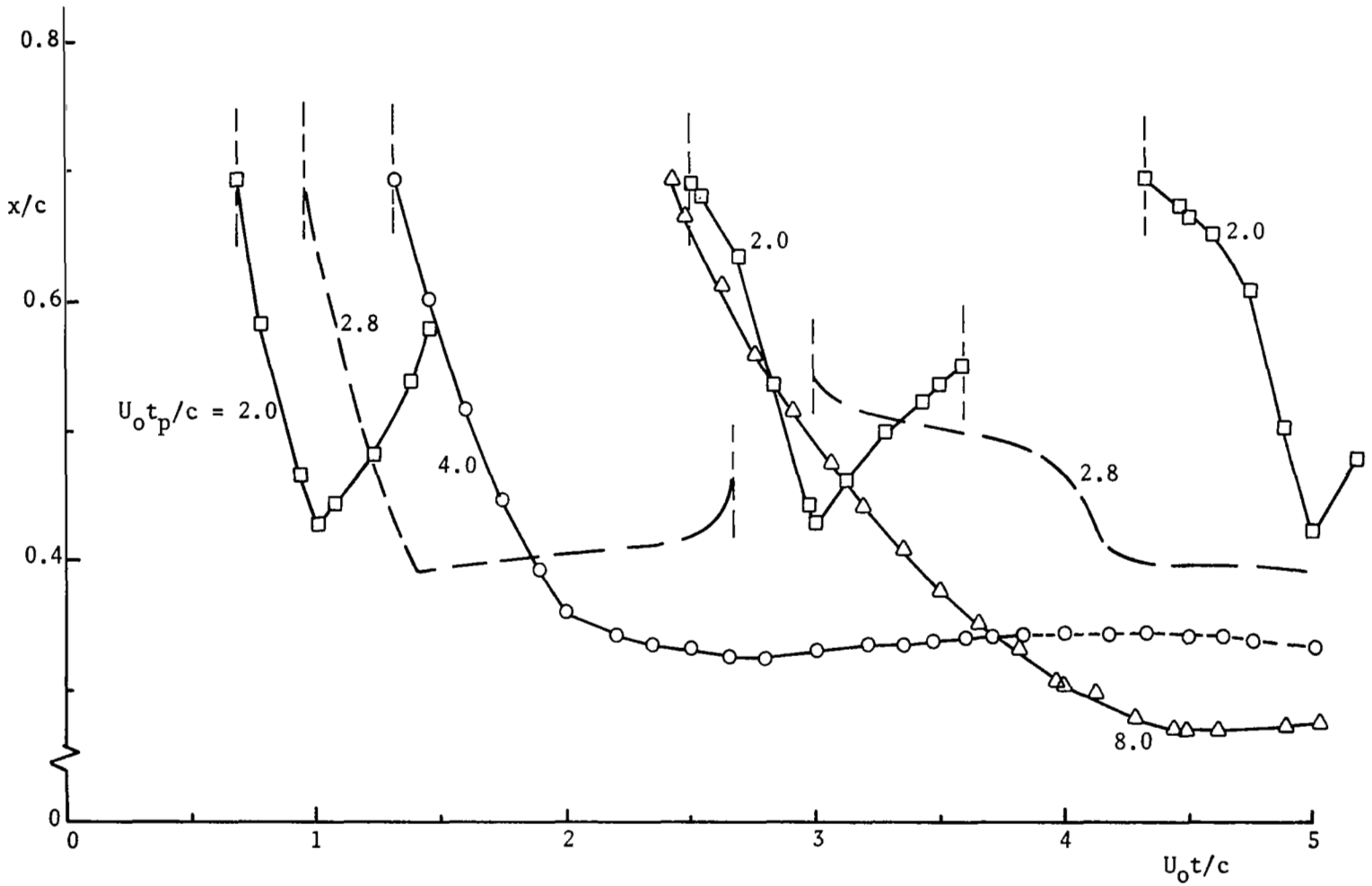


Figure 20 Movement of the Reversal Point with Time; Oscillatory Flow, $U_o t_p/c = 2.8$

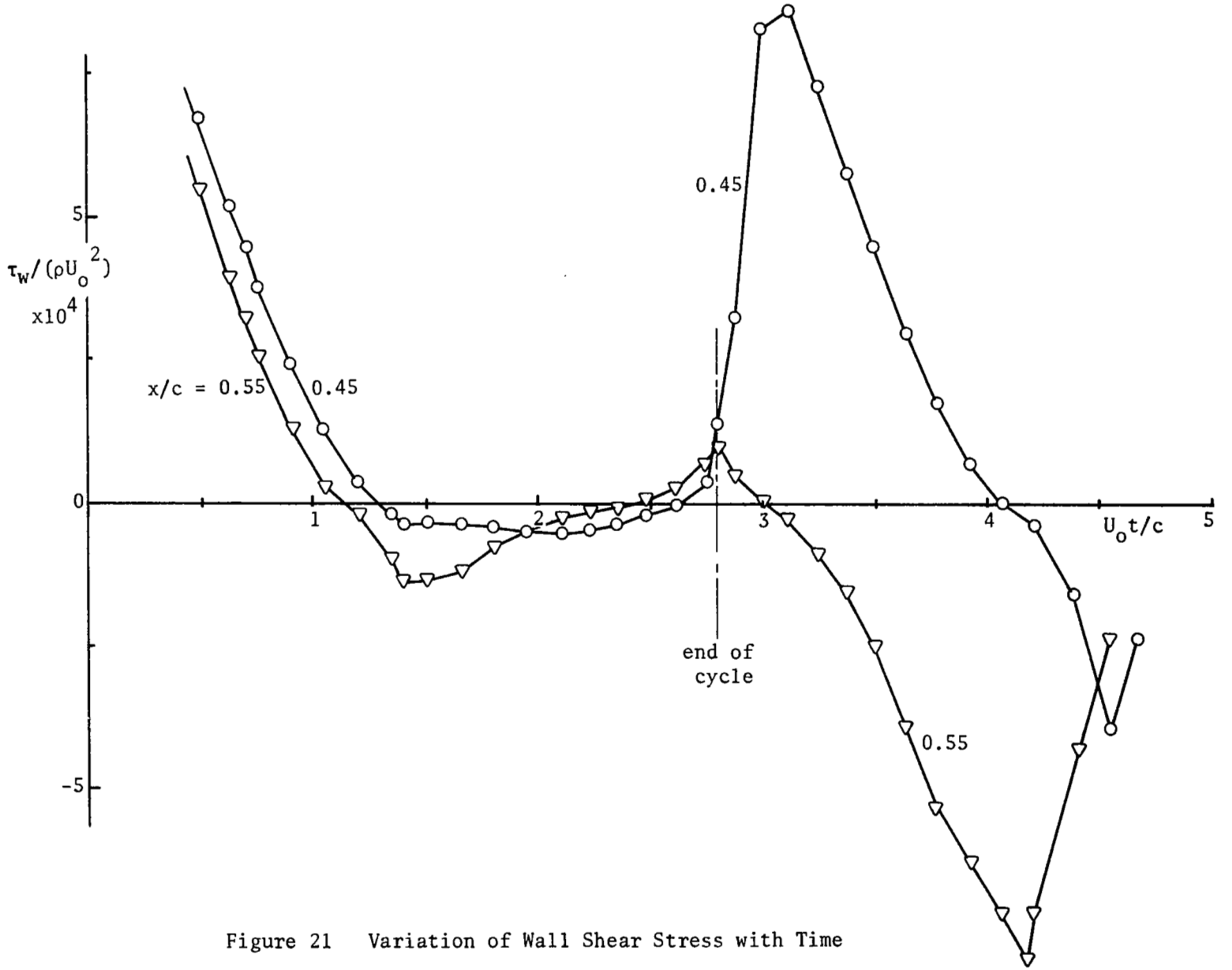


Figure 21 Variation of Wall Shear Stress with Time

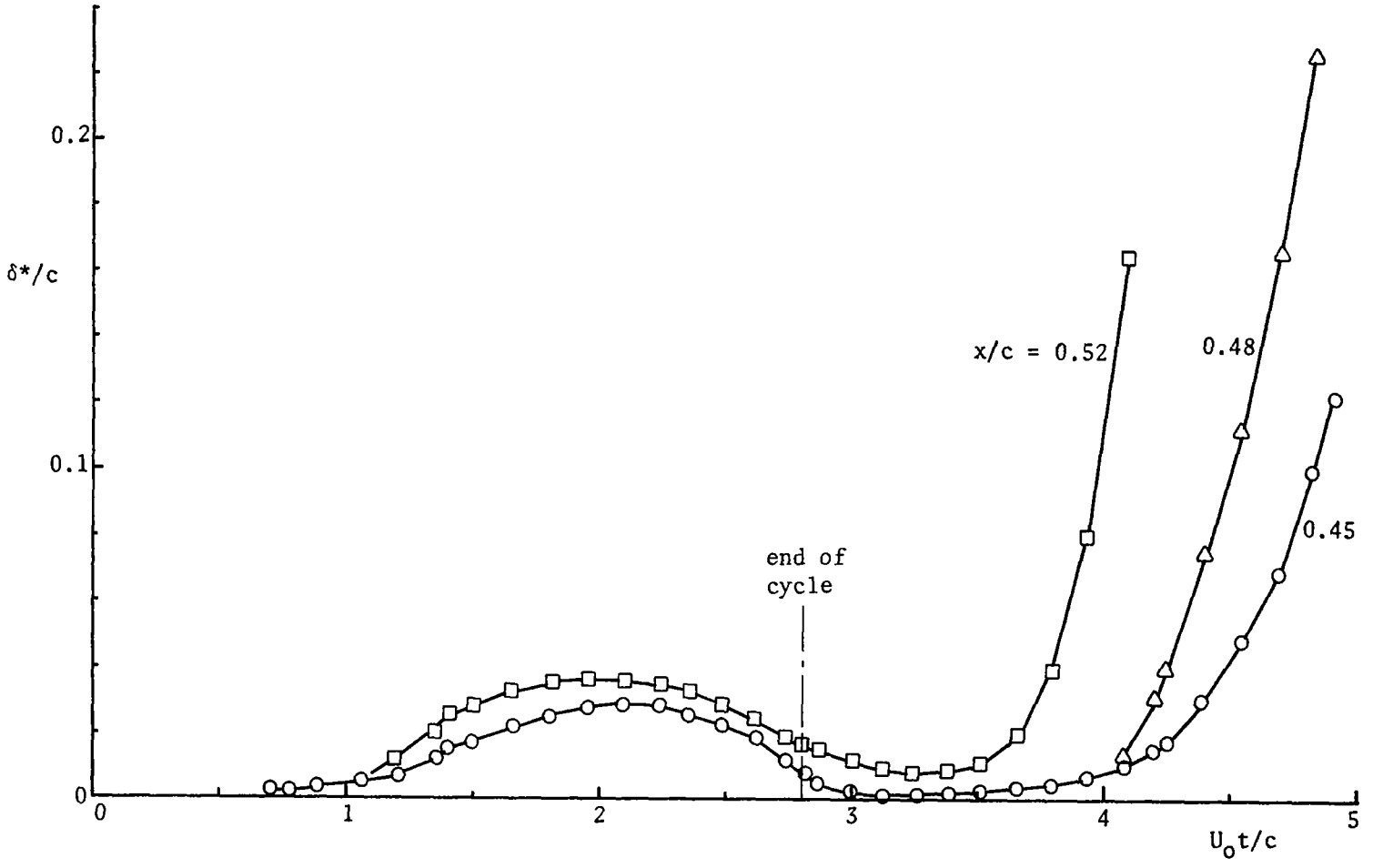


Figure 22 Variation of Displacement Thickness with Time; Oscillatory Flow, $U_o t_p/c = 2.8$.

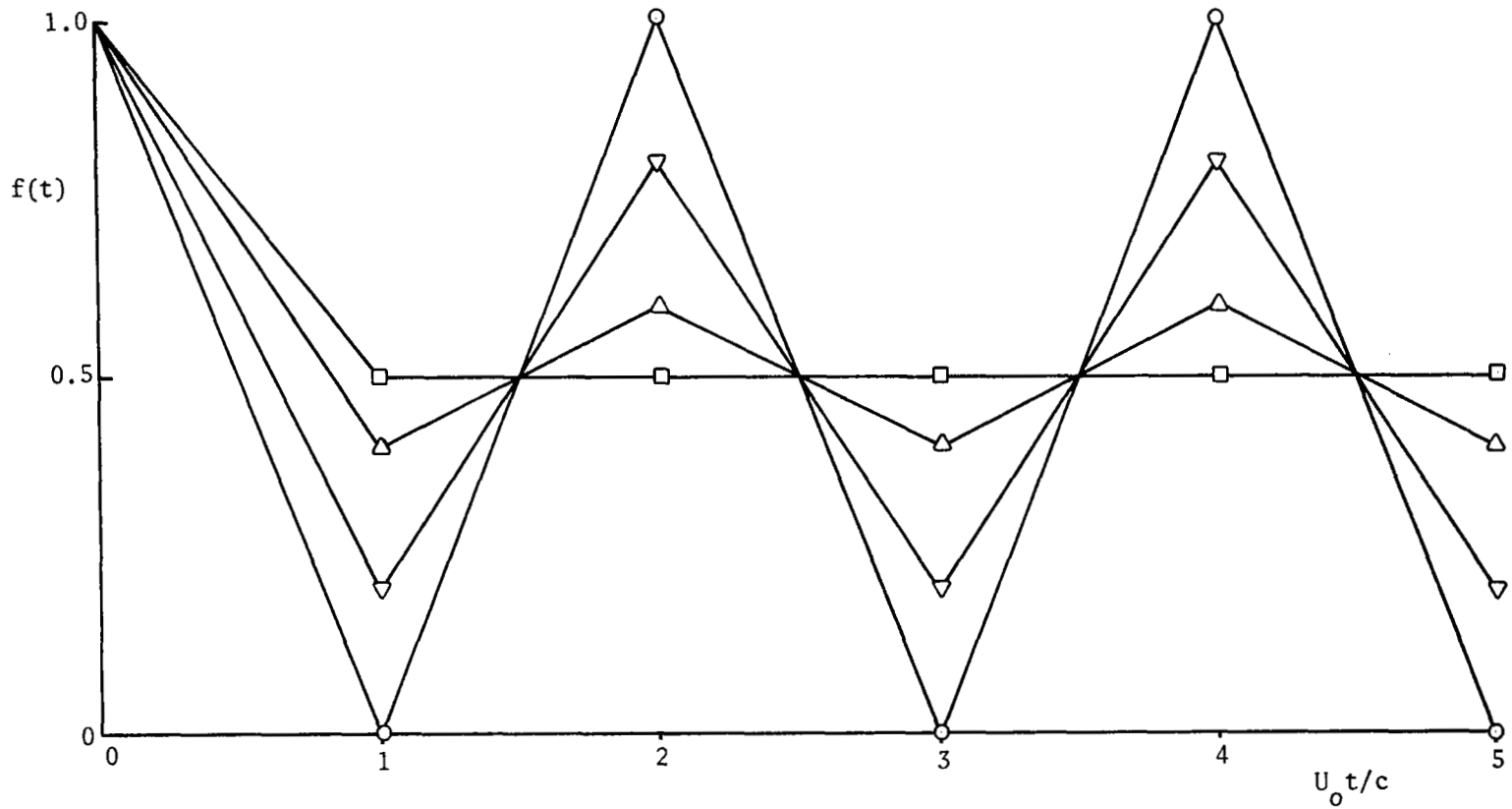


Figure 23 The Function f(t) for Oscillatory Flows of Various Amplitudes; $U_o t_p/c = 2.0$.

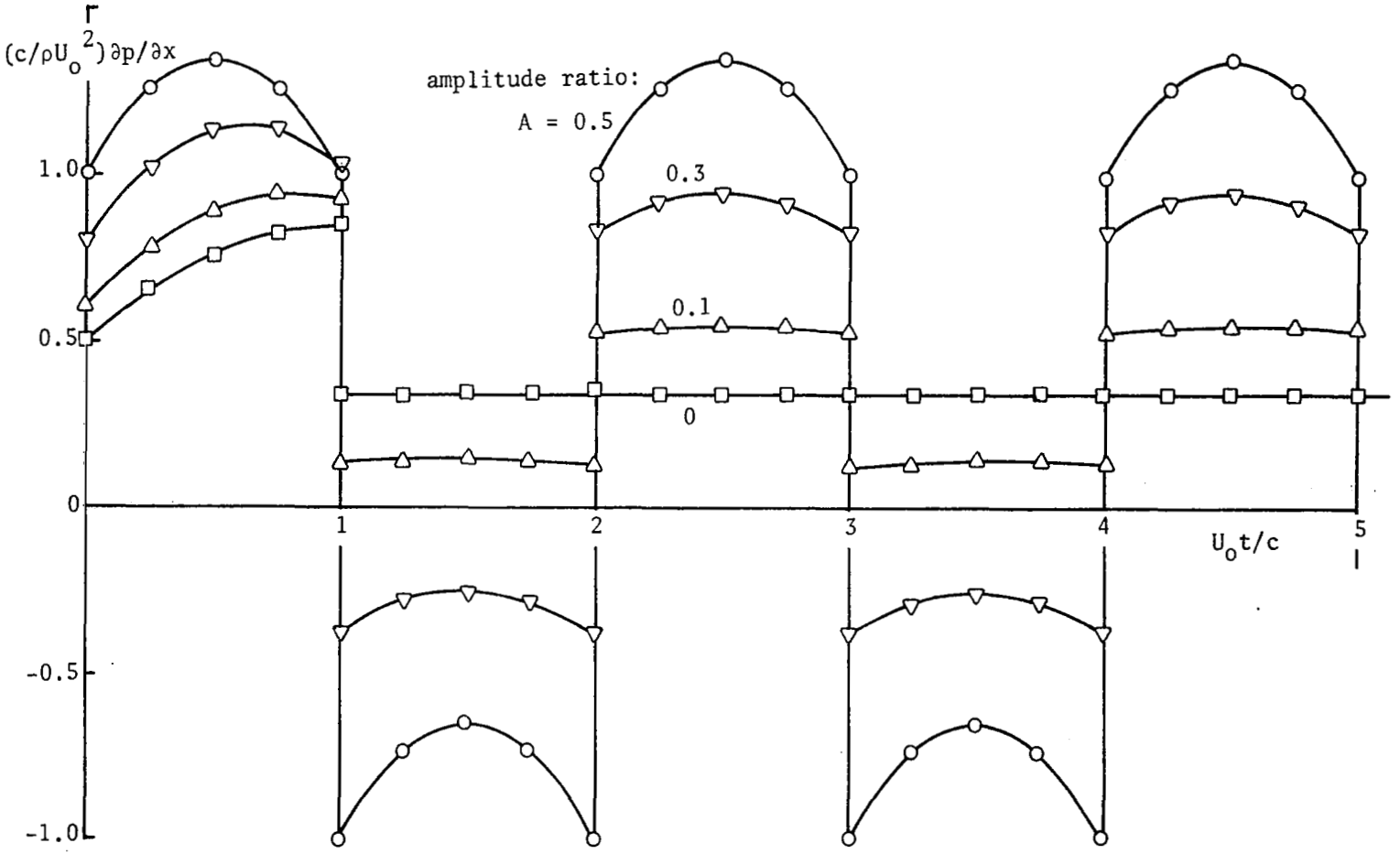


Figure 24 Variation of Pressure Gradient at $x = x_o$ with Time; Oscillatory Flow, $U_o t_p/c = 2.0$.

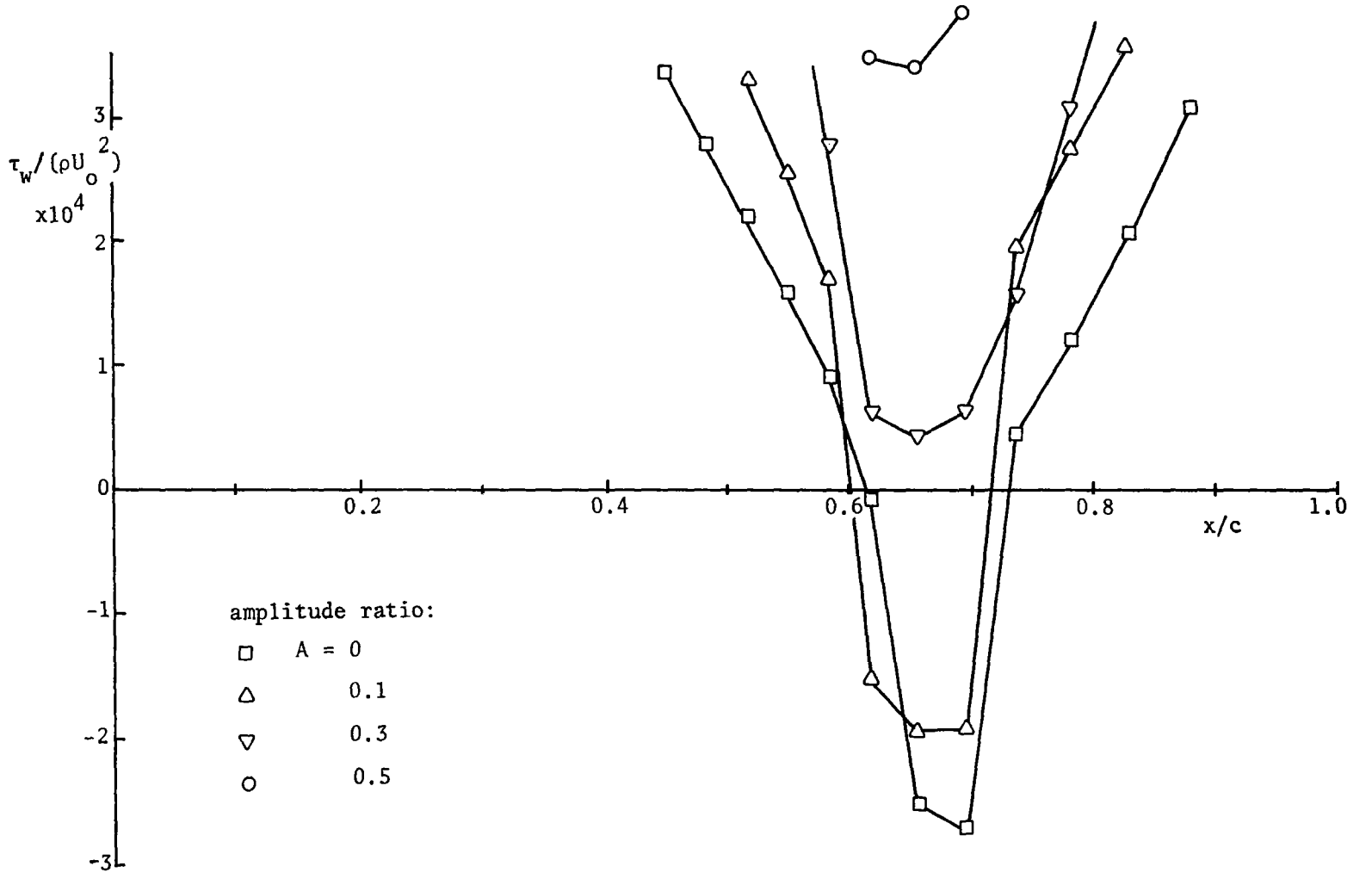


Figure 25 Wall Shear Stress Distributions for Various Amplitudes; Oscillatory Flow, $U_o t_p/c = 2.0$, $U_o t/c = 4.0$.

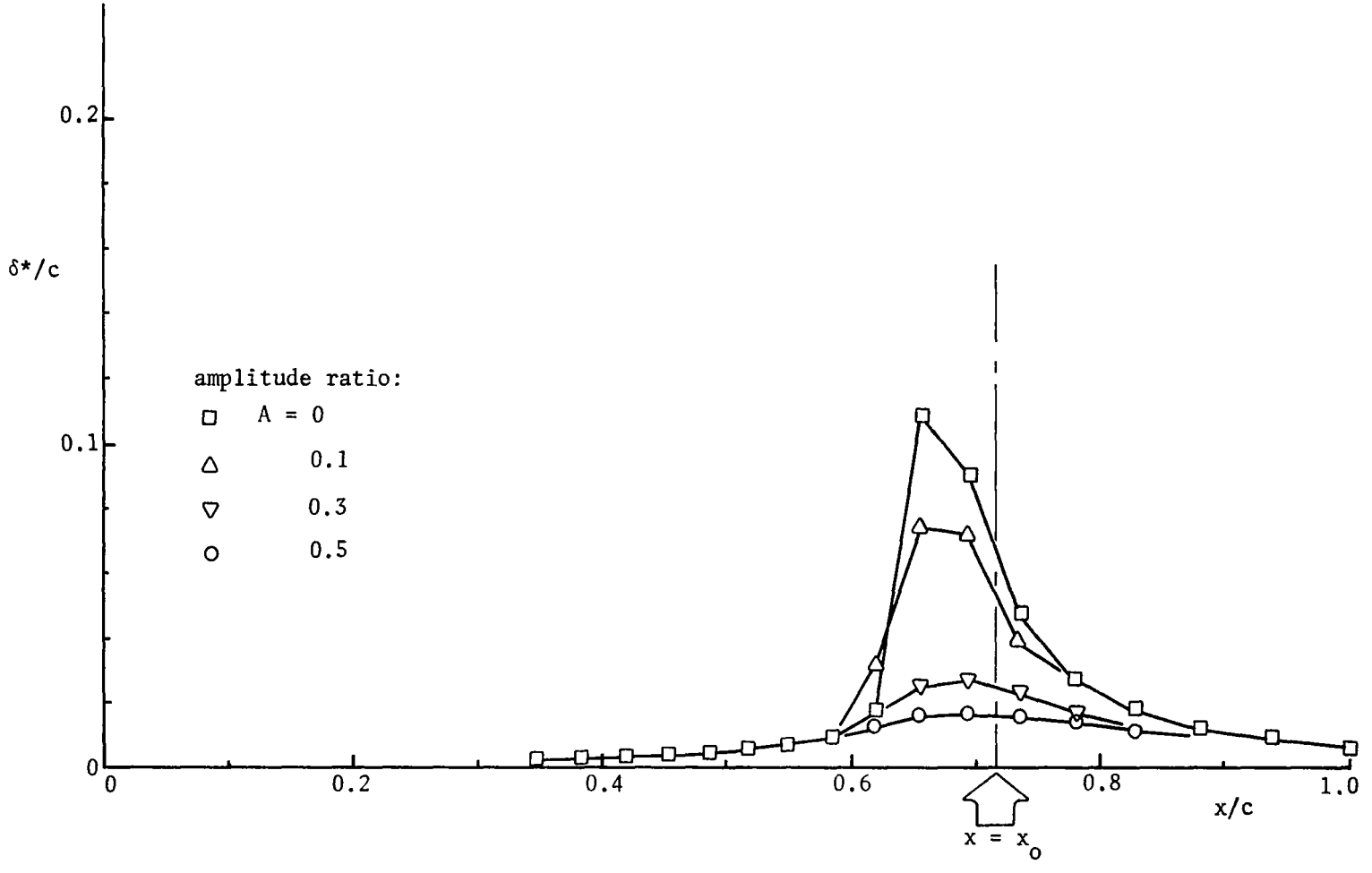


Figure 26 Displacement Thickness Distributions for Various Amplitudes; Oscillatory Flow, $U_o t_p/c = 2.0$, $U_o t/c = 4.0$.

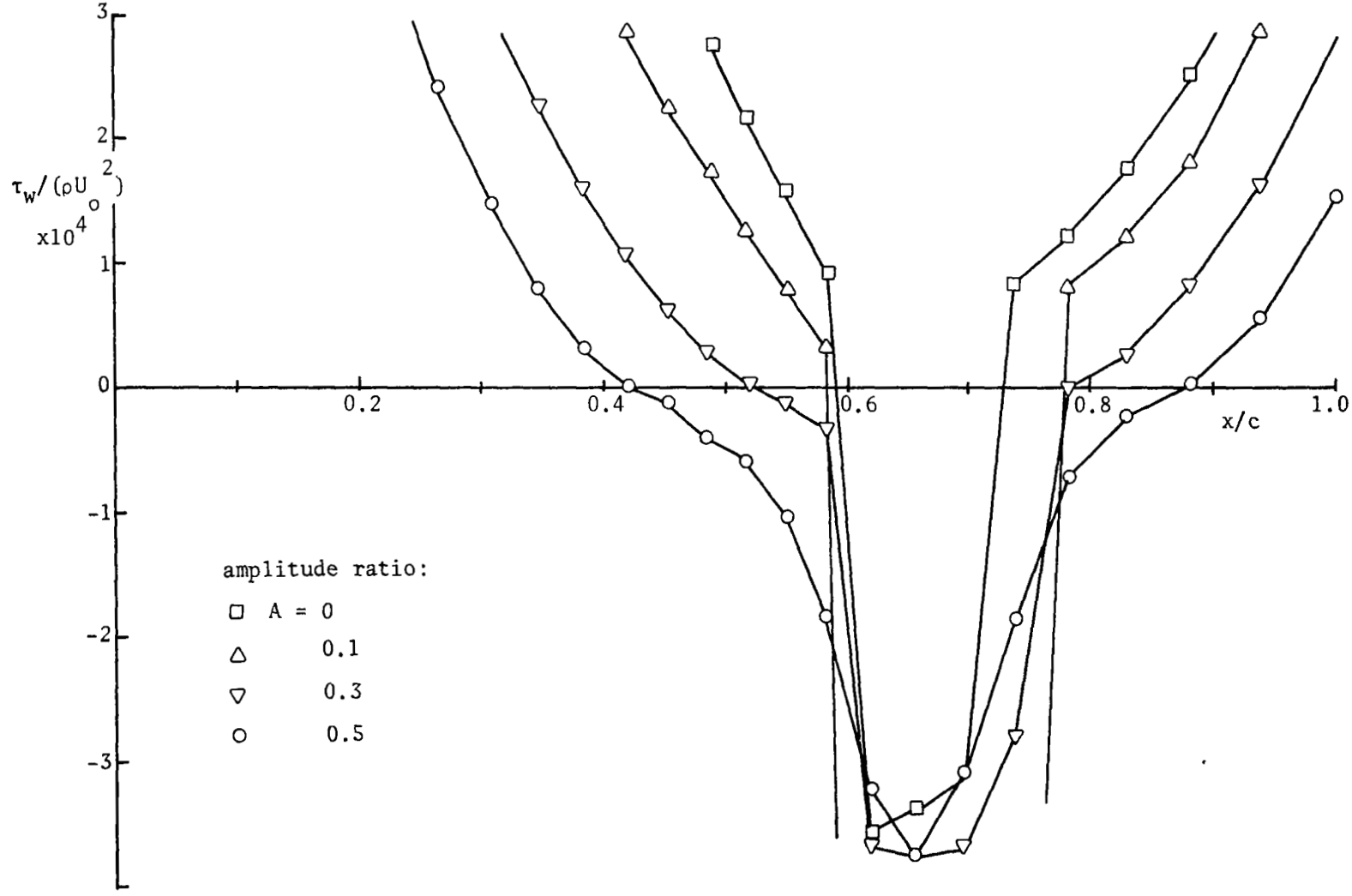


Figure 27 Wall Shear Stress Distributions for Various Amplitudes; Oscillatory Flow, $U_o t_p/c = 2.0$, $U_o t/c = 5.0$.

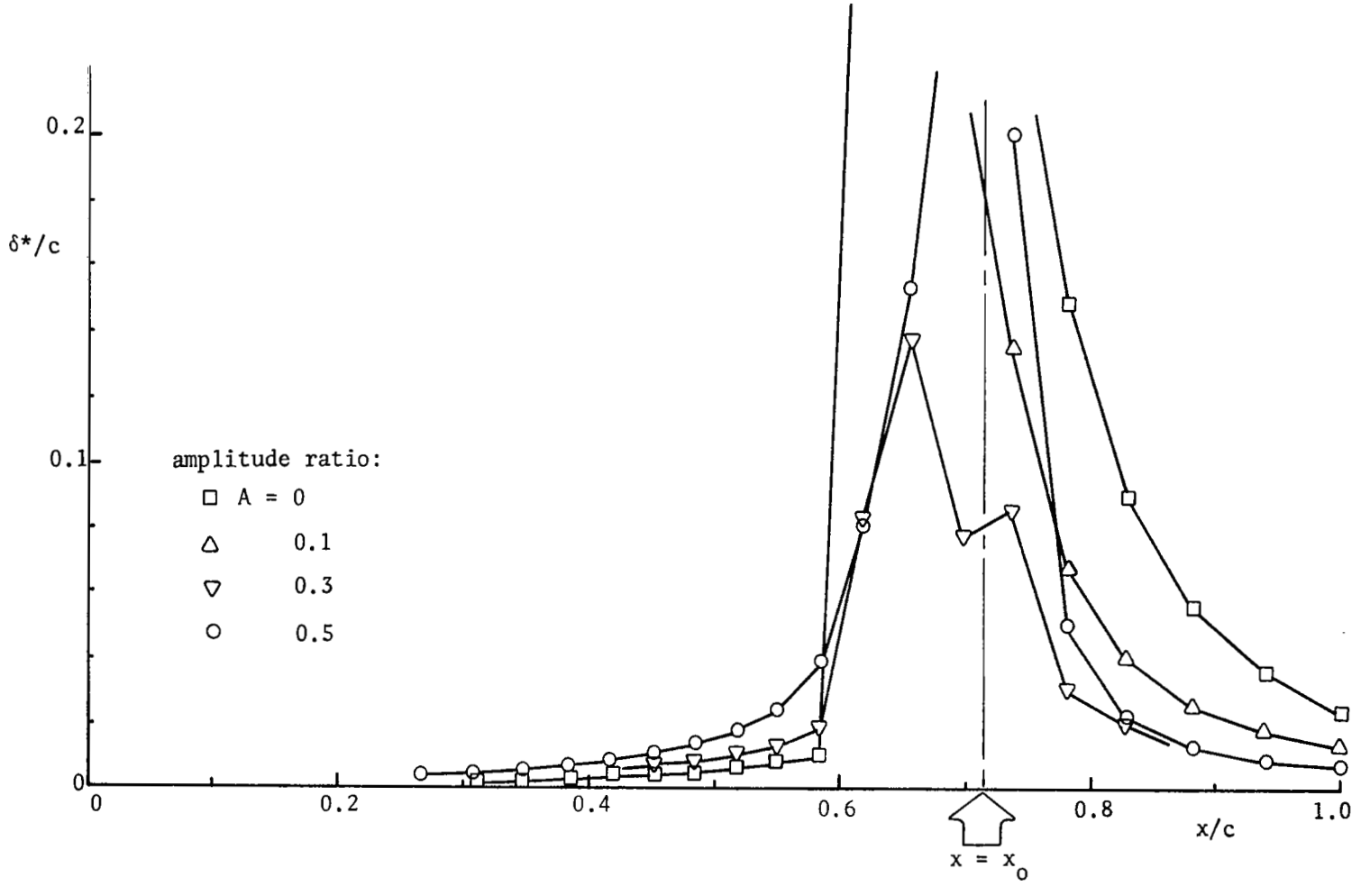


Figure 28 Displacement Thickness Distributions for Various Amplitudes; Oscillatory Flow, $U_o t_p/c = 2.0$, $U_o t/c = 5.0$.

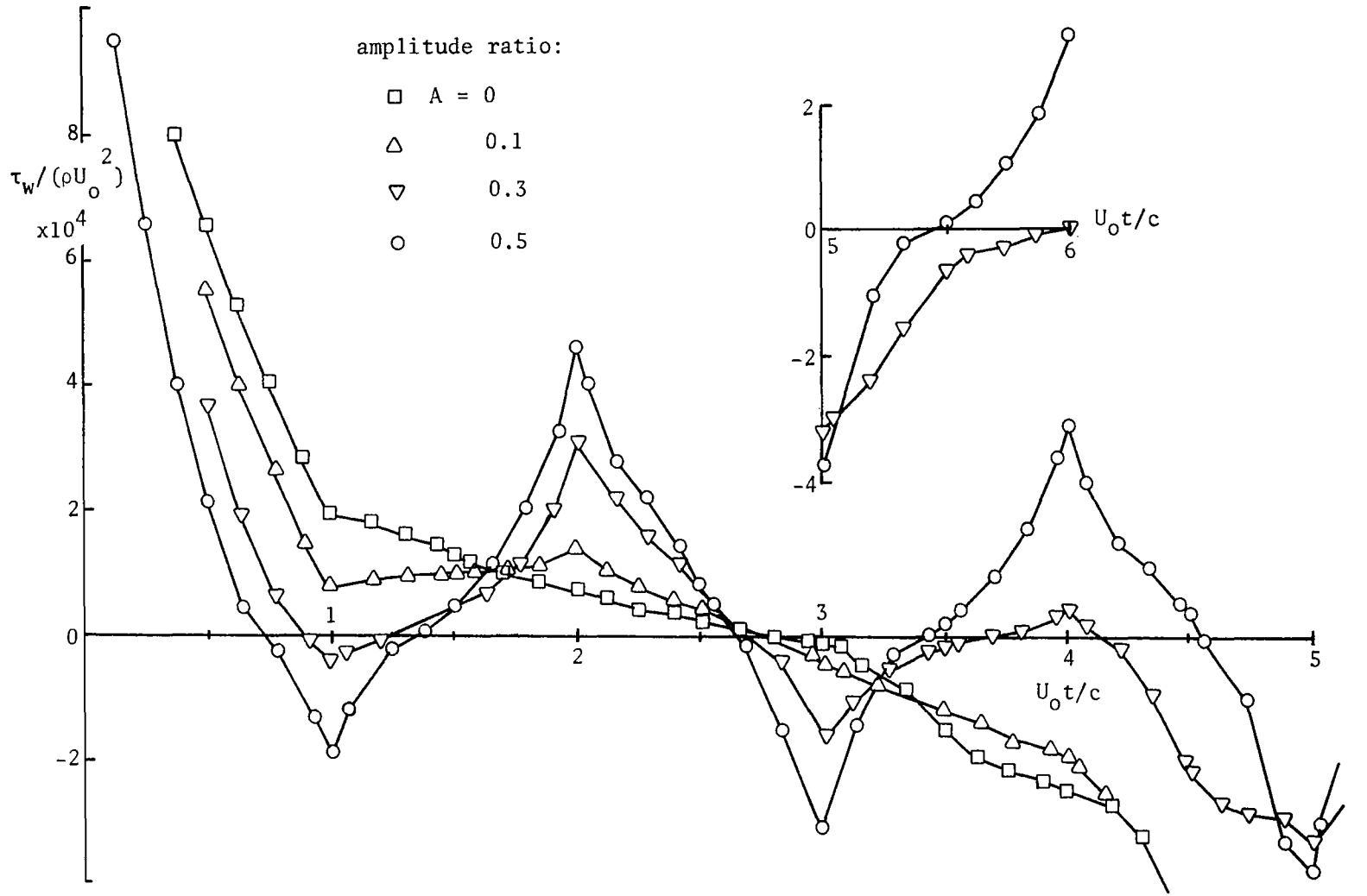


Figure 29 Variation of Wall Shear Stress with Time;
Oscillatory Flow, $U_o t_p/c = 2.0$, $x = 0.65c$.

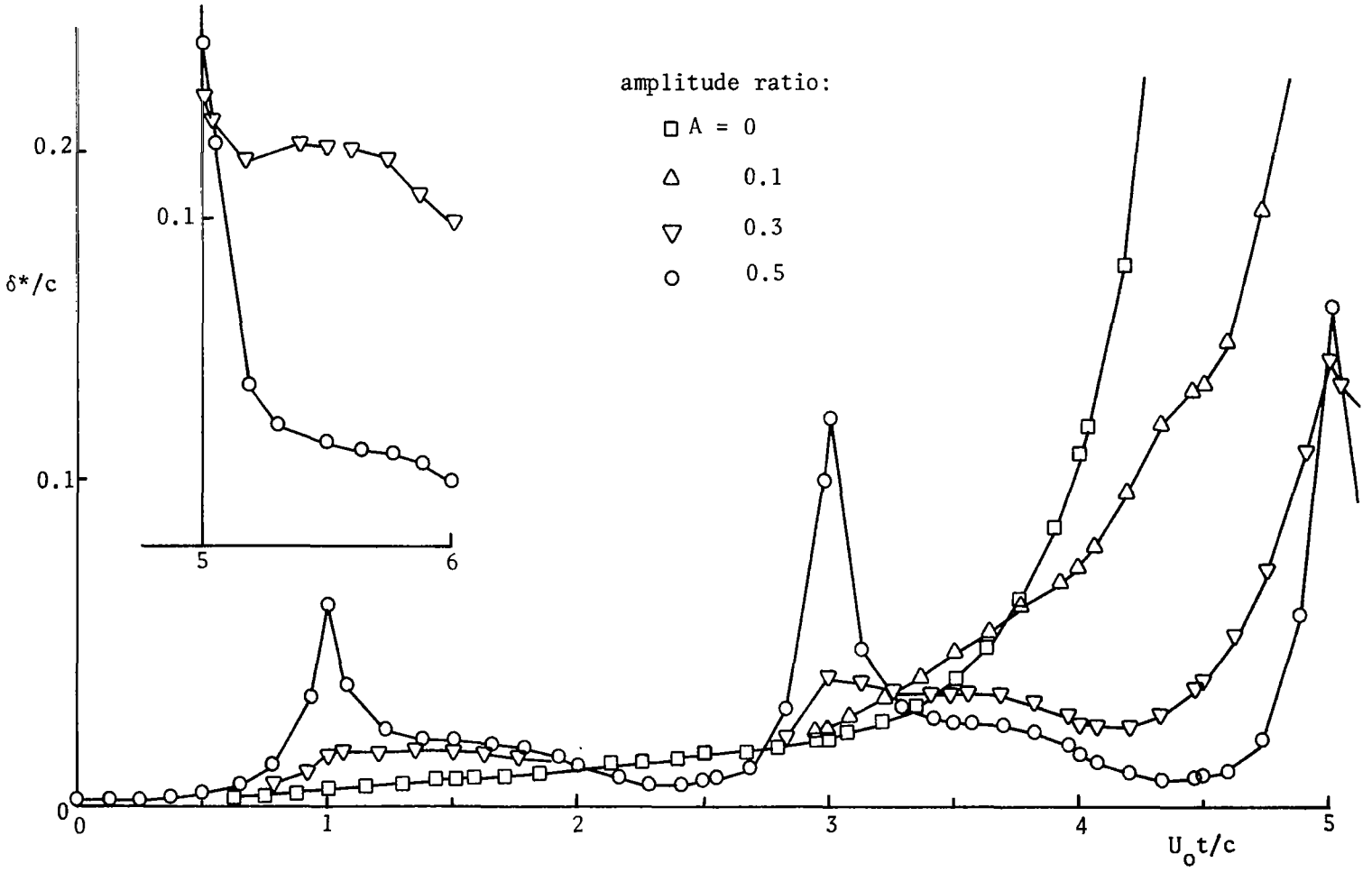


Figure 30 Variation of Displacement Thickness with Time; Oscillatory Flow, $U_o t_p/c = 2.0$, $x = 0.65c$.

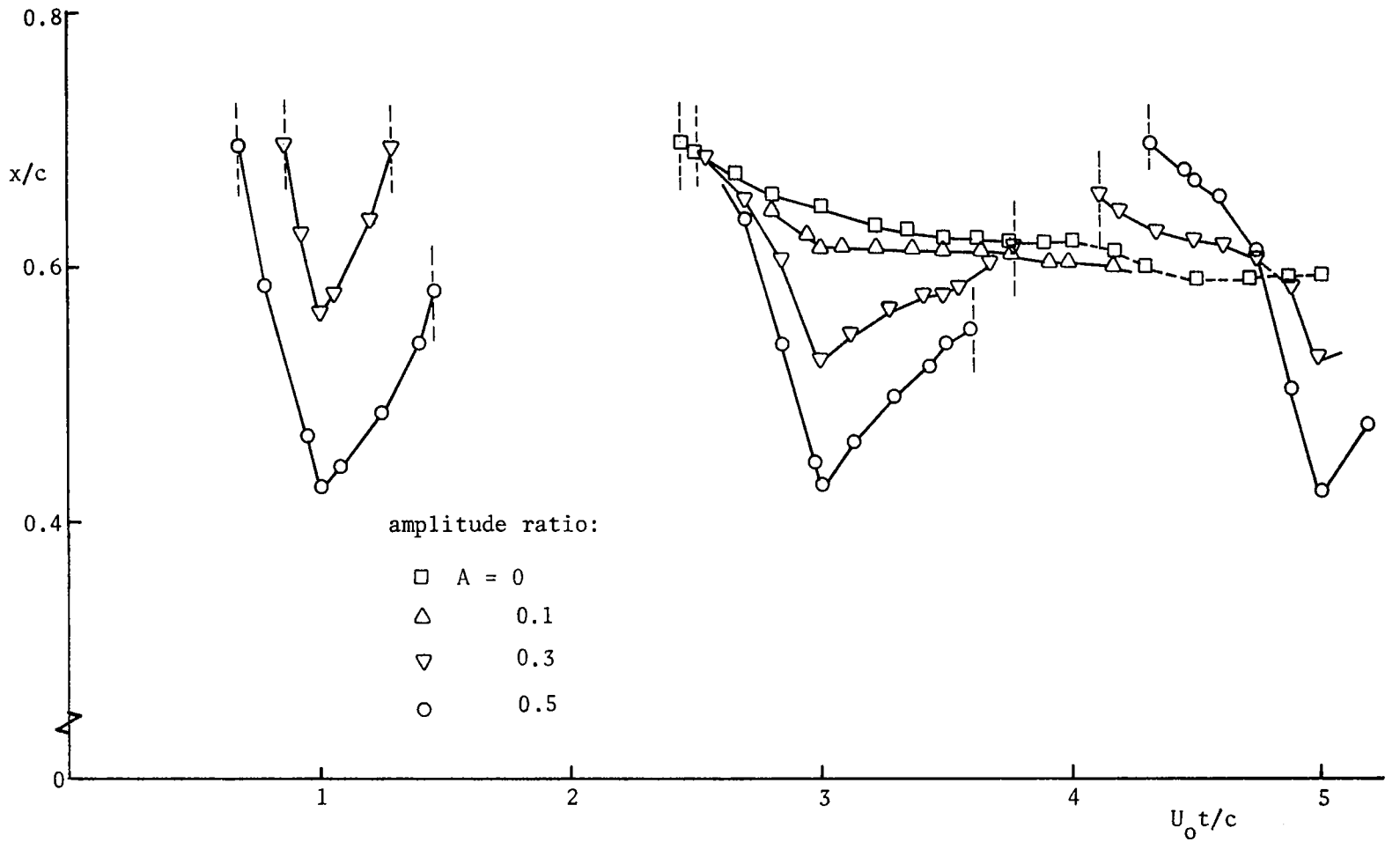


Figure 31 Movement of the Reversal Point with Time; Oscillatory Flow, $U_o t_p/c = 2.0$.

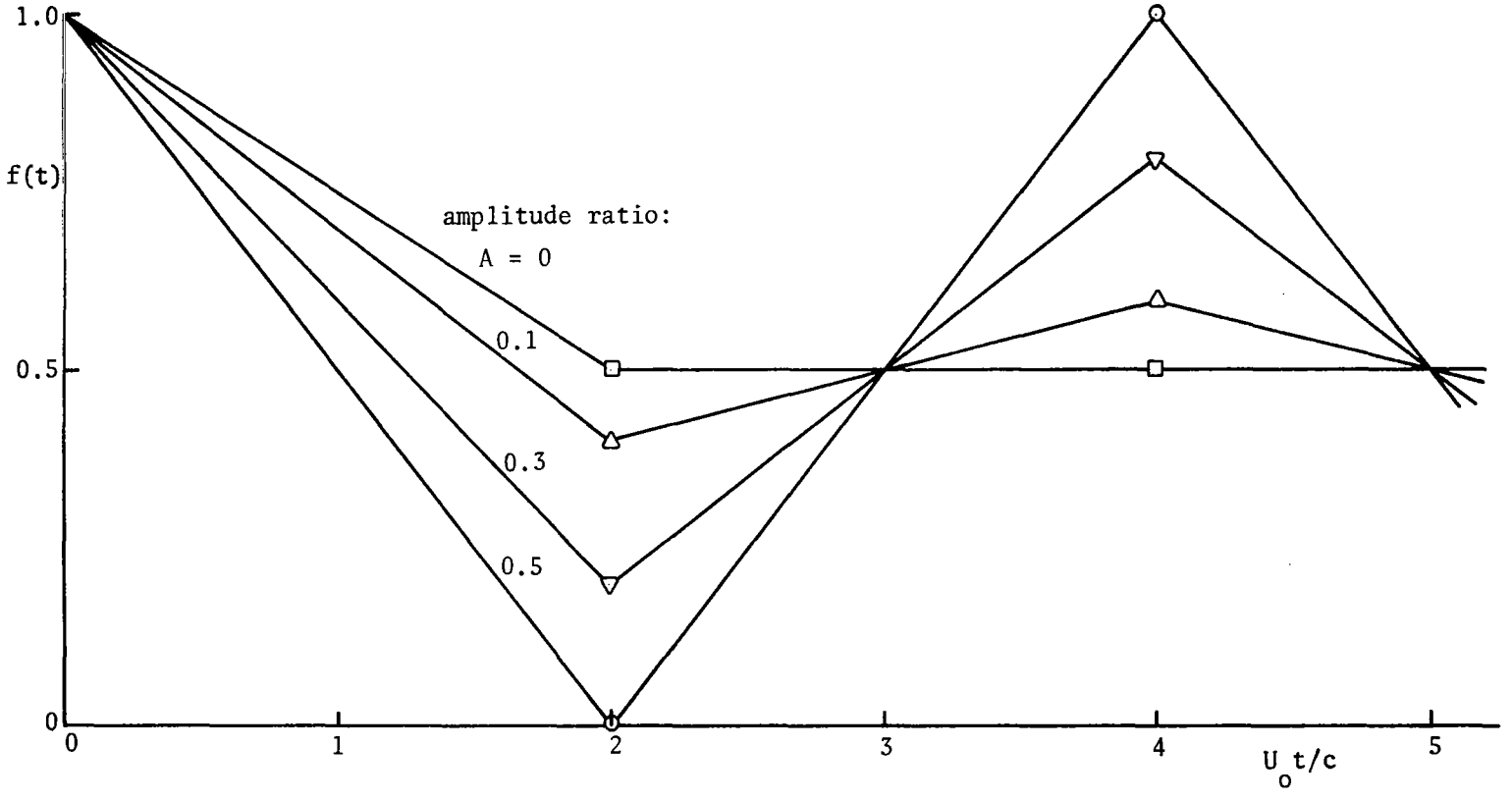


Figure 32 The Function f(t) for Oscillatory Flows of Various Amplitudes; $U_o t_p/c = 4.0$.

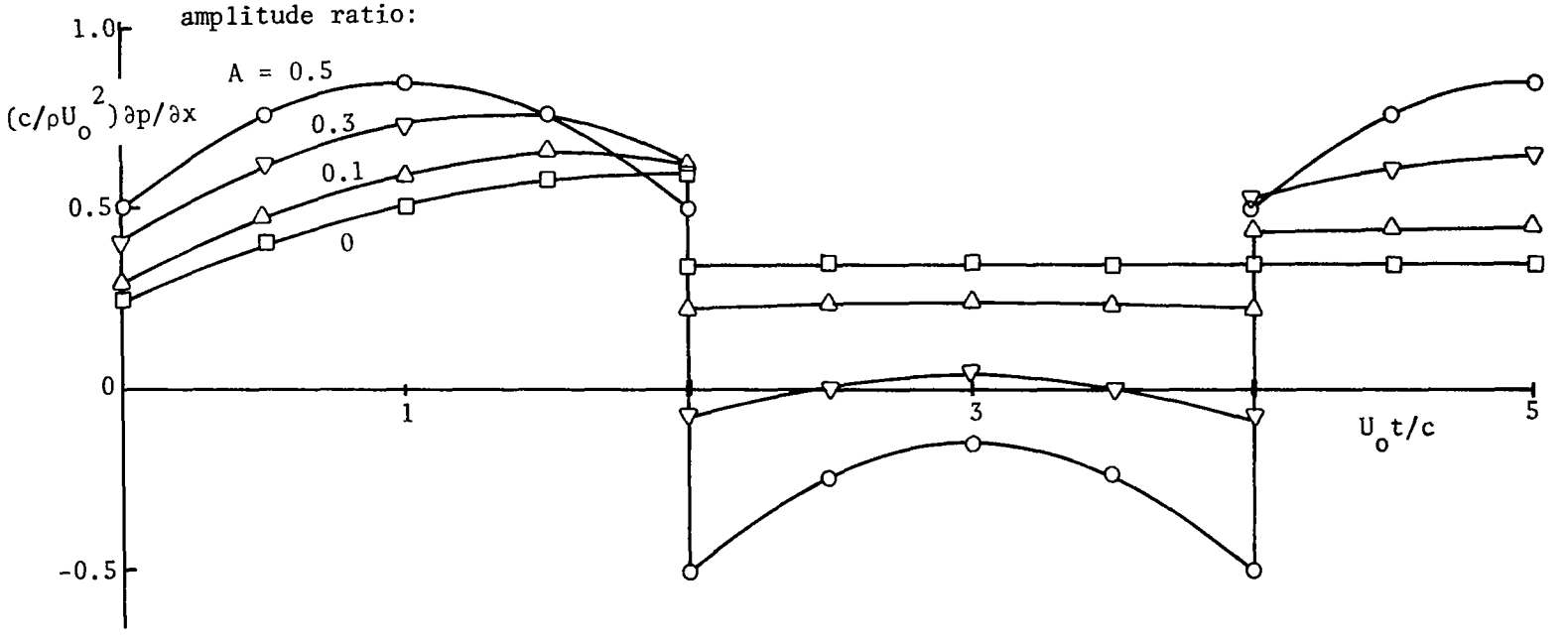


Figure 33 Variation of Pressure Gradient at $x = x_o$ with Time; Oscillatory Flow, $U_o t_p/c = 4.0$.

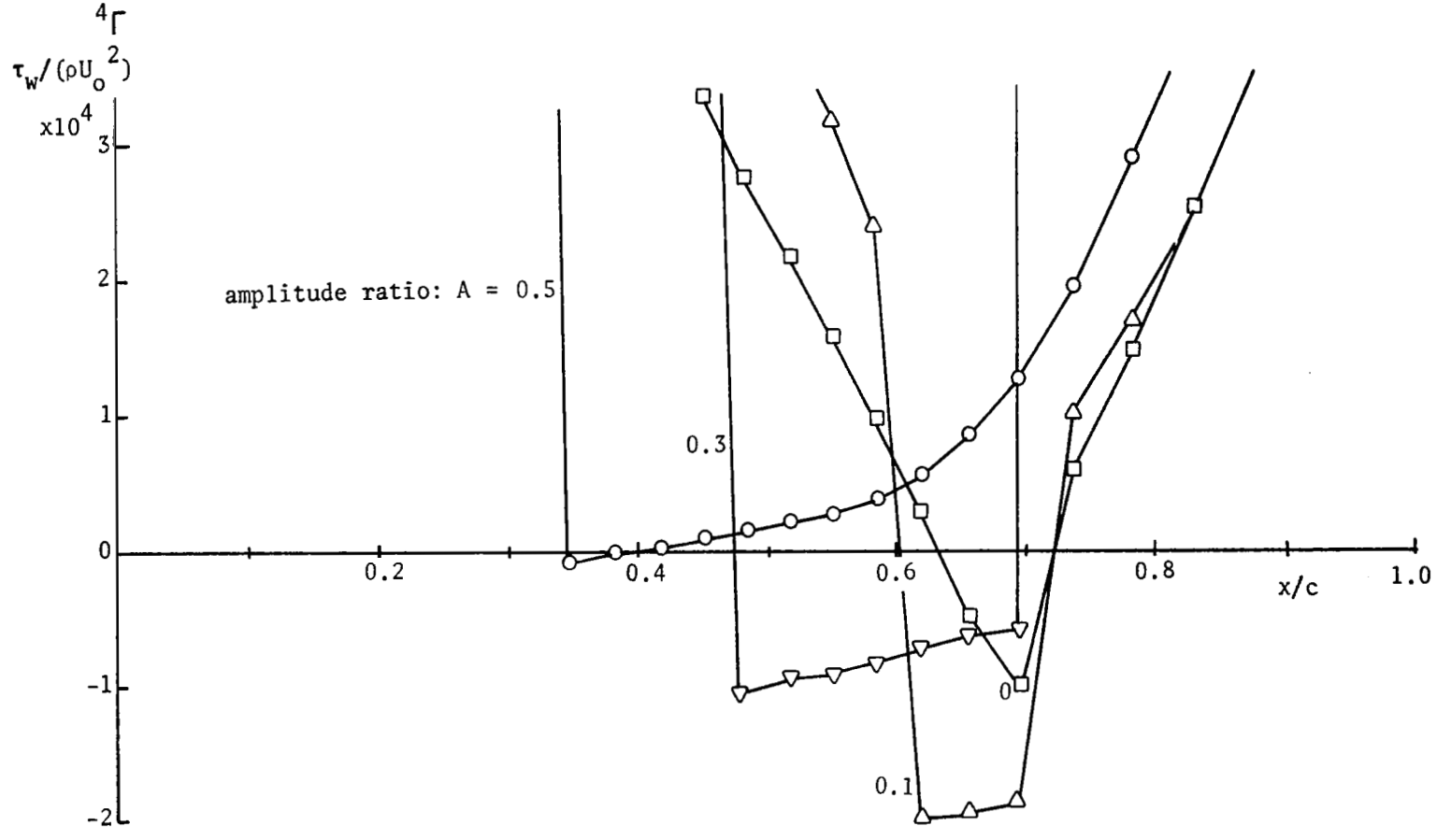


Figure 34 Wall Shear Stress Distributions for Various Amplitudes; Oscillatory Flow, $U_o t_p/c = 4.0$, $U_o t/c = 4.0$.

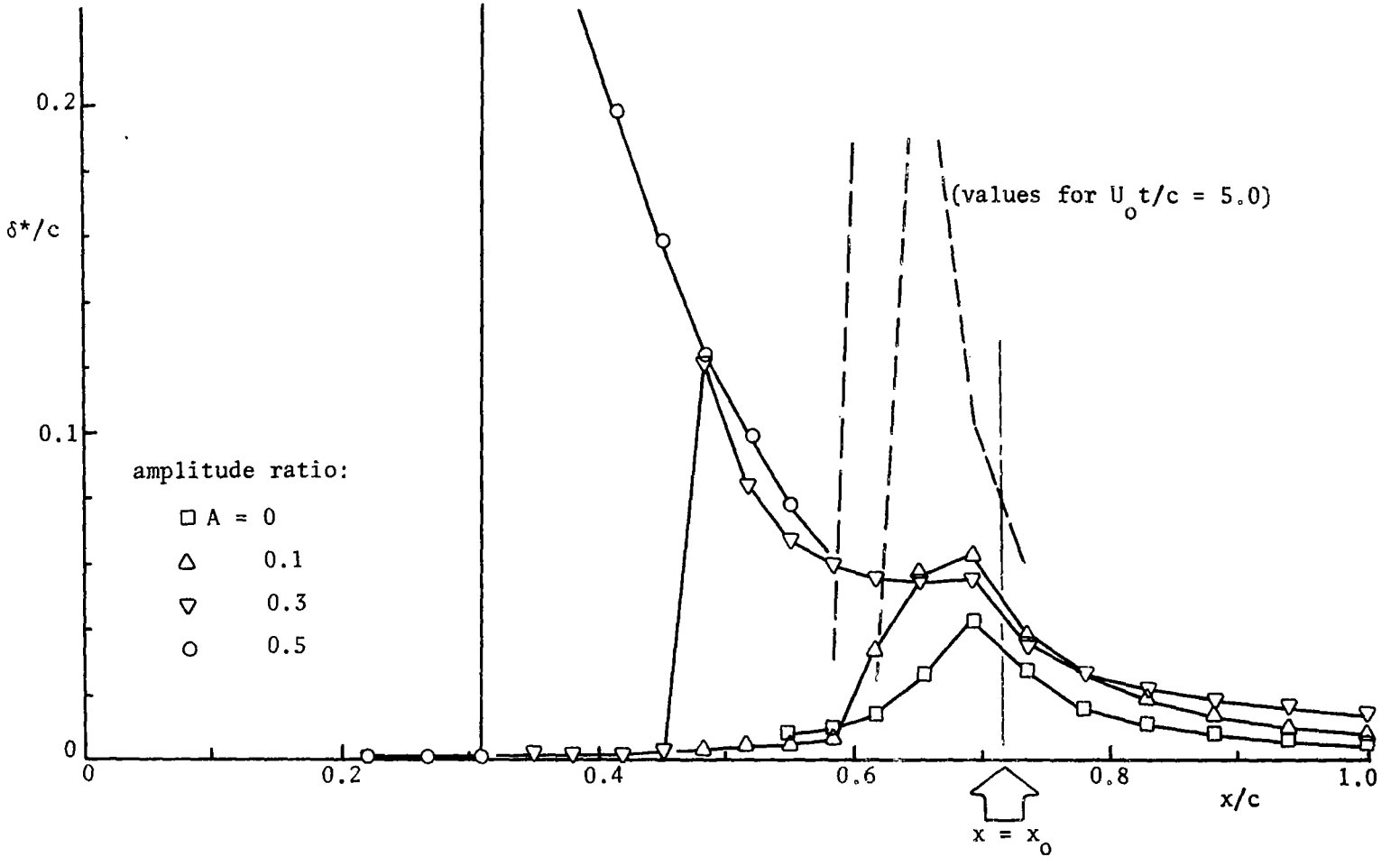


Figure 35 Displacement Thickness Distributions for Various Amplitudes; Oscillatory Flow, $U_o t_p/c = 4.0$, $U_o t/c = 4.0$.

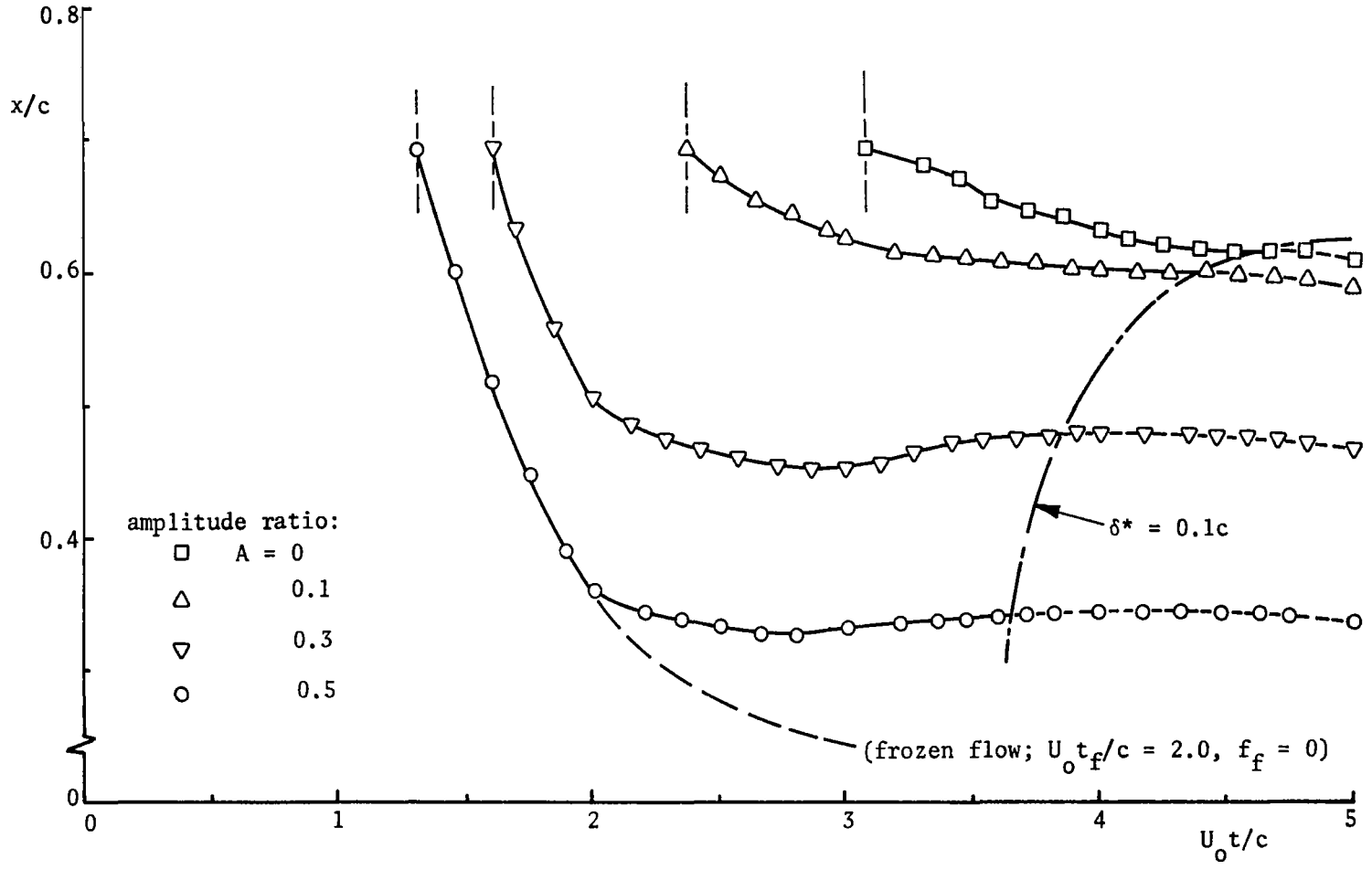


Figure 36 Movement of the Reversal Point with Time: Oscillatory Flow, $U_o t_p/c = 4.0$.

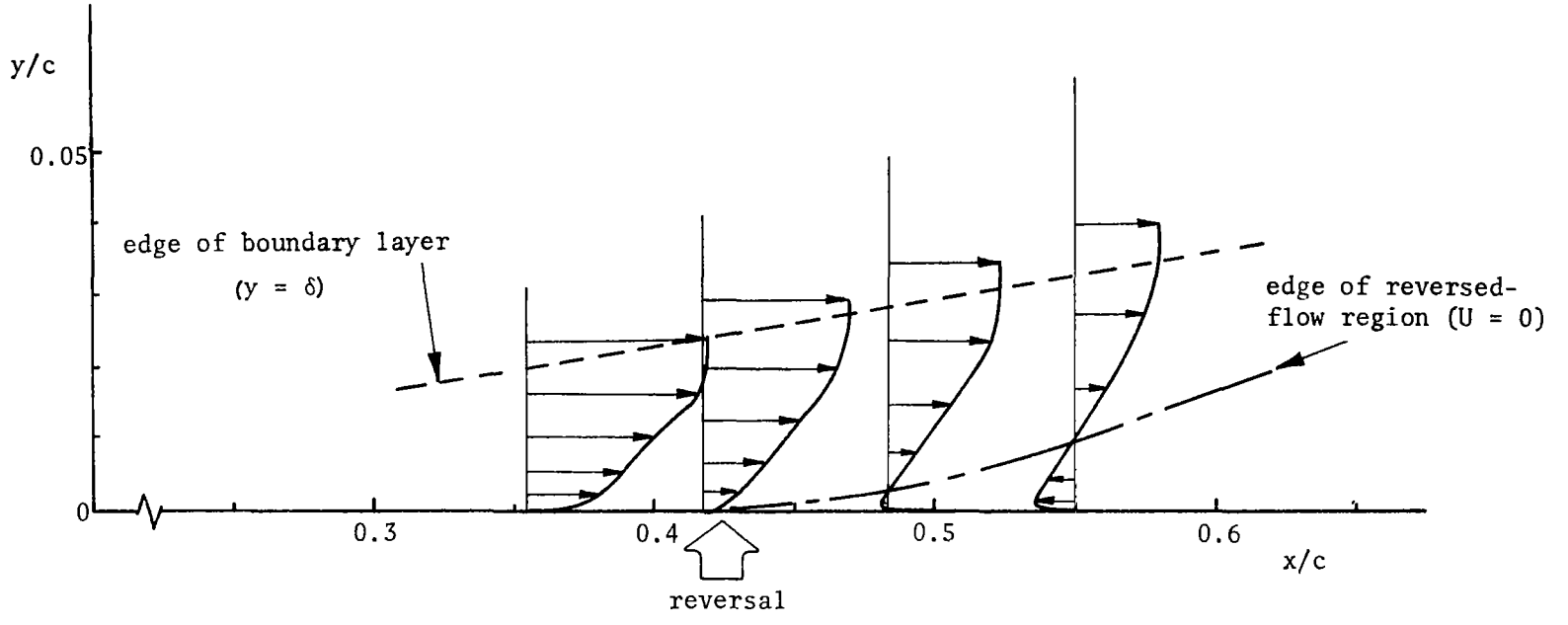


Figure 37 Velocity Profiles at $U_o t/c = 1.0$; Oscillatory Flow, $U_o t_p/c = 2.0$, A = 0.5.

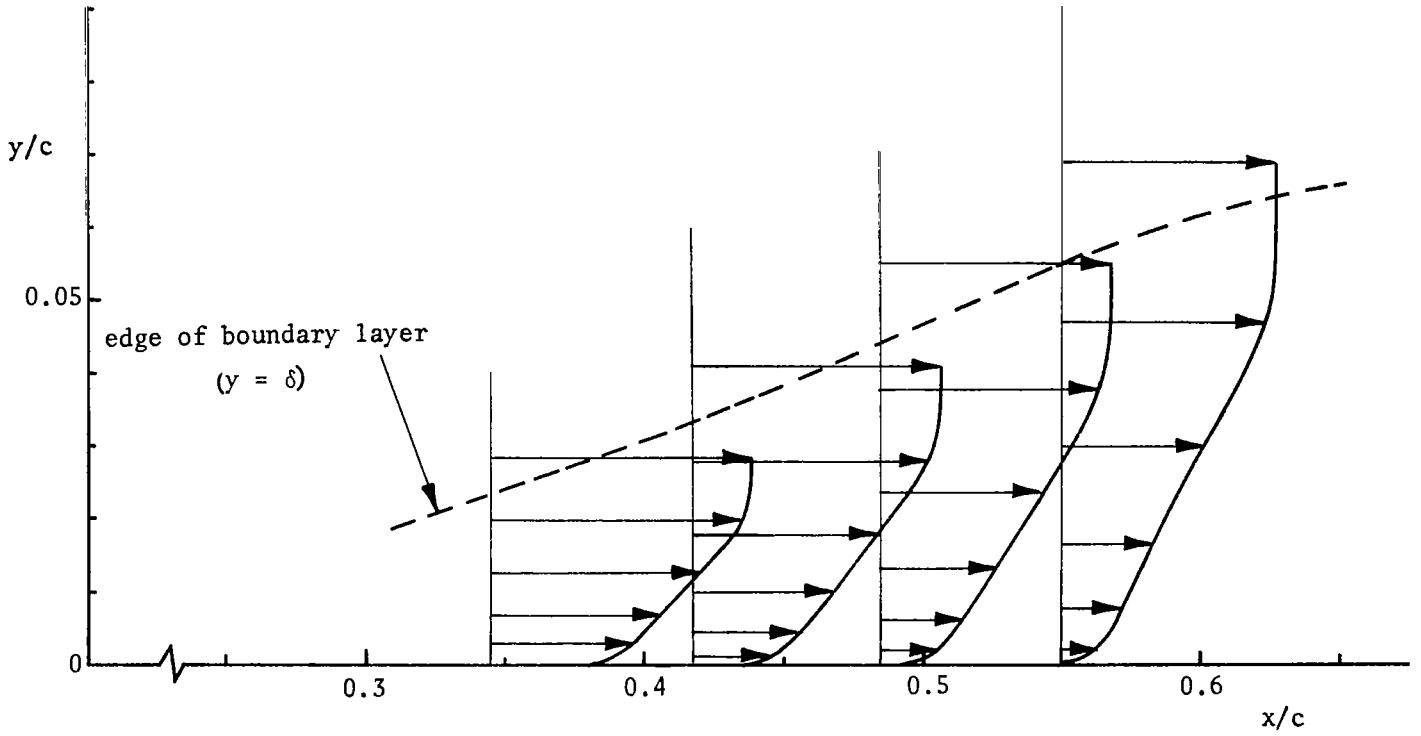


Figure 38 Velocity Profiles at $U_o t/c = 1.5$; Oscillatory Flow, $U_o t_p/c = 2.0$, A = 0.5.

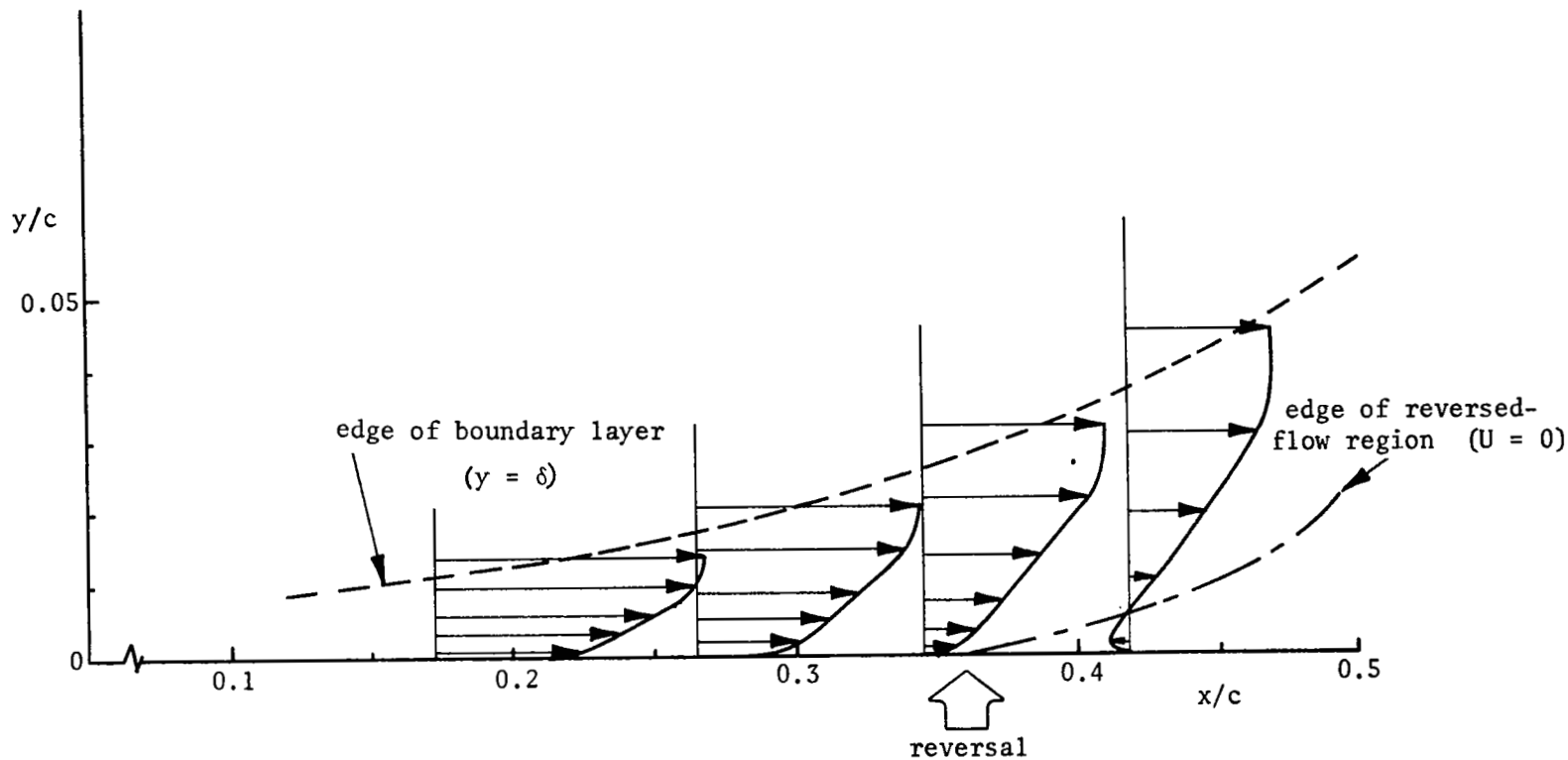


Figure 39 Velocity Profiles at $U_o t/c = 2.0$; Oscillatory Flow, $U_o t_p/c = 4.0$, A = 0.5.

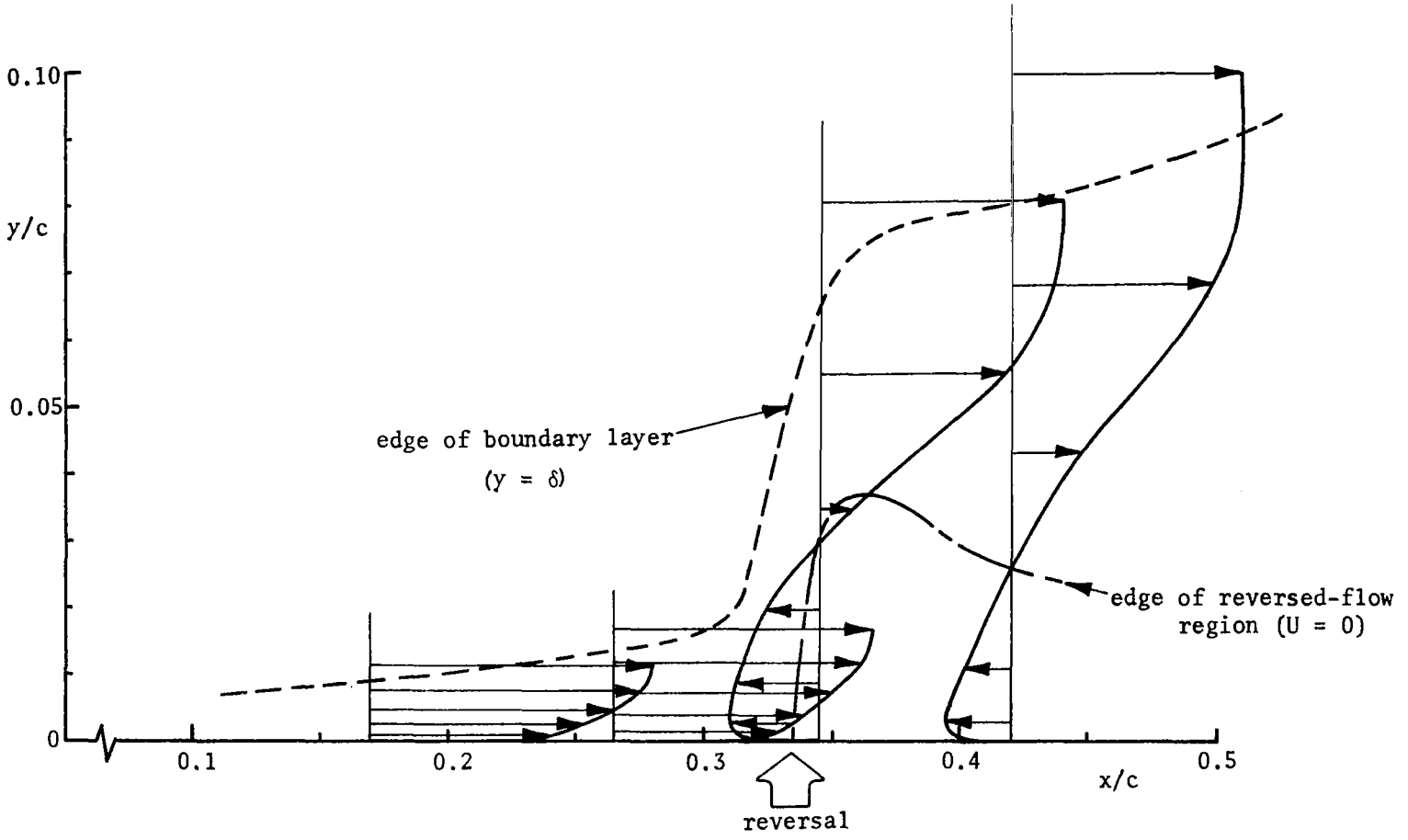


Figure 40 Velocity Profiles at $U_o t/c = 3.0$; Oscillatory Flow, $U_o t_p/c = 4.0$, A = 0.5.

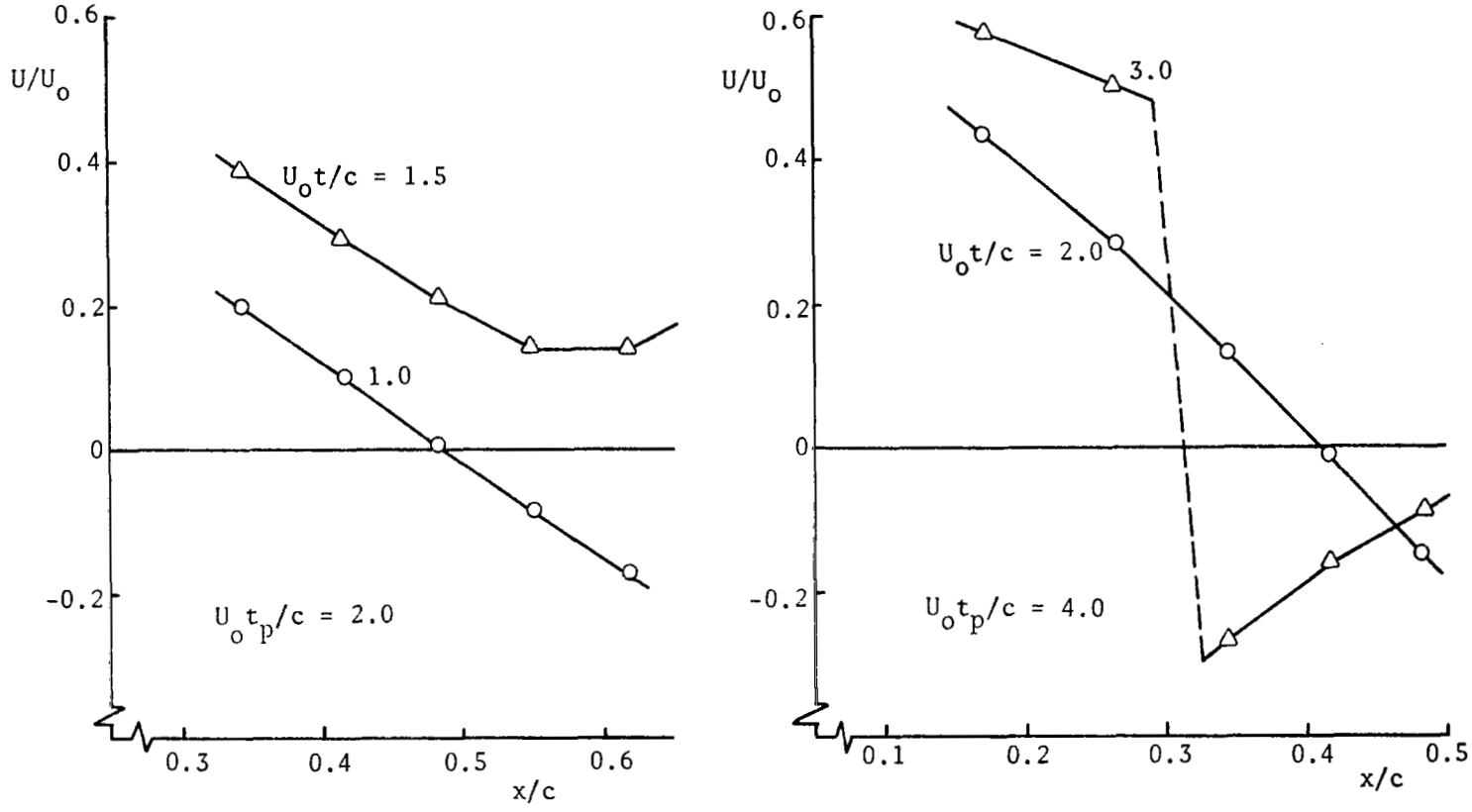


Figure 41 Velocities at y = 0.1δ; Oscillatory Flow, A = 0.5.

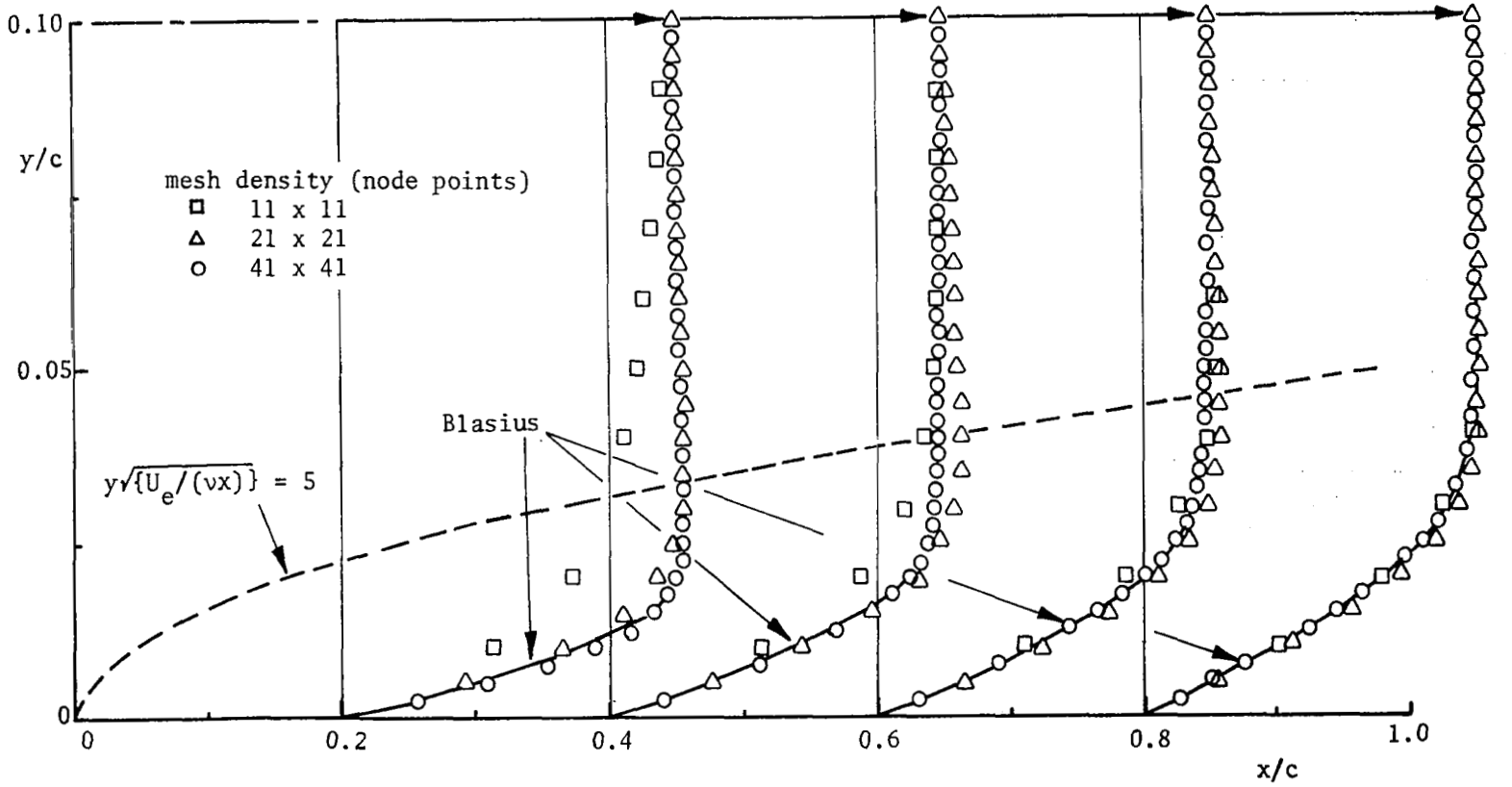


Figure 42 Computed Velocity Profiles Over a Flat Plate; Laminar Flow, $U_o c/\nu = 10^4$.

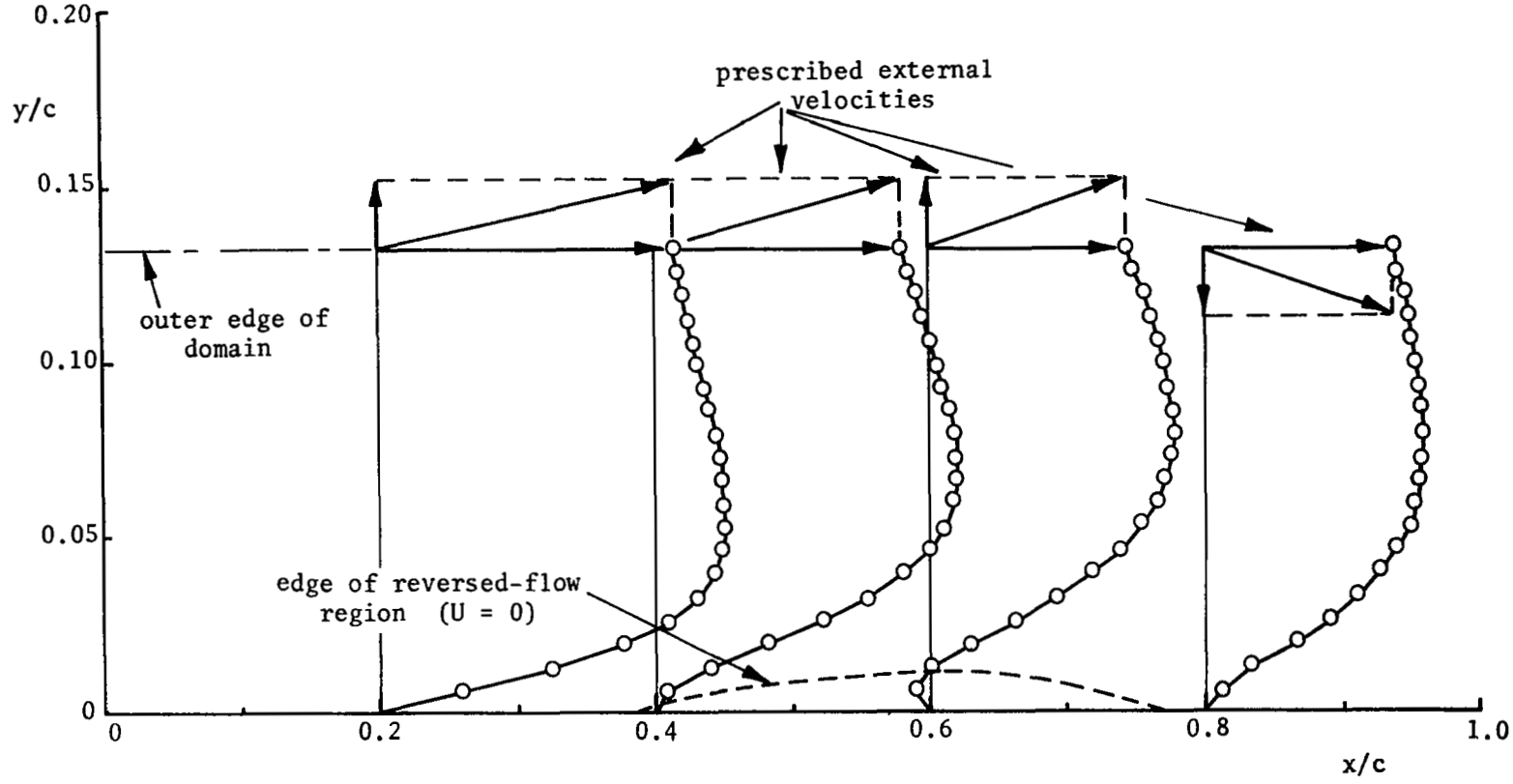


Figure 43 Velocity Profiles at $U_o t/c = 2.0$; Laminar Frozen Flow, $U_o t_f/c = 2.0$, $f_f = 0.5$.

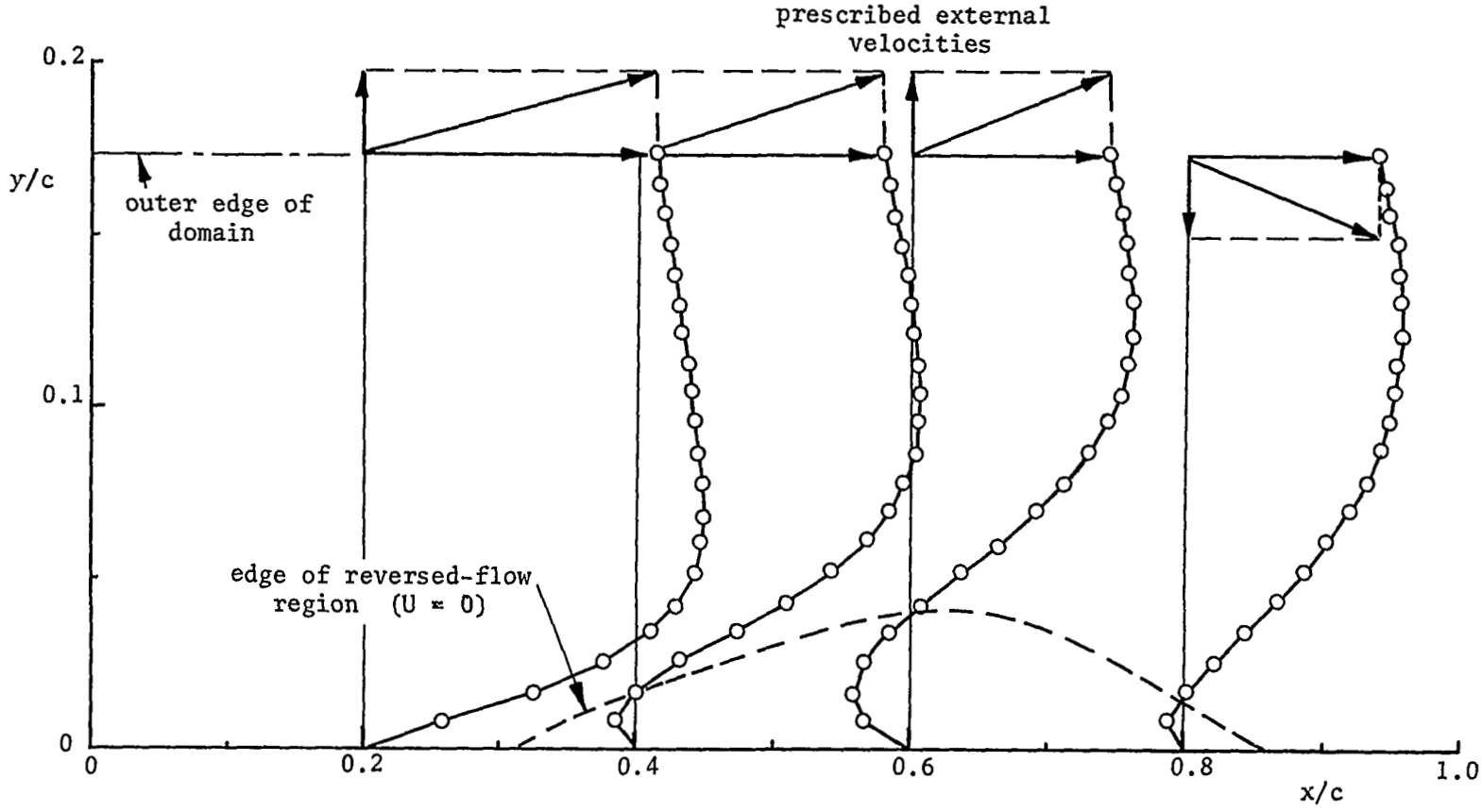


Figure 44 Velocity Profiles at $U_o t/c = 4.0$; Laminar Frozen Flow, $U_o t_f/c = 2.0$, $f_f = 0.5$.

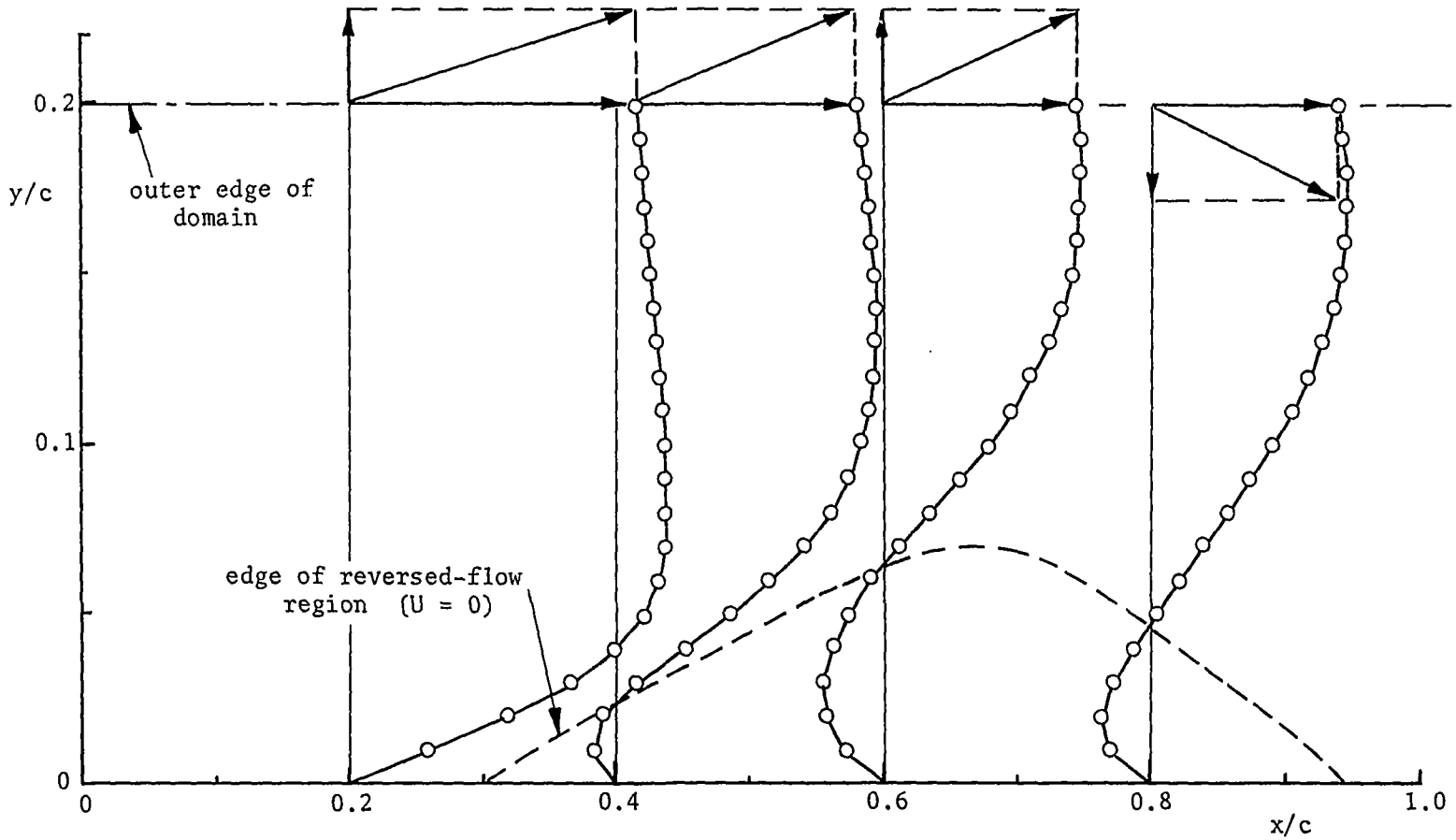


Figure 45 Velocity Profiles at $U_o t/c = 8.0$; Laminar Frozen Flow, $U_o t_f/c = 2.0$, $f_f = 0.5$.

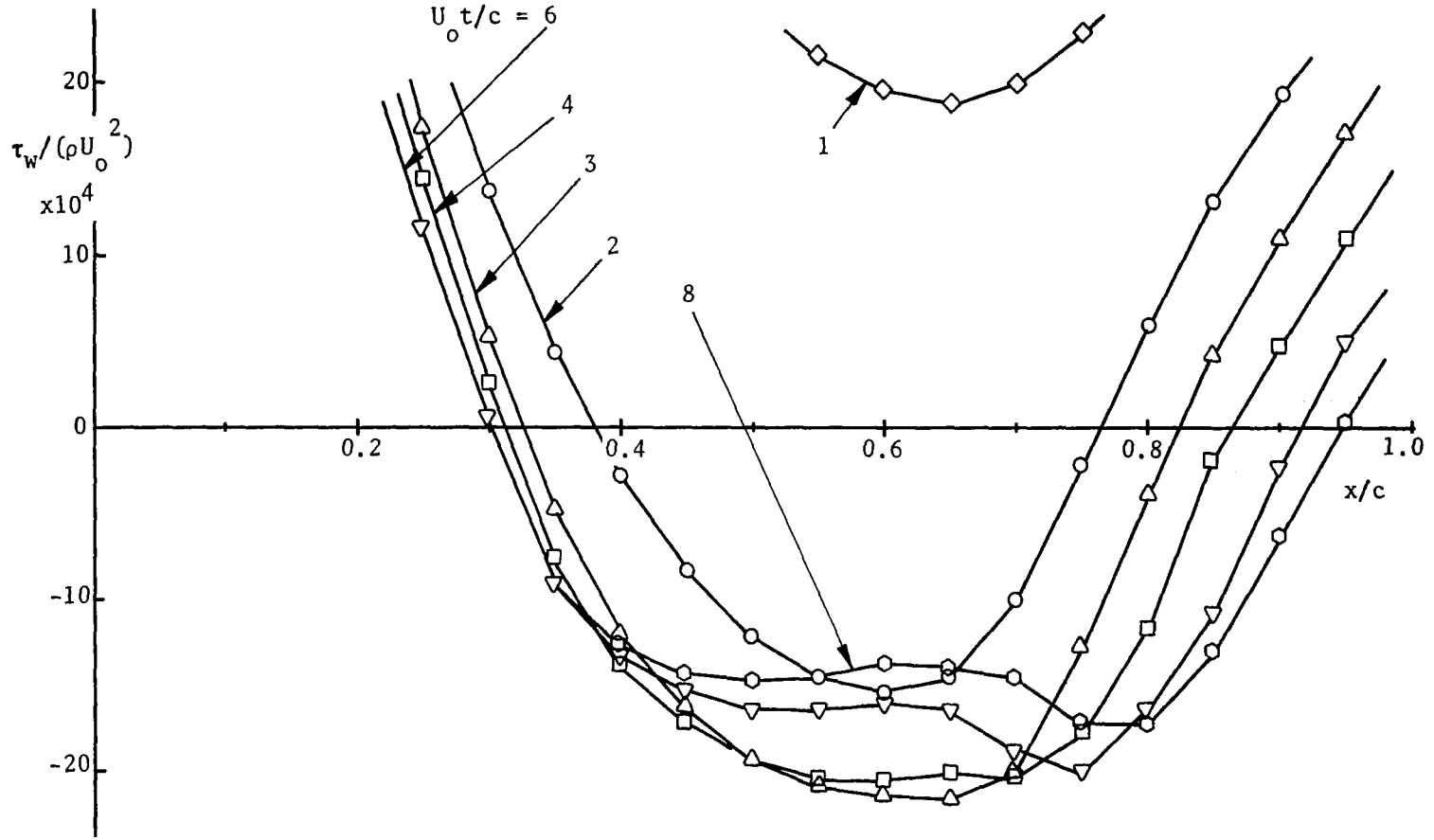


Figure 46 Wall Shear Stress Distributions for Increasing Time; Laminar Frozen Flow, $U_o t_f/c = 2.0$, $f_f = 0.5$.

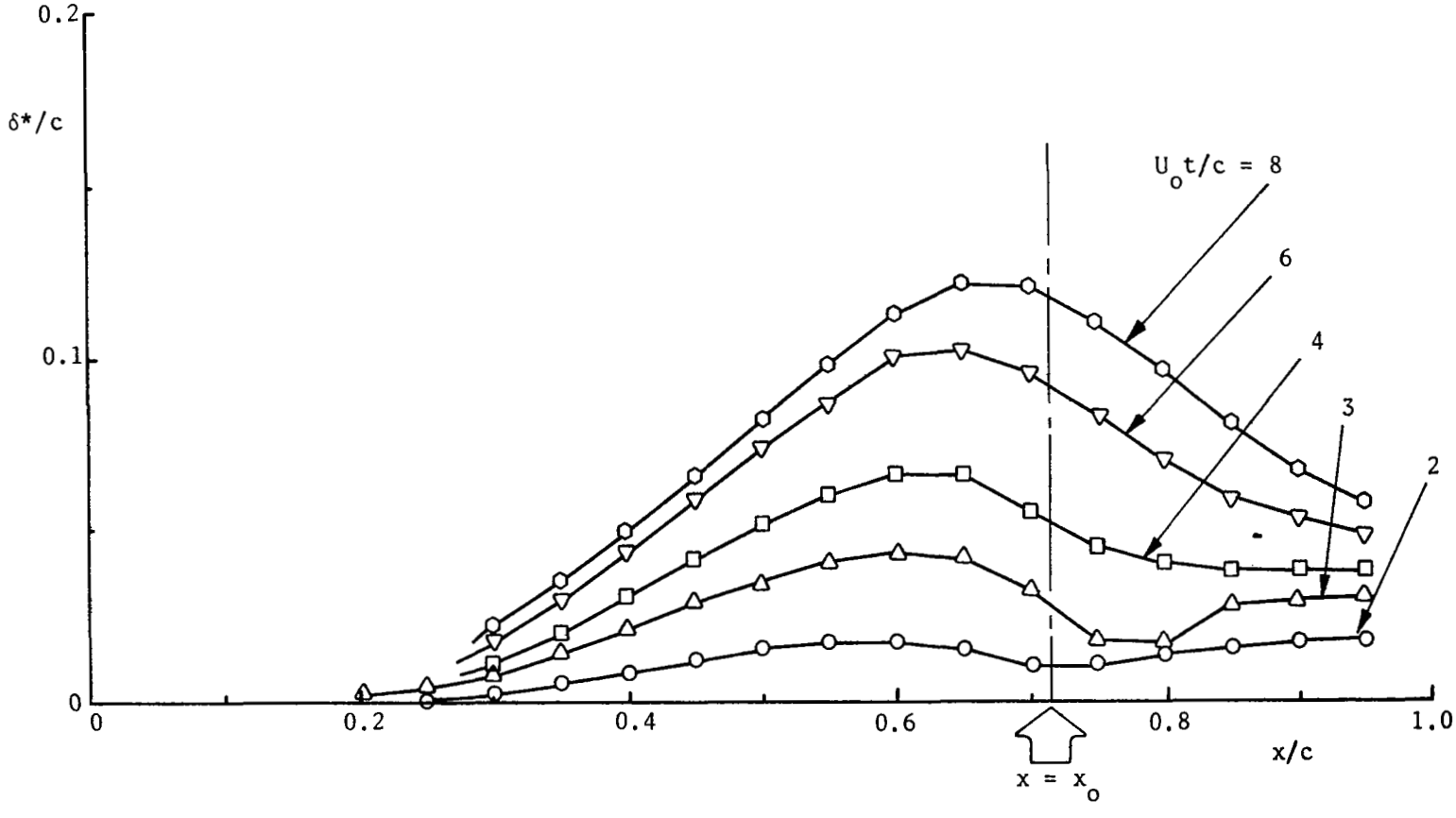


Figure 47 Displacement Thickness Distributions for Increasing Time; Laminar Frozen Flow, $U_o t_f/c = 2.0$, $f_f = 0.5$.

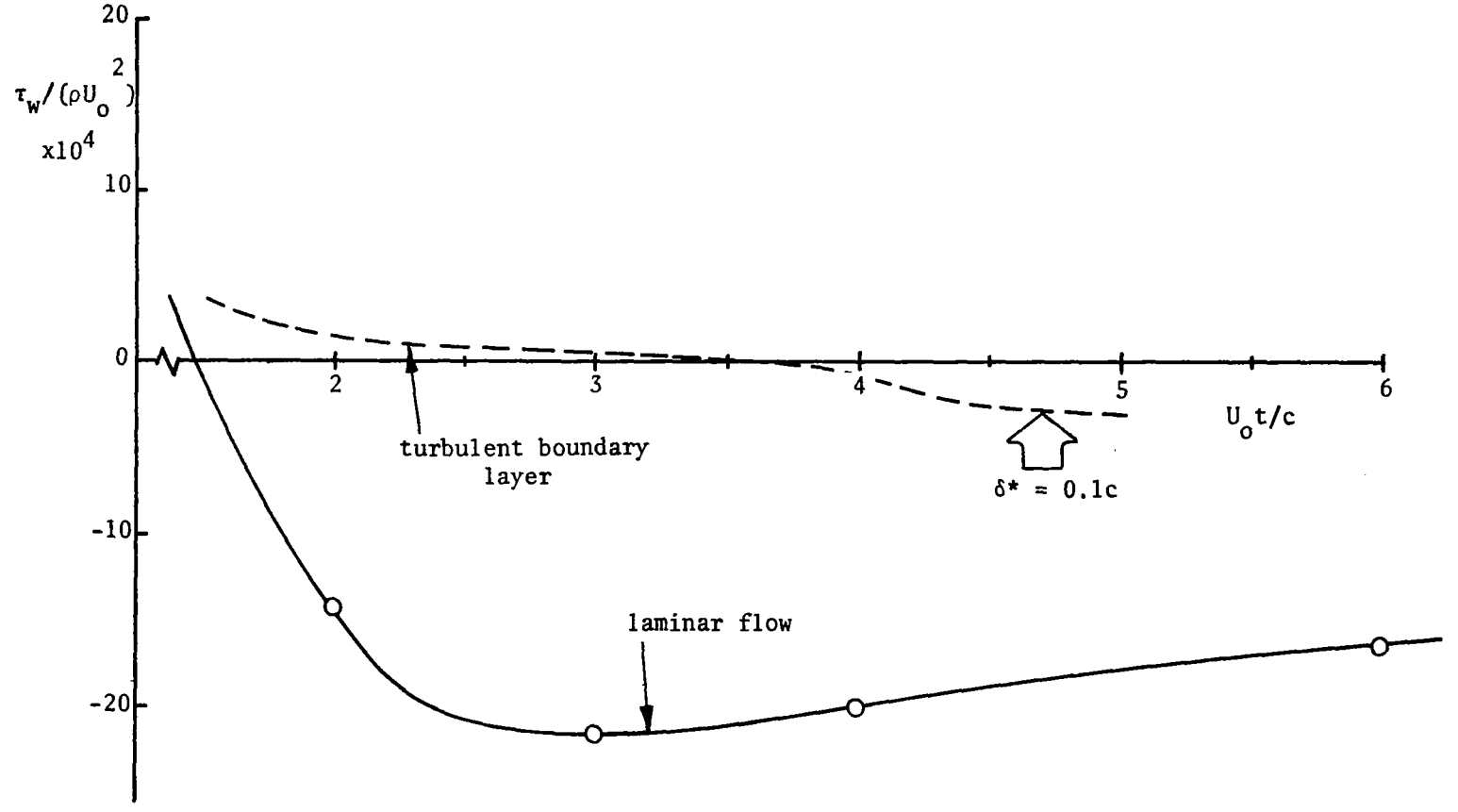


Figure 48 Variation of Wall Shear Stress with Time; Frozen Flow, $U_o t_f/c = 2.0$, $f_f = 0.5$, $x = 0.65c$.

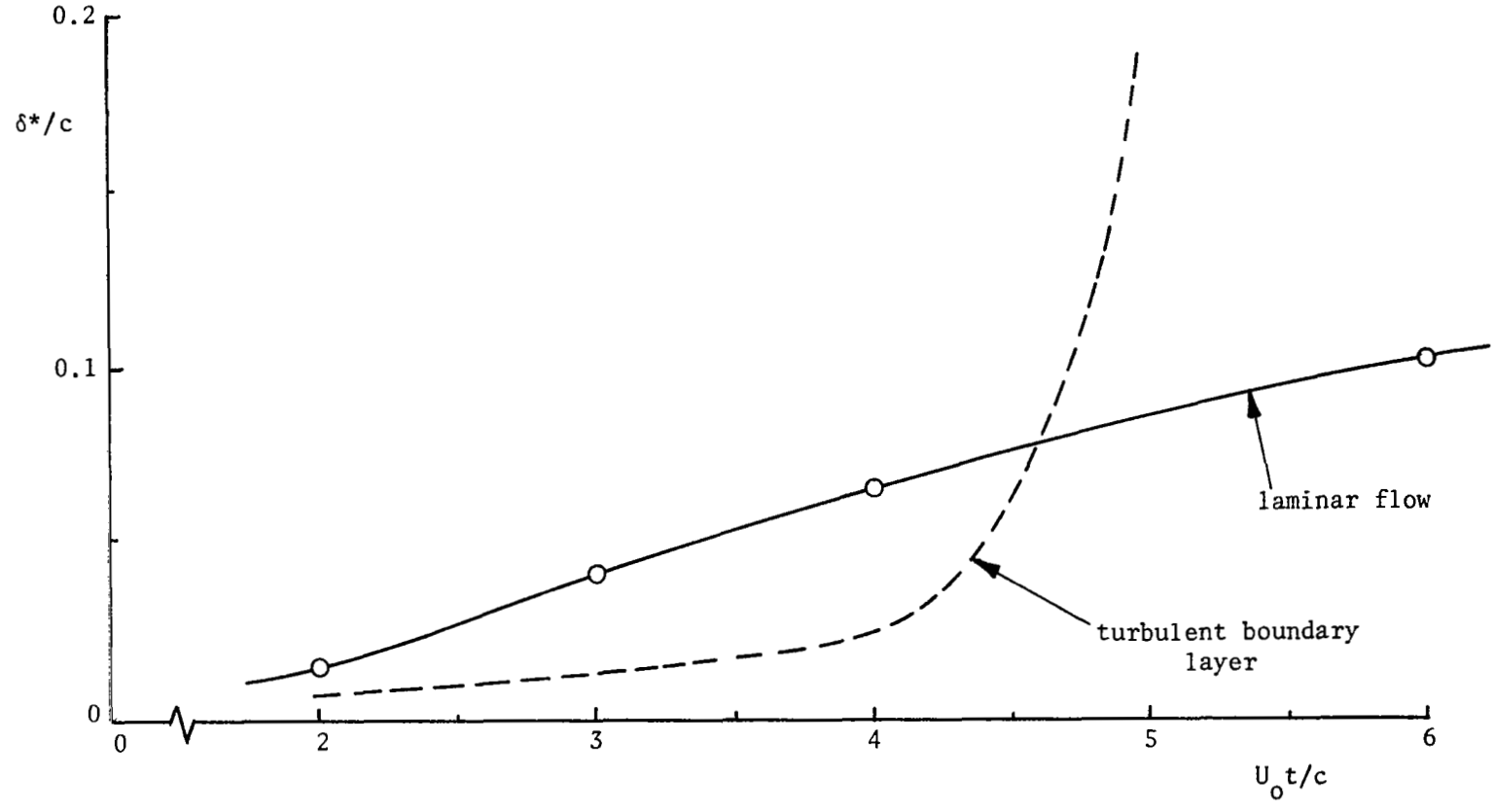


Figure 49 Variation of Displacement Thickness with Time; Frozen Flow, $U_o t_f/c = 2.0$, $f_f = 0.5$, $x = 0.65c$.

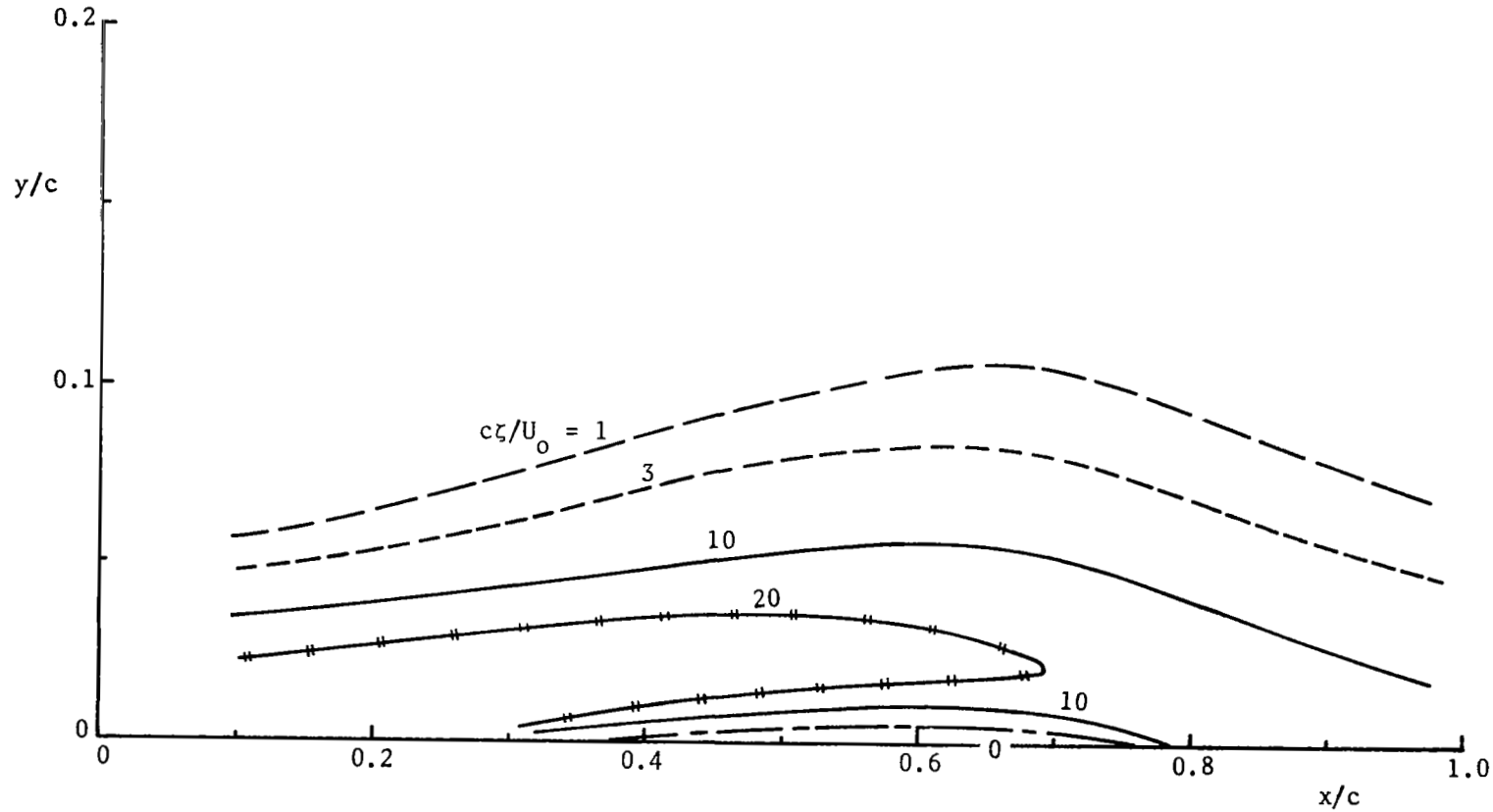


Figure 50 Vorticity Contours at $U_o t/c = 2.0$; Frozen Laminar Flow, $U_o t_f/c = 2.0$.

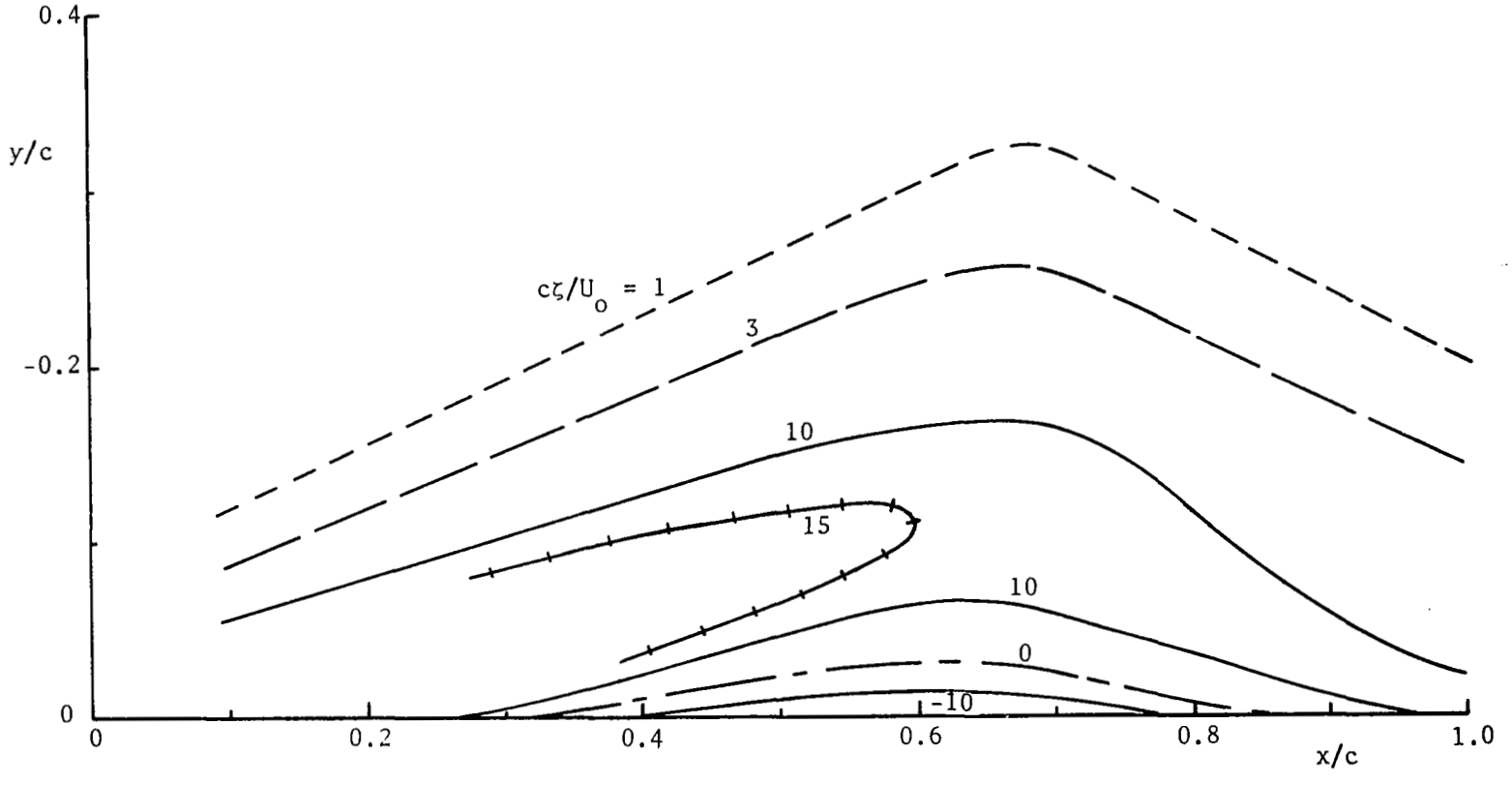


Figure 51 Vorticity Contours at $U_o t/c = 4.0$; Frozen Laminar Flow, $U_o t_f/c = 2.0$.

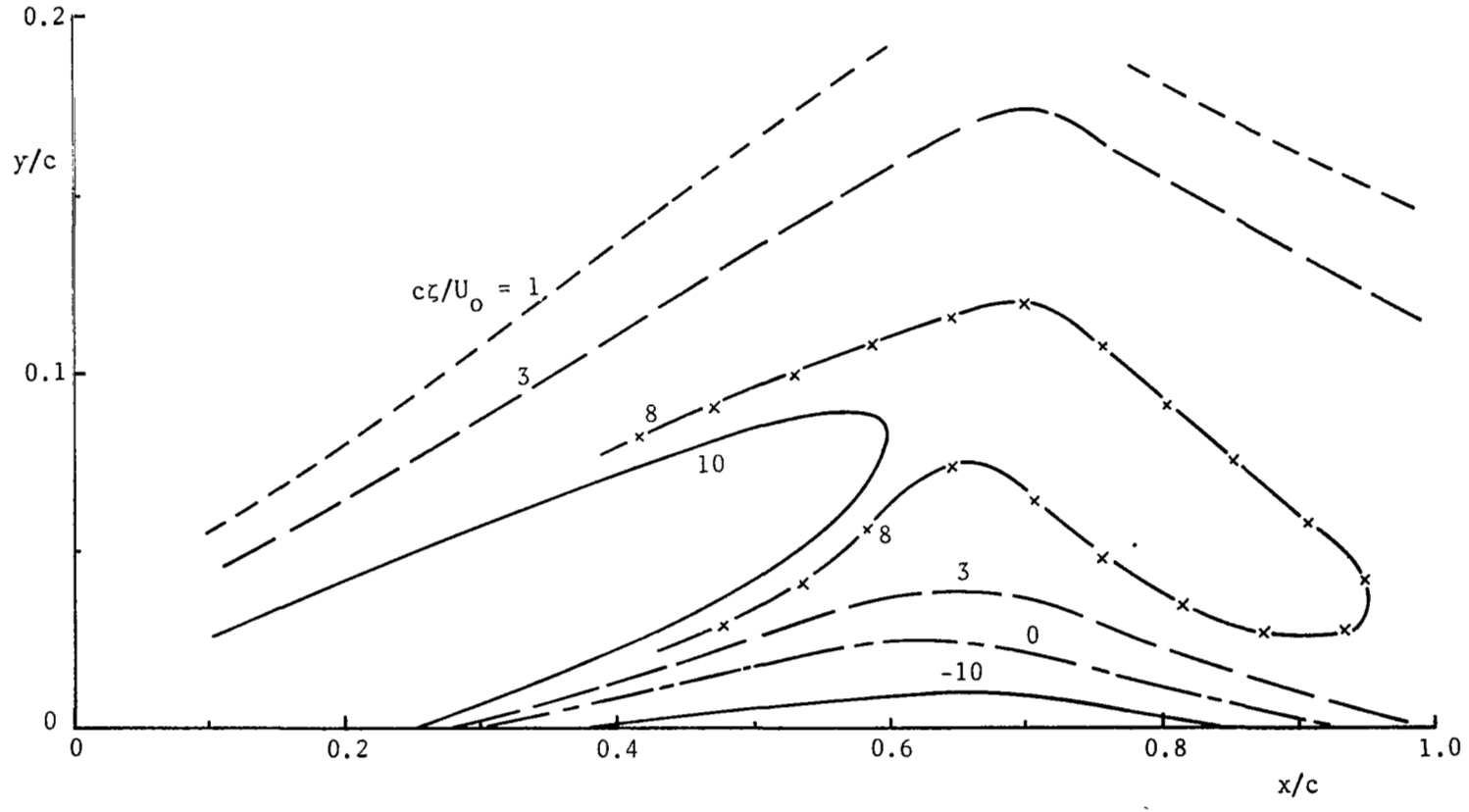


Figure 52 Vorticity Contours at $U_o t/c = 8.0$; Frozen Laminar Flow, $U_o t_f/c = 2.0$.